MASTER

Development of a numerical model for the US-DoT side impact dummy a hybrid modeling approach

Teulings, A.M.G.L.

Award date:
2001

Technische Universiteit Eindhoven
Department of Mechanical Engineering
Section of Engineering Dynamics and Biomechanics

Development of a numerical model for the US-DoT Side Impact Dummy

-a hybrid modeling approach-

A.M.G.L. Teulings

WFW-report DCT.2001.42

Under supervision of:
prof. dr. H.Nijmeijer
prof.dr.ir. J.S.H.M. Wismans
dr. ir. N. van de Wouw
dr. ir. P.H.M. Bovendeerd
ir. R.S.J.M. Verhoeve

...Well yes, that all fine but General Motors doesn't build rigid cars...

-Paul F. Altamore- Manager, Engineering Services, TNO-MADYMO-NAO

Abstract

Virtual testing allows vehicle designers to assess the level of occupant safety, offered by a vehicle, in a very early phase of the vehicle design process. The occupant model, usually, is a representation of a crash test dummy that is used in regulatory testing. These occupant models have evolved from simple multibody models to complex finite element models.

Recognizing the strengths (and limitations) of both multibody and finite element occupant models in certain fields of applications, TNO, that in the past specialized in multibody models, is now developing a new numerical model for the US-DoT Side Impact Dummy (US-DoTSID)

The development methodology used for this new DoTSID model is based on the previously developed multibody model of the US-DoTSID, with the inclusion of a finite element mesh. Using a hybrid modeling approach, combining both multibody and finite element modeling techniques, this DoTSID model was validated and subjected to two vehicle crash applications.

The combination of multibody and finite element allowed for a very efficient and flexible model set-up. Overall, the model predictions are in good agreement with the assessed experiments. However, the lack of validation on material level deteriorates the models predictiveness. Therefore, the development methodology of these hybrid models should include a more thorough finite element based influence, starting with the validation of the material models.

Contents

Chapter 1

Introduction

This introduction to "*Development of a combined finite element-multibody model for the US-DoT Side Impact Dummy*" contains a framework for this thesis, the objective and the methodology adopted to attain this objective.

1.1 Framework

This section contains background information on the importance of crash safety research and the role that virtual testing plays in this field of science.

1.1.1 Crash safety of vehicles

Annually, motor vehicle crashes worldwide cause over a million road deaths and over a hundred million injuries, of which roughly 10% serious. In the Netherlands, it is estimated that approximately 25% of all deaths involving young adults can be attributed to traffic related accidents. The economic cost of traffic accidents are staggering. A minimum estimate for 1999 in the European Union alone is more than 160 billion Euro a year [1][1].

In an effort to reduce the number and severity of injuries both government organizations and automotive manufacturers continuously look at possibilities to improve and validate *crashworthiness* of road vehicles. Crashworthiness relates to a vehicle's structural capability to absorb the crash kinetic energy and the restraint system's ability to provide adequate protection in a survivable crash.

The relationship between loads and severity of sustained injury are described by *injury criteria* (see appendix A). These criteria make it possible for legislative organizations to set measurable standards for crashworthiness. This is done through the specification of standardized vehicle crash tests, where the loads that occupants of that particular vehicle model would incur are measured by sensor equipped crash test dummies. Only when these loads indicate that the likelihood of serious injury is negligible a vehicle complies to the required safety standards. In the US, the National Highway Traffic Safety Administration (NHTSA) issues the Federal Motor Vehicle Safety Standards (FMVSS) for assessing crashworthiness.

While most crashes are frontal, side impact is more severe accounting for almost 40% of all crash related fatalities [1]. This phenomenon can be attributed to the limited space between the occupant of the struck vehicle and the striking vehicle when compared to frontal collision. Also, since early crashworthiness research mainly focused on frontal impact, the crashworthiness of vehicles in these type of collisions has been further optimized with respect to side impact. Recognizing the importance of ensuring occupant safety in lateral collisions, NHTSA, has issued two test procedures for validating vehicle crashworthiness in side impact. Theses procedures are documented in Federal Motor Vehicle Safety Standard 201 (FMVSS201) and FMVSS214 [2][3]. The specifics of the FMVSS201 procedure requires the use of a standard anthropomorphic testing device: The US-DoT side impact dummy (US-DoTSID) [4][5].

1.1.2 Anthropomorphic test devices

Anthropomorphic Test Devices (ATD's) are mechanical models that can represent a specific human body region, such as a head, or the complete human body. Crash test dummies represent the latter category. These

[1] Numbers in brackets designate references at the end of the thesis

dummies, as illustrated in figure 1.1, can represent a range of occupants: male, female, newborns, infants and children of various ages.

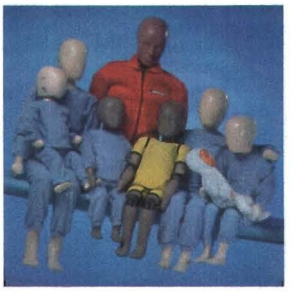

Figure 1.1: Family of crash test dummies.

Crash test dummies normally consist of a metal and/or plastic skeleton, including joints, covered by flesh-simulating plastic and/or foam. The dummy can be equipped with sensors to measure the accelerations, forces and deflections of different parts of the dummy during crash tests. In approval tests on vehicles and safety devices it is required that the measured values should stay below certain (human) tolerance levels. Since their introduction in 1973, the use of these crash test dummies in safety regulations has shown a clear increase [6].

Most dummies can be used in one specific impact direction only; frontal, lateral or rear. Attempts have been made to design "omni-directional" dummies, however without much success. Main requirements of an ATD are: anthropometry, biofidelity, durability, repeatability, reproducibility and durability.

Anthropometry is the ability of the dummy to represent a human being in terms of selected size and corresponding mass and mass-distribution. The dummy should interact correctly with the vehicle seat and safety belt system. For the representation of an adult male in automotive tests often a 50^{th} percentile adult male dummy is used. This dummy combines all the average anthropomorphic values for the adult male category. A total body mass of 77.5 kg and a standing height of 175 cm were defined for a 50^{th} percentile adult male.

Biofidelity deals with the level of human-like response a dummy displays and is probably the most difficult part of the design. Obviously a non-biofidelic dummy could guide the vehicle design process in a wrong direction.

In order for a dummy or subcomponent test device to function as an effective industrial and governmental standard tool, or even as a research tool, it must not only provide a biofidelic response, but it must also demonstrate that it can give similar results in repeated tests. This quality is captured in the repeatability of an ATD.

Reproducibility means that any two ATD's built to a particular design must respond in a manner similar to each other. In order to maintain reproducibility, ATD's have to be certified. This certification is the tuning and checking of components to assert that they are within a predefined corridor or set of limits.

Finally, crash test dummies need to be robust. Each dummy should "survive" a number of tests without failure and remain within the specified certification limits. Values of 20 to 100 tests with a 50% overload compared to human tolerance levels are mentioned as durability requirements [7]. This requirement can be contradictive to, for instance, requirements regarding biofidelity.

1.1.3 Virtual testing in crash safety

Besides the crash tests required by legislation, car manufacturers usually also perform additional tests to gain insight into the crash behavior of their vehicle design. However, the cost in time and other resources limits the effectiveness of these full-scale tests as a means of fundamental research to gain a better understanding of side impact. Moreover, these tests find their primary use in a late (prototype) stage of the vehicle design process when changes to the design are very costly. These drawbacks make crash testing an inefficient tool for parametric studies and vehicle design. As a result, attention focused on developing an alternative method of assessing crashworthiness.

Developments in computer hardware and software have made simulations an alternative for many tests. Virtual testing is a tool that allows researchers to predict injury potential of occupants in a very early stage of the vehicle design. Through parametric studies the model can provide information that helps the designers to improve crashworthiness of their vehicle, thus minimizing the amount of hardware crash testing and shortening

the design phase. Moreover the simulations can serve as a means of research to gain a better understanding of crashes and (the improvement of) crashworthiness. The March 2000 VITES[2] proposal [8] included an objective to reduce the number of injured and killed road users by a factor two through the application of numerical crash simulations in vehicle design process. This reduction would entail 20.000 less fatalities in Europe with the corresponding economic benefits of approximately 20.000 million Euro.

The vehicle model will typically be unique for each study but the variety of occupants is limited to just a few instances, these being the models of the available crash test dummies. This allows for standard models to be made, just like the test dummies, prefabricated, and readily available for use by the engineer.

1.1.4 Evolution of numerical anthropomorphic test device models

Numerical ATD models used in virtual testing can, roughly, be divided in two classes.

- Lumped parameter or multibody (MB) models in either 2 or 3 dimensions, where the "occupant" is represented using a set of rigid bodies with prescribed masses and moments of inertia, linked by various types of kinematic and/or dynamic joints.
- Finite element (FE) models, where a continuous system is discretized in space using a finite number of elements interconnect by nodal points.

The following section provides an overview of the evolution from simple 2-dimensional lumped parameter models to the more complex finite element models. Furthermore, applications and limitations of these modeling methods will be discussed.

Multibody models

Almost 40 years have elapsed since McHenry [9] proposed one of the first mathematical simulation models to describe the dynamic response of a vehicle occupant involved in collision. This CAL-2D model consisted of a two-dimensional (2-d) lumped parameter model with seven degrees of freedom and was formulated to predict the major responses of the occupant in frontal collision and to determine the feasibility of more sophisticated models. The results were sufficiently encouraging to warrant the development of a more complex two-dimensional model that featured eight bodies and had 11-degrees of freedom. The updated model was subjected to a validation attempt as described by McHenry and Naab (1966) [10]. The simulated test series consisted of 15 instrumented sled tests at two levels of impact severity. The correlation between experimental and analytical results was considered reasonable, particularly in view of the fact that many of the joint properties and contact characteristics were estimated. Further improvements to this model were made by McHenry and Segal (1967) [11], Segal (1971) [12], Danforth and Randall (1972) [13] and Robbins *et al* (1974) [14]. This latest version of the CAL-2D model, shown in figure 1.2, was called MVA-2D and included features such as occupant interaction with: belts with inertia reels and belt sliding, collapsible steering column and air bag.

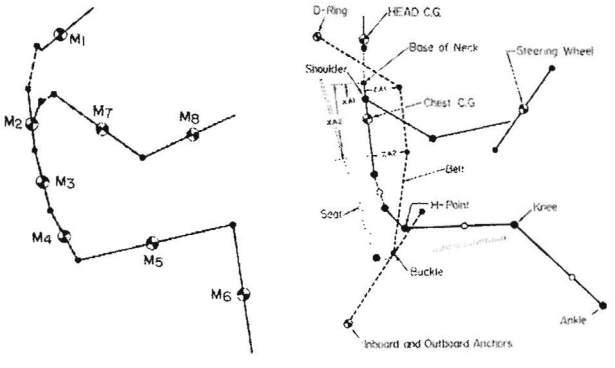

Figure 1.2: The MVA-2D model.

Despite all efforts, this model version could not be properly validated. The model was primarily used for frontal and rear impact.

[2] Virtual testing for Extended Vehicle passive Safety

Two-dimensional occupant models became inadequate for the simulation of accident victim kinematics, especially in cases of lateral or oblique collision, pedestrian-car impact and when asymmetric restraint systems are used [15]. The early and mid-seventies saw the emerge of several 3-dimensional models.

In 1972, Bartz [16] proposed a three-dimensional (3-d) model that was adapted by the Calspan Corporation for their CAL-3D release (figure 1.3). This model consisted of 15 rigid bodies, 10 ball and socket type joints and 4 hinge joints.

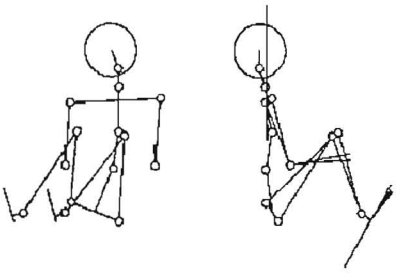

Figure 1.3: The CAL-3D model.

The model was validated by comparing model results with experimental data from sled impactors and full scale crash tests at velocities up to 48 km/h. Correlation between the simulated and experimental results was considered good. Further improvements to this model were made and in 1984 and the CVS version IV, as the model was called back then, was capable of handling belt slippage on deforming segments and rate dependent belt forces, aerodynamic forces, automatic equilibrium routines for seated occupants and air bag routines [17]. Applications for the model were found in pedestrian impact [18][19][20][21][22], side impact [23][24][25][26][27][28], rollover [29][30] and whole body ejection evaluation [31]. During this time frame, MADYMO [32] appeared with both a 2-d and a 3-d version of their numerical solver for occupant safety analysis. MADYMO with its solver also released numerical crash test dummy models using the lumped parameter approach. Steady evolution of this 3-d lumped parameter approach has earned this technique lots of merit in the simulation world with numerous examples of ATD models for a range of applications [33]. Figure 1.4 illustrates MADYMO's multibody SID-IIS ATD model.

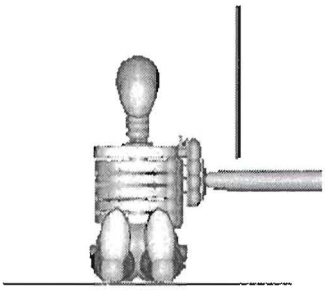

Figure 1.4: Multibody model of the SID-IIS dummy.

A drawback of these multibody models lies in the use of rigid ellipsoids that, by their nature, cannot mimic a detailed and deforming surface [34][35][36]. This concern is particularly valid for side impact crashes where the door trim undergoes large deformations before interacting with the occupant.

A spin-off of the lumped parameter models are the facet models [33], see figure 1.5. These models are in fact multibody models with the added capacity to describe contact surfaces with an accurate piece-wise geometry.

The lumped parameter models use abstract quantities, such as lumped masses and nonlinear springs, to model the dummy response. Therefore, the developer must know how to group properties, such as distributed mass and component structural stiffness into mass lumps and springs [37][38]. A shortcoming of this lumped approach is that model parameters may have little physical bearing to reality. This constraint limits the validity of these models to the same range of impact conditions as were used in the experimental validation tests, to a greater extent than is the case for a finite element model.

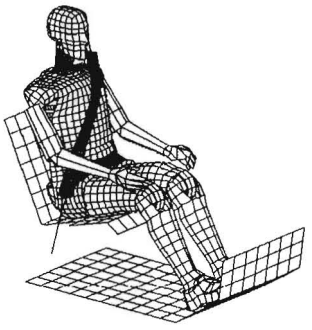

Figure 1.5: Facet model of the HYBRID-III ATD.

Finite element models

The second modeling technique for evaluating motor vehicle crashworthiness emerged in the early eighties. Finite element (FE) modeling is particularly useful for structural analysis when large and localized deformations come into play. This technique also allowed for the modeling of inflating air bags to a much higher degree of accuracy then can be attained with the lumped parameter approach. This feature proved indispensable in modeling "*out-of-position*-crashes" where the occupant of the struck vehicle is, for instance, leaning forward over the steering wheel and struck by the inflating air bag.

PAM-CRASH [39] is a FE code that has been used for crashworthiness engineering in the transportation industry since 1982 [40][41]. Rainer Hoffmann *et al* in 1990 [42] presented a technique for coupling the PAM-CRASH and MADYMO codes in one simulation. The coupling of the FE vehicle model, including air bag and knee bolster, with facet model of the HYBRID-III dummy [43] resulted in good correlation for this complex crash simulation. Figure 1.6 shows an example of such a combination.

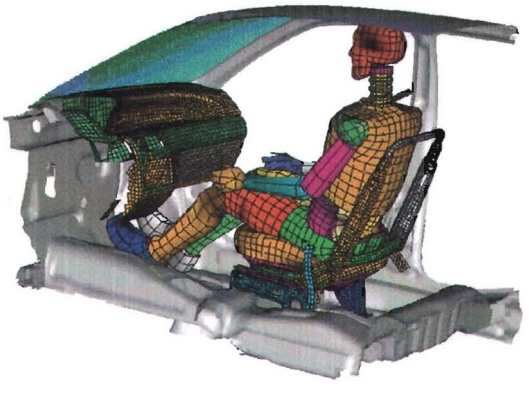

Figure 1.6: Example of FE and facet model combination.

Drawbacks of the higher level of modeling detail in the FE approach as opposed to multibody models are a long development time for the model and also the sharp rise in cpu time for the numerical integration scheme to complete a simulation run. Moreover, success of the FE approach requires an accurate geometric description of the dummy parts and accurate constitutive models for the materials of which these parts consist.

The apparent success of the FE approach in structural analysis and the inherent limitations of the lumped parameter occupant models restricting their use in certain application fields, such as side impact, motivated the development of FE models for dummies. In 1992, the German Forschungsvereinigung AutomobilTechnik (FAT) started developing finite element dummy models for side impact. In 1999, FAT released their 43.000 element US-DoTSID model version 2.5 (figure 1.7) [44]. Validation has been performed on material, component and full dummy level, showing good correlation according to the FAT developers [45].

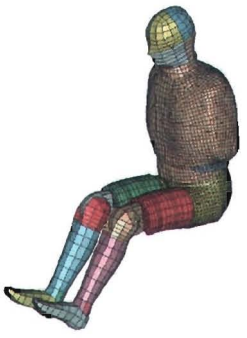

Figure 1.7: FAT finite element model of the US-DoTSID.

Despite this extensive validation, some manufactures found the predictably of this model to be insufficient for their applications. Moreover, the addition of a finite element based ATD model to a finite element (vehicle) environment often leads to an unacceptable long computational time for the analyses.

Multibody modeling versus finite element modeling

The major advantage of the multibody approach is its computational efficiency in simulating spatial motions of mechanical systems, such as the dummy and vehicle, using rigid bodies interconnected by complex kinematic or dynamic links. The advantage of the FE method is the added accuracy and the ability to describe (local) deformations and stresses in a realistic manner. However, the long computational times required to perform a finite element crash simulation makes the FE method less suited for optimization studies involving many design parameters. Both methods, therefore, have their place in a vehicle design process. Early "*concept vehicle*" studies can efficiently be performed in a multibody environment even when many parameters of the final vehicle design are not yet determined. Subsequently, when the design process reaches a more mature phase, finite element modeling can provide more accurate and reliable information.

1.2 Objective

MADYMO is a commercial software package that has extensive experience with the development of multibody dummy models. In the light of developments discussed in the previous section, and industrial demand, MADYMO is now investigating the possibilities of developing FE dummy models. MADYMO's existing resources, such as available models, modeling expertise and acquired test data, however, are still primed for the development of multibody models. TNO's aim is, to integrate these existing resources in the development of finite element models in order to facilitate the design process. Depending on the extent of the integration, one should speak of a hybrid MB-FE model.

This thesis will focus on:

1. The (methodology of) development a hybrid MB-FE numerical model for the US-DoTSID

The model should be able to be used as a design and evaluation tool in a production environment. This constitutes the following requirements:

2. The model should be predictive and accurate within a useful range of applications
3. The time step of the numerical integration scheme used to simulate side impact with this model should be large enough to allow it to be useful in a production environment, while still ensuring numerical stability and convergence
4. The handling (positioning, contact definitions, etc.) should be as similar as possible to MADYMO's multibody and facet models

Finally, in addressing point 2, some suggestions for the assessment of a given numerical model's quality will be discussed.

1.3 Methodology

Developing and validating any numerical model for such a complex system as a crash test dummy is a lengthy process, consisting of the model configuration, assembly of test series, model calibration and finally, the model validation.

1.3.1 Model configuration

As discussed in the objective, the DoTSID model will consist of both MB and FE parts. A dummy skeleton frame is modeled as a multibody system linkage derived from the multibody DoTSID model [33]. This system linkage includes all the joints, including joint properties such as joint stiffness and range of motion. Also the sensors are connected directly to this multibody core. The linkage in itself has no geometry since all contact ellipsoids have been removed.

Subsequently, the finite element mesh is largely derived from a FE numerical DoTSID model that NHTSA freely publishes for research purposes [47]. Based on measurements and documented information improvements were made to this mesh. The majority of material properties are derived from literature, test data or, where necessary, determined through (sub)system level calibration.

1.3.2 Test matrix

It is extremely important to validate the numerical model within the range of loading conditions (type and severity) of its intended application. First priority, therefore, is to identify this application area. Subsequently, test data should be gathered pertaining materials, components and the full-system based on these loading conditions. This collection of test data is referred to as the *test matrix*. Based on this matrix the model can be calibrated and validated.

Particularly test data on material level was lacking, this can be attributed to TNO's predisposition to develop multibody models, where material properties are often lumped.

1.3.3 Calibration and validation

Calibration is the tuning of a model to obtain good response in a selected series of tests. Validation is an assessment of the quality of the calibration. Therefore test data used in validation should be derived from tests not used in the calibration. Using the test matrix of existing test data as reference the DoTSID model was calibrated and validated using an iterative optimization process (See section 3.1.3).

Validation quality assessment

When numerical models of hardware crash tools are not sufficiently validated to test data, they are not likely to accurately predict (trends of) real-life responses. This can render the models useless as tools for numerical vehicle design optimization with respect to crash safety.

A crucial problem in communication between developers and users of numerical models concerns the judgement of the quality of the models. So, even though there is a clear need for classification of a numerical models quality, a method could never be agreed upon [48]. Currently, a European Union project called Virtual Testing for Extended Vehicle Passive Safety (VITES) [8] is investigating such a model classification method. VITES published their project proposal in March 2000 where it was stated that:

"... major improvements in model predictiveness can be obtained through the definition of procedures and criteria allowing an objective assessment of the quality of models and of the accuracy of the virtual test results ..."

Issues such as, the number and range of validation tests to be performed, the repeatability and reproducibility of the tests, the accuracy of the prediction, and the models sensitivity all need to be taken into account before classification of a numerical models quality can be made.

In chapter 7.2, the DoTSID model will be evaluated by applying a method proposed by Prasad *et al* [48].

Chapter 2

The US-DoT Side Impact Dummy

The DoTSID, see figure 2.1, is specified in the Code of Federal Regulations (CFR)-subpart F [49]. DoTSID was adapted from the Hybrid II 50^{th} percentile male test dummy [50] and implemented in safety regulations in 1990 to provide human-like acceleration responses in the lateral direction.

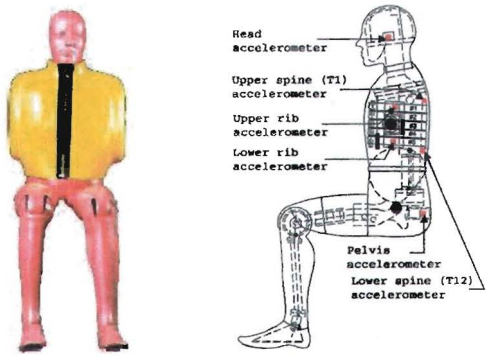

Figure 2.1: The US-DoT Side Impact Dummy.

2.1 General description

The United States Department of Transportation Side Impact Dummy (US-DoTSID) represents a 50^{th} percentile male with a standing height of 175 cm, erect sitting height of 89.9 cm and a total non-instrumented body mass of 76.5 kg [5]. Lower arms have been omitted, since it was found in earlier prototype simulations that these extremities cause a significant disturbance in repeatability. Furthermore, the upper arm is represented by low density urethane foam blocks. The loss of stiffness and mass as a result of these design choices are compensated in the thorax assembly.

2.1.1 Instrumentation and assessable injury criteria

For the evaluation of injury criteria ATD's can be equipped with a range of sensors. Figure 2.1 shows a instrumented US-DoTSID.

While there are a multitude of injury criteria in use (for both humans and ATD's), the FMVSS214 US side impact regulations only specify tolerance levels for two: the maximum lateral pelvis acceleration and the Thoracic Trauma Index (TTI(d)), see appendix A.1. The DoTSID is therefore equipped with sensors in the pelvis, spine and thorax that can register the signals required for the assessment of these two criteria.

Optional instrumentation can be fitted, for instance: head accelerometers for Head Injury Criterion (HIC) assessment. When evaluating the HIC, however, the dummy is usually equipped with the newer and more biofidelic HYBRID-III type neck and head. This upgraded ATD is generally referred to as the SID/HIII or FrankenSID. Table 2.1 specifies the DoTSID's default and optional sensor array.

Table 2.1: DoTSID Instrumentation

Instrumentation for compliance and certification testing	Optional instrumentation
Thoracic Uniaxial Accelerometer (Upper Rib)	Triaxial Accelerometer in the Head
Thoracic Uniaxial Accelerometer (Lower Rib)	Triaxial Accelerometer at T1
Thoracic Uniaxial Accelerometer (T12)	Triaxial Accelerometer at T12
Pelvic Uniaxial Accelerometer (Pelvis)	Six-Axis Lumbar Spine Load Cell Triaxial Accelerometer in the Pelvis

In FMVSS214 the tolerance level for the maximum lateral pelvic acceleration is specified at 130 g. For TTI(d) the limit is set at 85 g (4-door cars) and 90 g (2-door cars).

The effect of FMVSS214 crashworthiness assessment has been studied [52] by comparing vehicles performance prior and after the introduction of this safety standard, see table 2.2.

Table 2.2: Average TTI(d) in the FMVSS 214 test configuration

	2- Door Cars	4-Door Cars
FMVSS214 requirement	90	85
Model Year		
1981-90	110	80
1993 (just before FMVSS214)	97	74
1997 (post-FMVSS214)	74	65

From this table it could be concluded that American cars, nowadays, offer more occupant protection. However, since DoTSID lacks the ability to assess abdomen related injuries, some of this added thoracic safety was possibly gained at the expense of other body regions. In many US cars it can be observed that the armrest is positioned in such a manner that during side impact the abdomen is directly struck. This provision cushions the blow on the regulatory protected thorax and pelvis at the expense of the abdomen and the real overall occupant safety.

2.1.2 Biofidelity

Biofidelity issues of the hardware dummy are less relevant when developing a numerical model. Therefore DoTSID biofidelity issues are only briefly covered in this section.

There is a general consensus in the scientific community that improvements in the biofidelity and instrumentation capabilities of the US DoTSID dummy is needed [53][54]. In 1990, the International Standards Organization (ISO) Working Group on Anthropomorphic Test Devices, labeled the overall biofidelity of the DoTSID as *unacceptable* for side impact analysis [55]. The 1990 ISO ratings were based on a set of biofidelity requirements that did not account for muscle tone effects which are currently more widely accepted [54]. When these muscle tone effects are taken into account, the overall rating for the SID changes to a *marginal* classification.

2.1.3 Reproducibility and repeatability

While DoTSID biofidelity remains an issue, the DoTSID dummies are very humanlike in the sense of having variations in their components. For instance, the thickness of the PVC skin varies significantly from dummy to dummy. The thickness of the jacket varies by more than 50% depending on the manufacturer [44]. Furthermore, inhomogeneities can be observed in many foam materials as shown in figure 2.2.

Studies made in the past [56] have stated that the reproducibility of the DoTSID ATD is an area of concern with values of recorded signals varying up to 25 % for reproduced tests. Especially the thoracic signals are prone to large deviations whereas the pelvis area has a rather good reproducibility. These observations need to be taken into account when criteria for the accuracy of a numerical DoTSID model are set.

Test repeatability of the DoTSID was found to be adequate with a relative maximum error of 7% pertaining the sensor output between repeated tests [51].

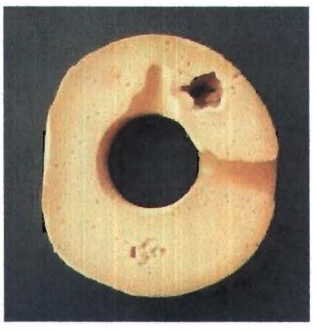
Slice of upper leg foam

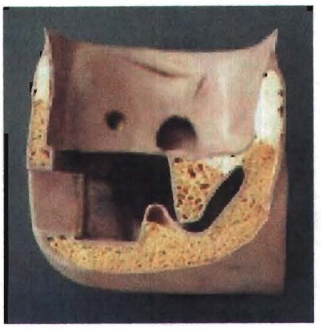
Cut through of pelvis

Figure 2.2: Inhomogeneities of foam parts.

2.2 DoTSID setup

This section will discuss DoTSID's hardware set-up in detail. For descriptive and modeling purposes the dummy is divided in several segments. Each part of the dummy that has a significant mass and a flexible connection with other parts is considered a segment. Dummy parts that do not show any relative motion are considered to be part of one segment.

Each segment is weighed and a segment local coordinate system in terms of physical points on that segment is chosen. The segments centre of gravity, expressed in the local coordinate system, is experimentally determined using a device called moment table-scale [57]. The principle moments of inertia and the transformation matrix that relates the principle moments of inertia to the segment local coordinate system have been determined using the STandard Automated Mass Properties (STAMP) procedure [57].

2.2.1 Lower torso

The lower torso assembly, depicted in figure 2.3, consists of a metal pelvis bone, metal femur stubs with retaining flanges for connection to the femurs, flesh simulating polyurethane foam, plasticized PolyVinylChloride (PVC) skin and an aluminium adaptor for connection to the lumbar spine. The axis denote the lower torso's local coordinate system.

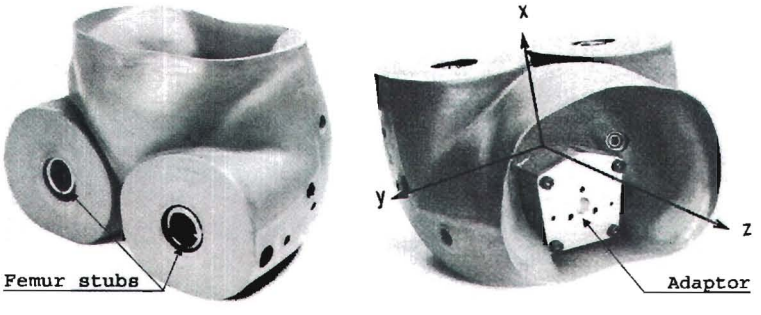

Figure 2.3: The US-DoTSID lower torso.

The lumbar adaptor has provisions for mounting x-, y- and z-directional accelerometers. Table 2.3 lists the inertia properties of this segment, excluding the contribution of the sensors.

Table 2.3: Inertia table for the US-DoTSID lower torso

Mass [kg]	13.845		
Centre of gravity [m]	x	y	z
	-0.0066	0.0000	0.0141
Principal moments of inertia [kgm^2]	I_{xx}	I_{yy}	I_{zz}
	0.1442	0.2059	0.2610

2.2.2 Abdominal insert

The abdominal insert, depicted in figure 2.4, consists of a polyurethane foam covered with PVC skin and has a mass of 1.455 kg. This component is not fixed to the DoTSID but is retained by the confining shape of the pelvis, jacket and rib cage assembly.

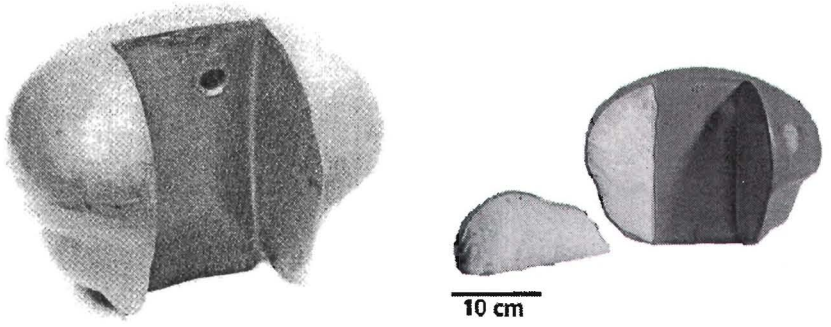

Figure 2.4: The US-DoTSID Abdominal Insert.

No information pertaining the center of gravity or moments of inertia are available for this component.

2.2.3 Lumbar spine

The lumbar spine, depicted in figure 2.5, connects the lower torso to the thoracic spine.

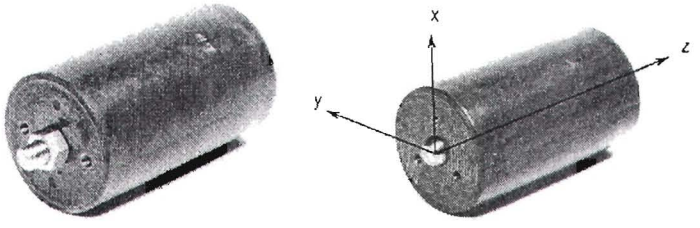

Figure 2.5: The US-DoTSID lumbar spine.

The spine is made of dense rubber (hyperlast) and a metal spine cable runs through the center line z-axes giving the spine the appropriate bending stiffness. Inertia properties are listed in table 2.4.

Table 2.4: Inertia table for the US-DoTSID lumbar spine

Mass [kg]	1.400 kg		
Centre of gravity [m]	x	y	z
	-0.0024	0.0000	0.0643
Principal moments of inertia [kgm^2]	I_{xx}	I_{yy}	I_{zz}
	0.0042	0.0040	0.0009

2.2.4 Upper torso assembly

The upper torso segment, depicted in figure 2.6, consist of a damper unit, shoulder foam and two subcomponents: the thoracic spine and the rib cage assembly. The rubber jacket and urethane arm foam are also a part of the upper torso segment.

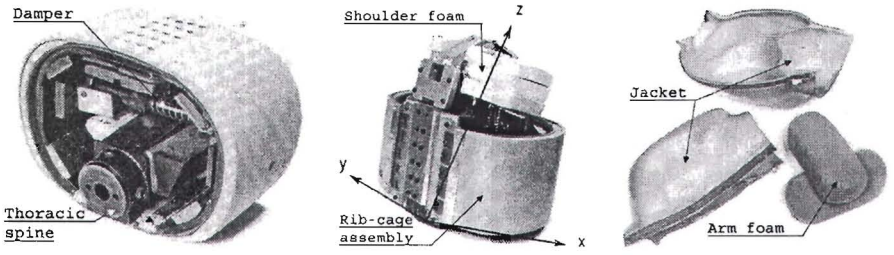

Figure 2.6: The US-DoTSID upper torso, containing the thoracic spine and rib cage assembly (left and middle) and the jacket and arm foam (right).

Given the relative complexity of this segment, the thoracic spine, rib cage assembly, jacket and arm foam will be discussed separately. Inertia properties of the complete segment are listed in table 2.5

Table 2.5: Inertia table for the US-DoTSID upper torso

Mass [kg]	29.600		
Centre of gravity [m]	x 0.0269	y 0.0000	z 0.1353
Principal moments of inertia [kgm^2]	I_{xx} 0.4271	I_{yy} 0.3435	I_{zz} 0.3512

Thoracic spine

The thoracic spine, depicted in figure 2.7, connects the lumbar spine to the neck and connects to the rib cage assembly via the damper (see figure 2.6).

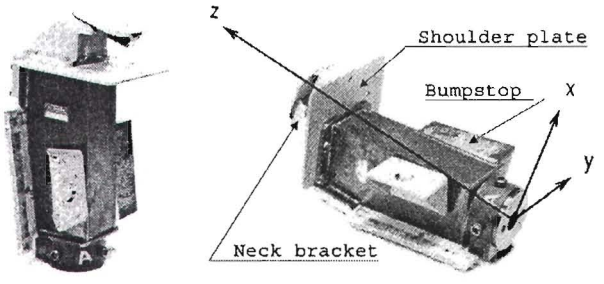

Figure 2.7: The US-DoTSID thoracic spine.

The spine is made of metal and has provisions to mount the rib cage damper unit and two accelerometers at 1^{st} and 12^{th} vertebrae height for assessment of the TTI injury criterion. The metal shoulder plate allows the fixture of the shoulder foam. The rubber bumpstop prevents damage to the rib cage due to excessive deformation. Inertia properties are listed in 2.6.

Table 2.6: Inertia table for the US-DoTSID thoracic spine

Mass [kg]	10.440		
Centre of gravity [m]	x -0.0291	y 0.0000	z 0.1455
Principal moments of inertia [kgm^2]	I_{xx} 0.0761	I_{yy} 0.0820	I_{zz} 0.0198

Rib cage assembly

The rib cage assembly, depicted in figure 2.8, is made of steel rib strips and steel rib ballast bars connected to the inside with rubber dampening cushions. The exterior of the steel rib strips is wrapped in four layers consisting of a dense, closed cell, urethane foam rib damping material, a plastic wrapping and finally, two

layers urethane foam rib padding. The left side rib ballast bar features a clevis that connects the damper unit (not shown) to the thoracic spine. The rib cage assembly is also connected to the thoracic spine by two leather strips allowing the assembly to hinge around the thoracic spine.

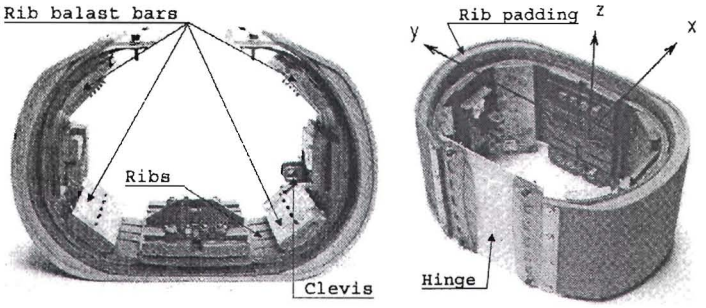

Figure 2.8: The US-DoTSID rib cage assembly.

Mounts for two accelerometers are placed at the upper and lower rib. The inertia properties are listed in table 2.7.

Table 2.7: Inertia table for the US-DoTSID rib cage assembly

Mass [kg]	12.530		
Centre of gravity [m]	x	y	z
	-.0808	0.0000	-.0027
Principal moments of inertia [kgm^2]	I_{xx}	I_{yy}	I_{zz}
	0.1479	0.0847	0.1799

Damper unit

The damper unit actually consists of a damper and a spring mounted in parallel. The unit connects the thoracic spine to the rib cage assembly, giving the ribs a more biofidelic dynamic behavior. This components mass equals 1.387 kg.

Jacket and arm foam

The rubber jacket weighs 5.375 kg and provides room for insertion of the arm foam and a shelf for retaining the abdomen (see figure 2.9). The arm foam is made of low density urethane foam and weighs 0.150 kg.

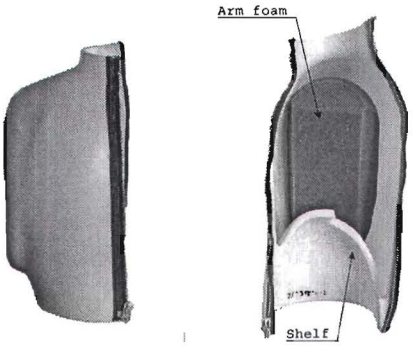

Figure 2.9: DoTSID jacket and arm foam.

The inner side of the jacket is lined with a fabric that provides a high resistance in tension.

2.2.5 Neck

The neck, depicted in figure 2.10, is a relatively simple segment made of hyperlast rubber and connects the thoracic spine to the head.

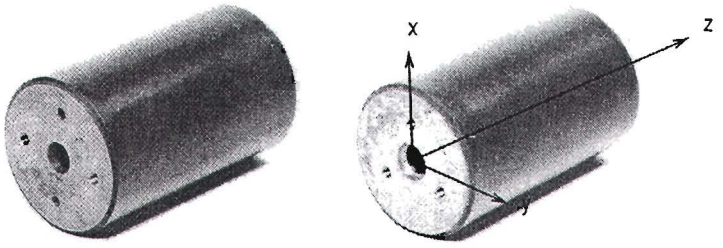

Figure 2.10: The US-DoTSID neck.

The inertia properties are listed in table 2.8.

Table 2.8: Inertia table for the US-DoTSID neck

Mass [kg]	0.870		
Centre of gravity [m]	x	y	z
	0.0000	0.0000	0.0606
Principal moments of inertia [kgm^2]	I_{xx}	I_{yy}	I_{zz}
	0.0020	0.0021	0.0006

2.2.6 Head

The head, depicted in figure 2.11, comprises a aluminium skull covered with PVC skin.

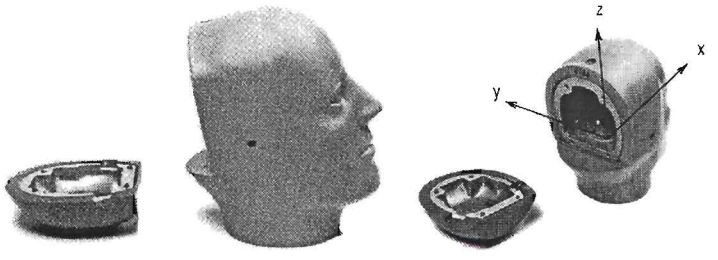

Figure 2.11: The US-DoTSID head.

The skull provides an accelerometer mount. The accelerometer is used for HIC injury criterion assessment. Inertia properties for this segment are listed in table 2.9.

Table 2.9: Inertia table for the US-DoTSID head

Mass [kg]	4.180		
Centre of gravity [m]	x	y	z
	0.0118	0.0000	0.0310
Principal moments of inertia [kgm^2]	I_{xx}	I_{yy}	I_{zz}
	0.0245	0.0294	0.0188

2.2.7 Upper leg assembly

The upper leg, depicted in figure 2.12, is attached to the pelvis via the retaining flanges and is, very unhumanlike, divided in two parts by a hinging joint allowing the post knee assembly to display a relative angle with respect to the femur. This design protects the DoTSID from damage when the hard knees make contact during impact.

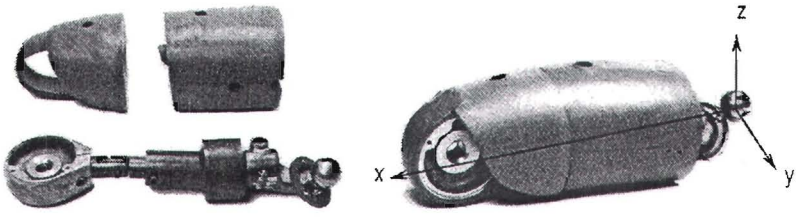

Figure 2.12: The US-DoTSID upper leg.

The "bones" are again made of steel, the flesh and skin are made of foam and PVC respectively. Inertia properties for this segment are listed in table 2.10. Note that the center of gravity y value is valid for the left upper leg, for the right upper leg the value is -0.0135.

Table 2.10: Inertia table for the US-DoTSID upper leg

Mass [kg]	9.550		
Centre of gravity [m]	x 0.2010	y 0.0135	z 0.0031
Principal moments of inertia [kgm^2]	I_{xx} 0.0125	I_{yy} 0.1355	I_{zz} 0.1383

Post knee assemblies

The post knee assembly, depicted in figure 2.13, connects the femurs to the tibia with a hinging joint.

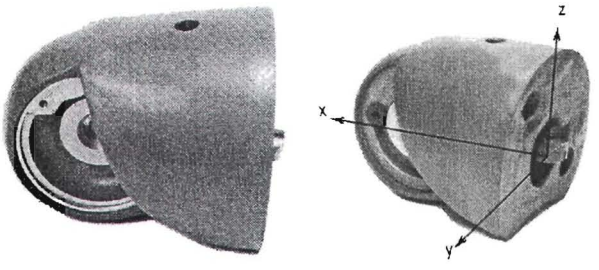

Figure 2.13: The US-DoTSID post knee assembly.

This assembly consist of steel (bones), urethane foam (flesh) and PVC (skin). The inertia properties are listed in table 2.11.

Table 2.11: Inertia table for the US-DoTSID post knee assembly

Mass [kg]	2.660		
Centre of gravity [m]	x 0.0573	y 0.0000	z 0.0137
Principal moments of inertia [kgm^2]	I_{xx} 0.0027	I_{yy} 0.0091	I_{zz} 0.0090

2.2.8 Tibia

The tibia or lower legs, depicted in figure 2.14, connect the post knee assembly to the feet with a hinging joint.

Figure 2.14: The US-DoTSID lower leg.

The materials used are steel and PVC and this segments inertia properties are listed in table 2.12.

Table 2.12: Inertia table for the US-DoTSID tibea

Mass [kg]	3.18		
Centre of gravity [m]	x	y	z
	0.0185	0.0000	-0.2056
Principal moments of inertia [kgm^2]	I_{xx}	I_{yy}	I_{zz}
	0.0661	0.0642	0.0027

2.2.9 Feet

Finally the feet, depicted in figure 2.15, are made of steel and covered with PVC skin

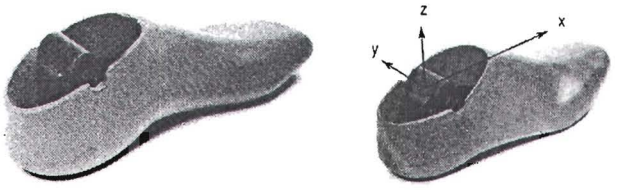

Figure 2.15: The DoTSID foot.

Usually for approval testing shoes are specified. This is primarily done to ensure a realistic friction between the feet and vehicle interior. The DoTSID numerical model will not include shoes as the proper friction can be directly applied to the contact. Inertia properties are listed in table 2.16.

Figure 2.16: Inertia table for the US-DoTSID foot

Mass [kg]	1.240		
Centre of gravity [m]	x	y	z
	0.0543	0.0000	-0.0461
Principal moments of inertia [kgm^2]	I_{xx}	I_{yy}	I_{zz}
	0.0009	0.0057	0.0055

Chapter 3

Modeling of the US-DoTSID

The hybrid multibody-FEM US-DoTSID, as depicted in figure 3.1, has been developed in the MADYMO code (version 5.5 developers release).

MADYMO stands for: MAthematical DYnamic MOdel and is a computer software package that can be used to simulate crash situations and assess injuries sustained by victims. MADYMO allows for modeling based on multibody (MB) and finite element (FE) techniques. Also, the code allows for combining these techniques into one model. The MADYMO solver will be discussed in appendix B. Additional information pertaining this numerical solver can be found in [58] and [32].

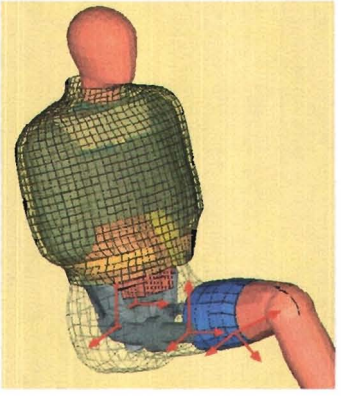

Figure 3.1: Hybrid multibody-FE DoTSID.

3.1 Methodology of model development

Developing and validating any numerical model for such a complex system as a crash test dummy is a lengthy process. This process consist of: the modeling, assembly of test series, model calibration and, finally, the model validation.

3.1.1 Modeling approach

When modeling the components of the SID as described in section 3.3, it became apparent that some of the components where especially suited to be modeled using the MB technique while other components would benefit from a FE approach. Recognizing the strengths (and weaknesses) of both MB and FE modeling techniques an attractive solution would be to combine both modeling approaches in one model. The hybrid US-DoTSID model is based on a skeleton frame of TNO's multibody DoTSID model and the geometry of NHTSA's FE model (figure 3.2). Both these models are discussed in the appendix C.

Key geometry values of the FEM were compared to actual measurements performed on a DoTSID and to measurements on file. Corrections to the mesh were made were it was deemed necessary. These corrections entail either the complete re-meshing of a component (jacket, shoulder foam, thorax to lumbar adaptor) or a simple scaling of the existing components mesh (arm foam, spine box, bump stop and abdomen). Also some

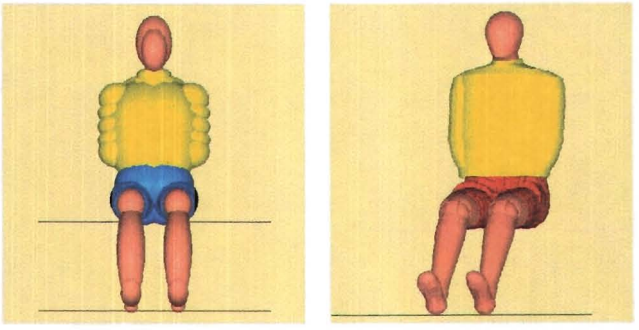

Figure 3.2: TNO's Multibody DoTSID model (left) and NHTSA's FEM DOTSID model.

doubt exists about the validity of the iliac wing width and height in the FEM geometry, upon inspection these wings appear to be larger than modeled. However, since the actual shape could not be accurately determined, the model is not updated.

Furthermore, the reference position of the model was compared to that of the physical dummy, resulting in a rotation of the upper torso 5^0 backward around the "thorax to lumbar adaptor" joint-axis in the model.

Key multibody parts of the model are: neck, damper and spine joint properties which are already validated components. Whereas in the multibody model the contact surfaces of these parts are represented by ellipsoids in the hybrid version the geometry of these components can be accurately captured by implementation of FE NULL-material. In MADYMO, this special material type gives a geometry the properties of being rigid and having no mass. When such a geometry is combined with a rigid body with specified mass properties, the result is a very cpu efficient representation that supersedes traditional ellipsoid-based multibody modeling in terms of geometrical accuracy.

Non-deforming and less crucial parts of the DoTSID model such as the steel bone structure, tibia and feet are modeled as rigid bodies combined with FE NULL-material with the advantage of stability and computational efficiency. The linked DoTSID multibody model, together with the bony structure comprises the *"skeleton"* of the FE DoTSID model (see section: 3.2.1). Apart from cpu and development efficiency this hybrid modeling approach yields following advantages:

- User-friendly positioning through MB joints
- Multibody sensor definition
- Allows for the implementation of FE NULL-material
- Crucial deforming parts, such as foams, skin, jacket and rib cage can be modeled using the FEM technique
- Complex joint-like interfaces, such as neck, lumbar spine and rib damper can be more conveniently modeled the using MB technique

Also, the presence of a rigid body in a FE component allows for a very precise control over the components mass properties. Using traditional FE techniques, the mass properties of a certain component (mass, center of gravity, moments of inertia) are derived from the geometry of the mesh and the specified material density. Thus, for a component to have accurate mass properties, the mesh needs to be very detailed. When using the hybrid modeling technique, however, any given component can be attributed the experimentally determined mass properties without the need of mesh refinement. This feature is extremely helpful when optimizing the model for cpu efficiency.

3.1.2 Acquisition of experimental data

A single test validation of any model may be misleading, since it is quite possible that the model parameters may be valid for only that test. As a result, calibration and validation should be conducted over various configurations and test severities covering the range of expected loading conditions in the expected application range for that model. Furthermore tests should be preferably performed at least twice to monitor repeatability. Test reproducibility is also an issue since results may vary due to the test operator, test site and dummy differences. Therefore, validation of models may require many tests to determine the quality of test results.

Assuming that repeatability and reproducibility of the test results are not in question, the best that any model can predict is within the known variability of these test results.

The total collection of tests that is used in calibrating and validating a numerical model is called the *test matrix*.

The test matrix should include tests on several levels:

1. Material level, in order to calibrate and validate the constitutive material models and parameters
2. Component level and assembled component level, in order to calibrate and validate material and component interaction
3. Complete dummy level, in order to calibrate and validate the model's assembled component interaction

Even though TNO has developed a multibody DoTSID model, it does not have access to a conclusive pool of material test data on the DoTSID. For the development of the multibody model this was not considered to be an issue, since multibody models not rely on accurate material models, as most of the material characteristics are lumped in a MB approach. The omissions of test data for certain materials, however, can well influence the attainable quality of a finite element model. The following sections will discuss the available data.

Material data

Some of the materials that are used in the DoTSID, such as the skin, have been evaluated in the past and material models in MADYMO are available. For other materials, such as the rib damping cushions, it was rather straightforward to implement experimental data obtained in previous experiments [59] into the appropriate MADYMO material model.

Many of MADYMO foam material models that were developed in the past [62], however, were validated under quasi static conditions or relatively low impact velocities. These velocities are hardly high enough to consider possible foam strain-rate dependency. Moreover, during validation, all of these foam material models are given a density of 1000 kg/m^3, for numerical efficiency reasons. For comparison: the real density of the considered foam materials ranges between 64 kg/m^{3}and 350 kg/m^3. While this is acceptable for these types of quasi-static simulations it makes the implementation into a dummy model impossible. Therefore, available experimental curves [61][60][62] pertaining foam materials were translated into MADYMO foam material parameters using a simplex optimization routine [63]. For a brief description of this approach, see appendix B.3.

Component data

The behavior of open cell foams depends on the outflow of air. Hence, the geometry of a specimen can influence its behavior. A small foam specimen, typically used in material testing, can therefore behave different than a larger piece of foam, especially under higher impact conditions. This observation holds even more true for an enclosed foam, such as the abdomen where the open cell foam is sealed airtight by the PVC skin. The resulting component behaves quite stiffer than the sum of its components. These phenomenons make component testing indispensable when calibrating the SID model.

Some components are pre-stressed. An example would be the lumbar spine. The lumbar spine consist of a rubber cylinder that is compressed by a steel cable. Depending on the load condition this segment will display a superposition of shear, bending, torsion tension and compression. While material data can be obtained for the rubber cylinder and the steel cable separately, it appeared very hard to capture the non-linear bending behavior and the different stiffness in tension and compression of the ensemble. Therefore, the material properties of this component were determined purely on the basis of literature and adjusted using component tests on the lumbar spine.

The modeling of multi-layered materials also proved difficult. One example is the jacket of the US-DoTSID, consisting of a thick rubber with a fabric lining. The fabric provides high resistance in tension, while in compression the rubber is predominant. In bending, the fabric determines the neutral fiber. Another example of a multi-layered material is the rib cage hinge, consisting of several layers of fabric embedded in an elastic rubber material. The hinge connects the ends of the steel ribs with the thoracic spine. Hence, it significantly contributes to the overall stiffness of the rib cage. The material properties of this component had to be determined purely on the basis of literature and adjusted using component tests on assembled thorax level.

Complete dummy data

This level needs to include tests that approximate the intended application area. This approximation to reality, however, does have its practical limits since every added complexity can make a test less suitable for model calibration.

For instance: the DoTSID numerical model needs to be suited for FMVSS214 analysis. This standard test describes a moving deforming barrier hitting a stationary vehicle with a DoTSID as occupant. A full scale simulation of vehicle, barrier and occupant interaction is not suited for model calibration because of its complexity and repeatability related issues. Also deficiencies in either vehicle or barrier model cannot readily be discerned from DoTSID model issues. An approximation would be to simulate DoTSID's interaction with sled test data (see appendix D) using a deforming barrier. But even this simplification introduces uncertainties to the model and puts high demands on the validity of the barrier model itself before these types of tests can be used for model calibration. Finally, rigid barriers are well suited to use in model calibration, since their structural behavior is straightforward to capture in a virtual environment. Naturally, the drawback is that these types of tests are relatively far from reality and can, therefore, limit the useful range of the models application. Appendix D discusses some of the available methods for acquiring suitable test data for side impact model validation.

Setting aside the aforementioned considerations, these full dummy tests often bring forward new phenomena mainly caused by component interaction. Hence, the proper modeling of contact interactions becomes a high priority in this stage. For some soft foam parts the correct modeling of the contact stiffness, allowing almost no nodal-penetration, caused difficulties for the numerical stability. This is a result of the high deformation (resulting in high stresses) as these foams frequently get squeezed between different interior part of the dummy. Particularly the arm foam needed additional consideration with respect to the contact stiffness. Interestingly the hardware dummy often exhibits damage after testing in these parts, indicating that in reality this component exhibits large deformations and stresses in impact conditions.

The significant advantage of deriving test data from more appropriate loading conditions as is the case in these full dummy tests might raise the question whether material and component tests would be dispensable. However, within simulations pertaining the fully assembled dummy model it is very difficult to identify the entities needed to modify the model correctly, as the results are determined by many factors affecting each other. In fact, complex model calibration can be seen as a nonlinear estimation problem. Material and (assembled) component tests provide a good starting point for the estimation process. For the dummy development this implies that the model must already have a certain quality before the model can be enhanced with data from fully assembled dummy test data.

3.1.3 Calibration and validation

Calibration is a process of tuning model response to approximate experimental response. Validation is an assessment of the quality of the calibration. This section addresses some of the issues concerned with the calibration and validation of the DoTSID model.

Iterative calibration procedure and validation

Intuitively, model calibration would start at the lowest (material) level and then progress from (assembled) components to full dummy level, thus gradually adding to the model's complexity while eliminating uncertainties. Experience, however, has showed that calibration for complex models cannot be achieved using a pure linear process. Suitable test data may not be available on all levels and an assembly of validated material and/or component models does not automatically result in a good response for the assembly. The later phenomenon can largely be attributed to component interactions that cannot be captured during isolated component tests. Also, often, assembled component tests are performed using higher (and more crash realistic) loading conditions that were not addressed during material and component testing.

To warrant good correlation on all levels, an iterative validation approach, as illustrated in figure 3.3, is proposed.

This approach is perhaps best illustrated by an example such as the thorax. The thorax of the US-DoTSID is an assembly of three main components (see Section 2.2): the rib cage, the thoracic spine and a damper unit. These components are made of various materials such as: metal, foam, rubber, etcetera. First the materials are modeled using values derived from literature and, when available, validated versus material test data (level I). These materials are then used to model the thoracic spine and the rib cage. The damper unit is separately modeled and validated on a component level (level II). These components are combined and validated using

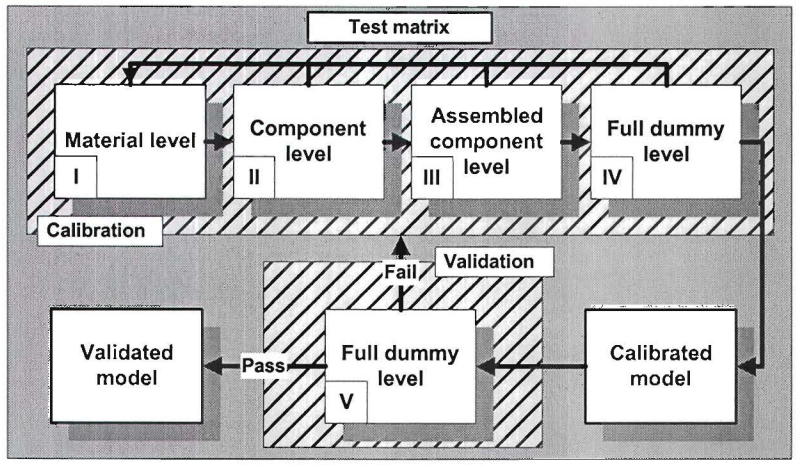

Figure 3.3: Proposed iterative validation approach.

test data on an assembled component level (level III). Information, derived in stages I and II, on the quality of the material and component models used in this assembly can help model calibration in level III. If as a result of level III calibration, material or component properties are changed, these entities must be reevaluated on their respective levels. When no conclusive test data on these materials of components is available, these entities can only be calibrated against data on the current level of assembly.

Assuming the completed thorax model is calibrated to satisfaction, the process continues to stage IV where the assembled components interactions are calibrated on a fully assembled dummy level using the same iterative mechanism.

Finally, when calibration is at a satisfactory level the model is validated against test data not used in the calibration process (stage V). When the model shows unacceptable insufficiencies in these tests, it could be assumed that the initial calibration tests do not properly cover the models intended application area. The additional tests should then be included in the calibration procedure. When model response is satisfactory, the validation process ends.

Validation priorities

The distinction between crucial and non-crucial dummy parts is primarily made on the basis of the influence of that part on the dummies response. When validating the DoTSID model response, emphasis is placed on good model-to-experimental correlation for the signals that are used in the regulatory specified TTI and pelvis acceleration injury criteria. These signals are:

- Lower spine (T12) acceleration
- Upper and lower rib acceleration
- Pelvis acceleration

The head acceleration may seem important as it is needed for the calculation of HIC, but HIC is not a required injury criterion for the DoTSID and, therefore, has no immediate priority. However, replacing the hardware's DoTSID head and neck with a HYBRID-III test dummy head and neck results in the SID/HIII dummy that is used for assessing HIC. Keeping in mind the future development of the SID/HIII model based on the DoTSID model, the top spine (T1) acceleration will also be assessed.

Since these injury criteria are based on maximum values of measured signals, the emphasis of the validation process lies in the accurate prediction of the regarded signals during that time interval where the highest peak occurs.

3.2 Multibody and NULL-material parts

Certain parts of the dummy were modeled as non-deforming material using multibody techniques combined with FE NULL-material. This section briefly covers the set-up of these parts, section 3.3 will describe the complete model set-up.

3.2.1 The "rigid skeleton"

The skeleton frame of the FEM dummy consist of a multibody system chain derived from the multibody DoTSID model. In this particular chain each dummy segment is represented by a *shapeless* body, with certain inertia properties. These segments are linked together to form a tree-like chain. The links between these bodies all represent a certain joint in the dummy, like ankle, knee, hip, etc. The system linkage in figure 3.4a comprises all the joints, including joint properties such as joint stiffness and range of motion, and sensors of the multibody DoTSID model. The coordinate systems in this figure are body fixed and denote the locations of the joints. FEM structures can now be supported to this linkage, allowing the user to position the dummy by rotating the joints.

Structures that are deemed non-deforming, such as pelvis bone, femur bones, femur stubs, head to neck adaptor and spine box are modeled as NULL-material that is supported to the multibody system chain. Figure 3.4b illustrates this set-up.

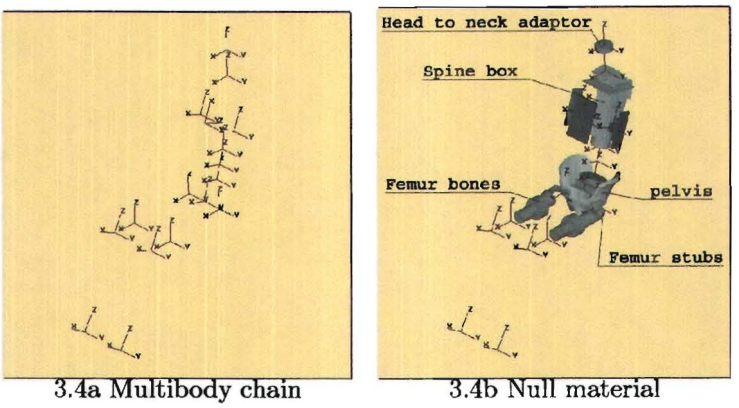

3.4a Multibody chain 3.4b Null material

Figure 3.4: The DoTSID skeleton.

As stated before, NULL-material is a non-deforming and massless material. Because these structures have no mass in the simulation, their real mass contribution is added to the supporting multibody.

3.2.2 Spine, neck and damper

The lumbar spine, neck and thorax-damper, depicted in blue in figure 3.5, are modeled using NULL-material shell elements that are supported to the corresponding rigid bodies from the multibody chain.

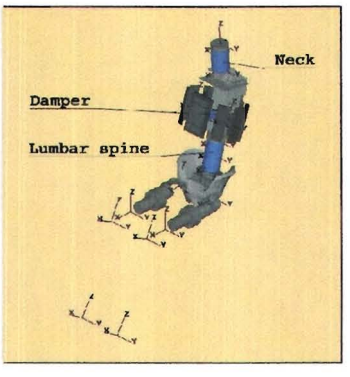

Figure 3.5: Spine, neck and damper.

Kinematic properties of these components are derived directly from the multibody DoTSID model. This implies that any deformation of these components is governed solely by the relative motion of the joints. This relative motion itself is defined through the joint degree(s) of freedom and the attributed stiffness and/or damping function(s). Section 3.3 describes the set-up of the spine, neck and damper unit.

3.2.3 Tibia, postknee's and head

Parts of the dummy that are considered to be non-critical for signal correlation are presently modeled using rigid bodies combined with FE `NULL`-material geometries for cpu efficiency and numerical stability.

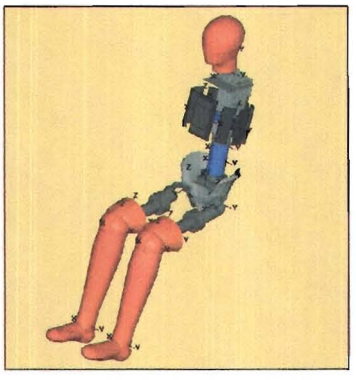

Figure 3.6: Tibea, postknee's and head.

These structures include the feet, tibia, postknee's and the head[1], shown in orange in figure 3.6. The contact compliance of these components is accounted for in pre-defined contact functions.

3.3 DoTSID model set-up

This section describes the assembly the hybrid MB/FE DoTSID model. For reasons of clarity, specific MADYMO keywords are in `typewriter` font and descriptions can be found in [32] and appendix B. A description of the material models can be found in appendix B.2.2. Appendix F summarizes this chapter and lists the exact material parameters used in the DoTSID model.

3.3.1 Lower torso

The lower torso, as specified in 2.2.1, includes three rigid bodies in the numerical model, one for the pelvis and one for each upper leg. The coordinate systems in figure 3.7 depict the local body coordinate systems of these bodies. The origins of these systems coincide with the joint locations of the hip joints and the pelvis. The joint properties, such as stiffness, that govern the rotation of the hip joints are derived from the DoTSID multibody model.

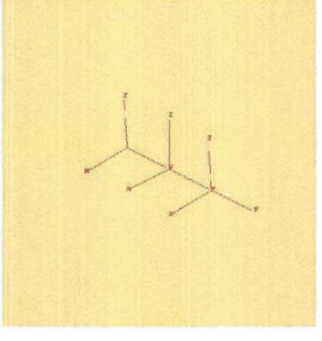

Figure 3.7: Pelvis and hip multibodies.

The steel femur stubs, see figure 3.8, are considered non-deforming and are modeled with FE `NULL`-material. The stubs are supported to the femur bodies and will rotate with these joints.

[1] Note that while the head is vital for HIC assessement, HIC is not a injury criterion for DoTSID.

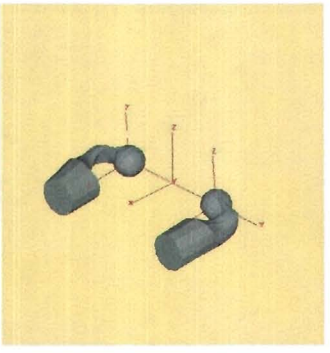

Figure 3.8: Femur stubs steel bones.

In order to compensate for the loss of mass, the mass contribution of these bones needs to be added to the femur bodies. The exact contribution in term of mass, center of mass and moments of inertia, however, has not been measured for these stubs. To derive accurate estimates of these quantities the following steps are taken. First, the upper femur are weighed and modeled in a mass supporting material type. The correct density can now be attributed to these structures. Subsequently a MADYMO simulation for the model in figure 3.8 is initiated. Standard output for a MADYMO run provides the inertia properties for all FE and MB systems with respect to their local body coordinate system. Finally these properties are added to the femur bodies and the upper femur bones are now reverted to `NULL`-material.

Both the pelvis steel pelvis bone and the aluminium pelvis to lumbar spine adaptor (figure 3.9) are considered rigid structures and are therefore modeled as NULL-material supported to the pelvis body.

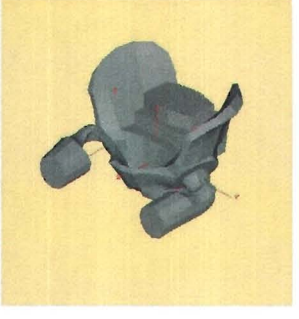

Figure 3.9: Pelvis bone and lumbar adaptor.

The pelvis foam is modeled using the `FOAM` material using `SOLID` mesh, see figure 3.10a. Experimental loading and unloading curves for different strain-rates were found in previous research [62] and this data is implemented in the pelvis foam material model. The PVC skin is modeled with a `SHELL` layer of `ISOLIN` material and shares the outer nodes of the pelvis foam, see figure 3.10b. Nodes of the skin that are adjacent to the pelvis bone are supported to the pelvis body. For the DoTSID skin, a satisfactory MADYMO material model has already been developed [62] and is therefore implemented in the DoTSID model.

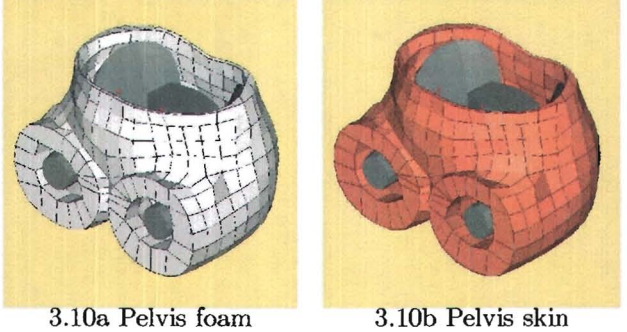

3.10a Pelvis foam 3.10b Pelvis skin

Figure 3.10: The completed pelvis model.

With all the components for the lower torso segment in place another MADYMO run is initiated. The inertia results are compared to those found in table 2.3. Discrepancies, that can mainly be attributed to the zero mass pelvis bone and adaptor, are compensated for in the pelvis body.

The inertia compensation procedure allows for a very accurate control over the models inertia. All the global mass related properties for this segment, as listed in table 2.3, are modeled accurately up to 3 digits. This is considered a big advantage over traditional FE modeling where the inertia properties are derived from geometry and density. Ensuring accurate inertia properties using FE modeling, one is forced to mesh every part in great detail, leading to cpu inefficient models. In traditional FE models, such as the FAT FE DoTSID model [44], mass discrepancies are compensated by adjusting the density of the heaviest dummy part in the dummy model. While this precaution does correct the total body mass for the model, it does not correct for the centre of mass nor the moments of inertia. Moreover, the global nature of this technique does not take into account the influence of local mass contributions. Furthermore, it is not known how this tuning of a certain density effects the models validity.

Note that inertia properties for rigid bodies are fixed throughout a simulations duration. The concern that centre of mass of a certain segment may not be a constant when deformation come into play, is not valid in this situation, because only the non-deforming structure's inertial properties are compensated in the rigid bodies.

3.3.2 Abdominal insert

The abdominal insert, shown in figure 3.11, is modeled as a `FOAM` material. Because the insert can undergo large deformations the skin is modeled as a `MEM` (membrane) layer of `ISOLIN` material. Membranes have no bending stiffness as opposed to `SHELL` layers. These membranes share their nodes with the outer foam. The abdomen is not supported to any other dummy part.

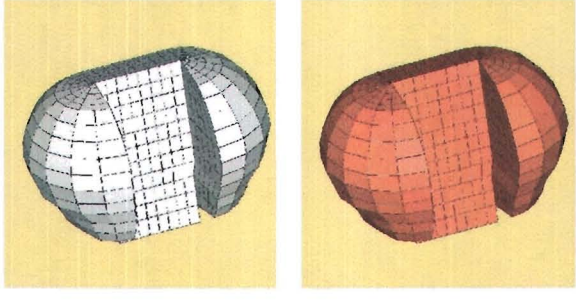

Figure 3.11: Abdominal insert.

The mass of the numerical abdominal insert corresponds with the hardware equivalent and is 1.455 kg. The exact foam properties are not known, so as a starting point the pelvis foam properties are used.

3.3.3 Lumbar spine

The spine consist of a rubber (hyperlast) cylinder that is compressed by a steel cable. Experimental data for this component is available for static testing only [57]. In dynamic loading conditions the spine could potentially display a stiffer performance then can be deduced from static testing due to mass and damping effects. The static tests showed that: depending on the load condition this segment will display a superposition of shear, bending, torsion tension and compression.

While material data can be obtained for the cylinder and the cable, it appeared very hard to capture the non-linear bending behavior and the different stiffness in tension and compression of the ensemble by using FE modeling techniques. This finding is supported by literature [45].

In the existing multibody DoTSID model though, this components global behavior was captured by applying the aforementioned experimentally derived stiffness functions. The lumbar spine of the hybrid MB/FE DoTSID model was therefore derived from the multibody model. Figure 3.12 shows the model of the lumbar spine consisting of rigid bodies.

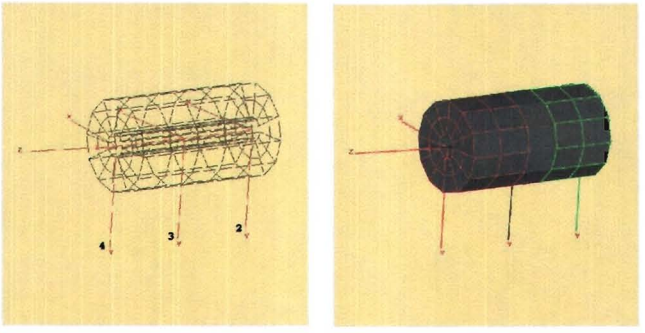

Figure 3.12: Lumbar spine.

The two joints positioned at locations 2 and 4 are LOCKED with respect to the pelvis and thoracic spine respectively. Joint 3 is a FREE JOINT where displacements and rotations are resisted by forces and moments. Any flexible connection between two rigid bodies has six degrees of freedom: three rotations and three translations. The corresponding resisting forces and moments are described in a SIXDOF RESTRAINT, that has been attributed the experimentally derived stiffness functions for bending, shear, torsion, tension and compression as well as interactions between the degrees of freedom.

The geometry of the spine is modeled using NULL-material where the lower part of the nodes (green) is supported to the pelvis and the upper part (red) to the thoracic spine. Bodies 2 and 3 are both assigned half the total mass contribution of this segment. The offset of these masses with respect to their body local coordinate systems is such that the total centre of mass for this component coincides with joint location 3. Contact with other geometries is based on a penalty function that applies a contact force based on penetration.

The elongation stiffness contribution of spine cable is modeled with a KELVIN ELEMENT connecting joint 2 and 4.

The exact parameters that are used in this lumbar spine model can be found in [64], but are considered to be confidential.

3.3.4 Upper torso assembly

The most complex of DoTSID segments is undoubtedly the upper torso assembly. This section will discuss the damper unit, thoracic spine, rib cage assembly, anti-sag device and the jacket with arm foam.

Damper unit

The damper unit includes two rigid bodies that are interconnected by means of a KELVIN-ELEMENT, see figure 3.13a. The dynamic behavior of this element has been calibrated to correlate with damper component tests (see Table 4.1) and includes nonlinear stiffness and damping [65].

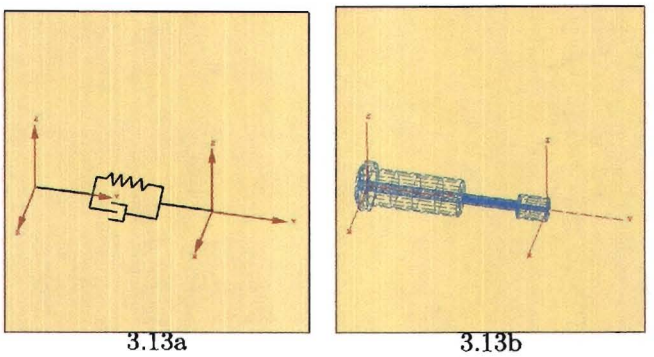

3.13a 3.13b

Figure 3.13: Thoracic damper unit.

The geometry of the damper unit, depicted in figure 3.13b, has been modeled using FE NULL-material. Both rigid bodies support half of the geometry, allowing the damper to compress and extend.

The mass distribution of this component needed no updating with respect to the multibody DoTSID model from which it is derived, since only NULL-material has been added.

Thoracic spine

This segment includes the sterno-thoracic spine, bumpstop, neck bracket and shoulder plate. The bulk of the thoracic spine model, depicted in 3.14, is generated using NULL-material SHELL elements and one multibody. Only the rubber bumpstop, depicted in black, is modeled using MOONEY-RIVLIN solid elements. The material properties were derived from literature [59]. Using similar inertia compensation techniques as explained in subsection 3.3.1, the supporting rigid body is given the correct mass attributes to provide this segment the same inertia properties as listed in table 2.6.

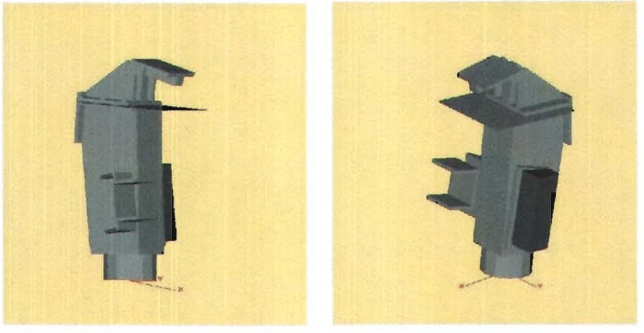

Figure 3.14: Thoracic spine.

After measurements performed on a DoTSID crash dummy and review of documentation [49], the geometry of the bumpstop and shoulder plate was corrected in order to better represent the reality. For the same reason, the complete thoracic spine, including the rigid body chain, was rotated 5^0 degrees backwards.

Rib cage assembly

The rib cage assembly consists of two rigid bodies. These bodies connect the clevis to the damper and the sternum plate to the anti-sag device. The clevis and sternum plate, depicted in figure 3.15, are supported to these bodies and modeled using FE NULL-material.

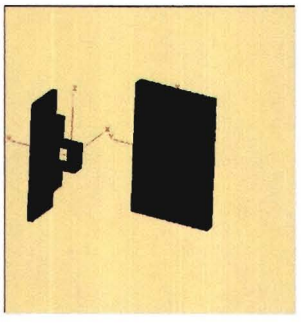

Figure 3.15: Left ribbalast bar, clevis and sternum plate.

Figure 3.16a shows the addition of the rib steel strips (light gray), the rubber rib ballast bar damping cushions (red) and the metal ballast bars (dark gray).

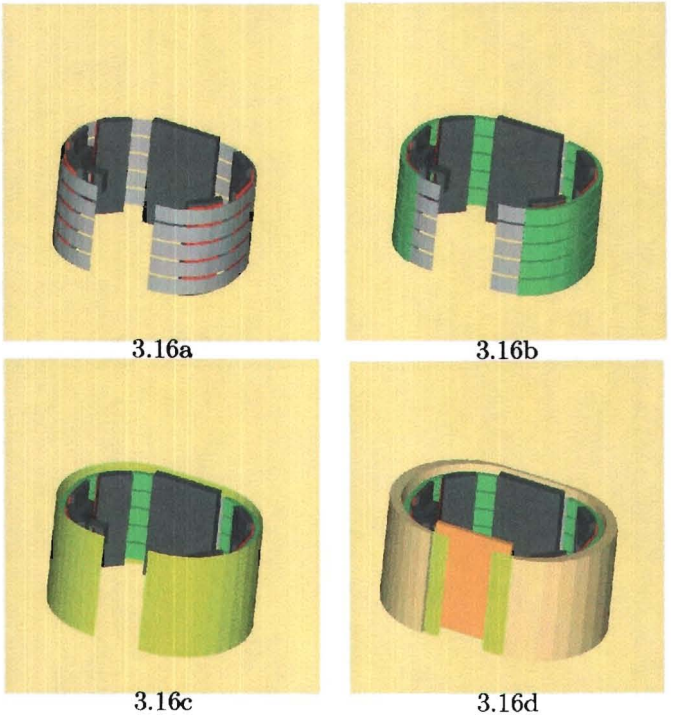

Figure 3.16: Build up of the ribcage assembly with a) the rib steel strips, rib ballast bars and dampening cushions. b) Rib damping material. c) Rib wrap and d) Rib padding and hinge.

The rib steel strips are modeled using `ISOLIN` shell elements, the rib ballast dampening cushions are modeled in `MOONEY-RIVLIN` solids. Both materials properties are derived from literature [59]. The rib ballast bars are `ISOLIN` solids but as they are considered to be non-deforming they are made `RIGID` at the start of the simulation. The advantage of `RIGID ISOLIN` over `NULL`-material is that all mass properties in the former method are retained, while the solver treats the two entities almost equally efficient. The clevis and sternum plate are not modeled in RIGID ISOLIN because MADYMO does not allow `RIGID` material to be supported.

The rib damping material, shown in figure 3.16b, is modeled as a solid mesh of `ISOLIN` material that includes damping. Material values are derived from literature [63]. The plastic rib wrap sheet (figure 3.16c) is modeled as `ISOLIN` shell elements. Finally the leather hinge (orange in 3.16d) and the rib padding are modeled in `ISOLIN` and `FOAM` respectively. No conclusive literature or test data was available for both these structures and their, initial, material parameters are therefore deduced from the LS-Dyna model [47].

Using the inertia compensation method, the rigid bodies mass properties are adjusted to satisfy the values as listed in table 2.7.

Thorax assembly

Figure 3.17a shows how the thoracic spine is attached to the rib cage assembly by fastening the hinge to the spine using the hinge mount block (light gray). Figure 3.17b shows the insertion of the damper unit (blue) extending from the clevis multibody to the thoracic spine damper retainer block.

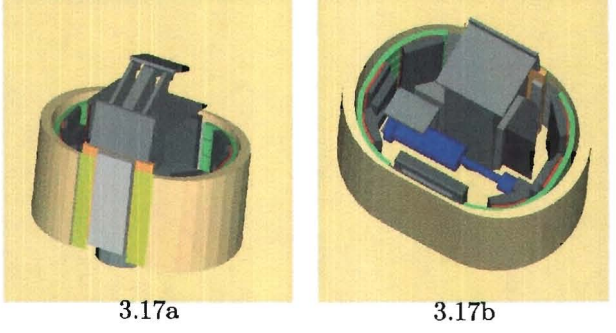

Figure 3.17: Connecting a) the thoracic spine assembly and b) the damper unit.

Finally, the shoulder foam is added (see figure 3.18). The shoulder foam has been completely remodeled because measurements indicated that the original mesh did not satisfy geometric requirements. The material properties of the shoulder foam are derived from the LS-Dyna model.

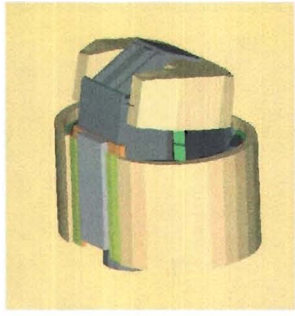

Figure 3.18: The completed thorax assembly.

The jacket and arm foam are added and subsequently, the completed upper torso components inertial properties can be compared to table 2.5. The mass is modeled correctly and the centre of mass and moments of inertia are modeled within a 3 % error margin. These small deviations can be attributed to the additions of especially the jacket and to a lesser extent the arm foam, damper unit and shoulder foam.

Anti-sag device

The anti-sag device is a small spring attached to the shoulder plate and sternum. It prevents the rib cage from sagging when the dummy is placed in upright position. A `KELVIN ELEMENT` with an experimentally derived loading curve is used to model this spring. This curve is derived from the multibody DoTSID model [33].

Jacket and arm foam

The original jacket mesh from the LS-Dyna model was very coarse and did not include the shelf geometry. Since the jacket was thought to have an important effect on the dummy response this mesh was completely remodeled in a rather early stage of the model development. Using a FARO 3D measuring instrument [65] an approximation of the outer jacket geometry is obtained.

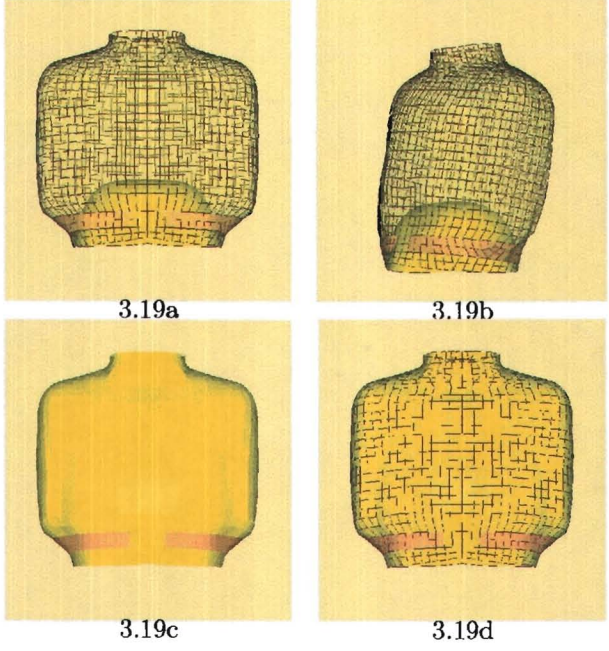

Figure 3.19: Build-up of the jacket geometry. a) and b) the outer jacket in wireframe, the shelf in solid yellow and the brigde in solid orange c) Jacket mesh in single layer ISOLIN shells d) Jacket mesh in dual layered shells (one ISOLIN and one ISOTEN).

The mesh for the shelf consist of two parts, first the shelf itself (solid yellow in fig. 3.19a and b) and secondly, the bridge (in orange) that connects the shelf with the interior of the jacket. In reality the jacket has a variable thickness, that cannot be measured using FARO measurements. In this model an average jacket thickness is applied to the entire collection of jacket shells (yellow in figure 3.19c).

In a later stage of the design the fabric lining of the jacket was also modeled giving the jacket more stiffness in tension. A second layer of shell elements with `ISOTEN` material properties was used to achieve this. `ISOTEN` is a material model that is frequently used to model fabrics since it supports linear isotropic material behavior in tension only and discards negative principal stresses. Since no relative motion between these layers can occur, this layer shares the nodes of the original shell `ISOLIN` mesh. Figure 3.19d shows the final jacket mesh.

3.3.5 Neck

Since the neck and lumbar spine are similar in design, the methodology used in modeling is identical. The joint parameters are derived form the multibody DoTSID model.

3.3.6 Head

The head is modeled using `NULL`-material shells and a multibody. The coordinate system frame in figure 3.20a designates the body local coordinate system for the head. This rigid body is attributed the measured mass properties as listed in 2.9.

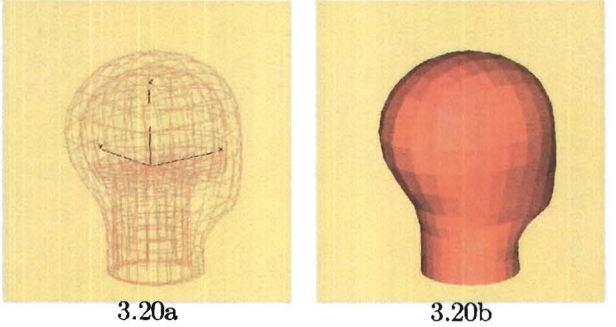

3.20a 3.20b

Figure 3.20: The DoTSID head.

Subsequently, a mesh of `NULL`-material is supported to this body, figure 3.20b. The head compliance is taken into account in the contact function.

3.3.7 Upper leg assembly

The upper leg assembly consists of two rigid bodies. The coordinate system frame in figure 3.21a designate the right upper leg and right post knee bodies.

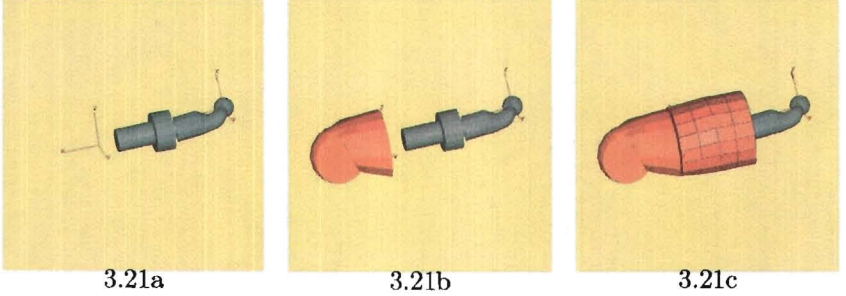

3.21a 3.21b 3.21c

Figure 3.21: Upper leg assembly.

The femur stubs were already discussed in section 3.3.1. Figure 3.21a also displays the upper femur bones. This geometry is modeled in NULL-material and supported to the upper leg rigid body. Subsequently, the post knee, added in figure 3.21b, is modeled in `NULL`-material, using the post knee body and the inertia information provided by table 2.11. The upper leg flesh, shown in figure 3.21c, is modeled with `FOAM` solids and the

skin using ISOLIN shells. The material properties are derived from literature [47]. Using the same approach explained in section 3.3.1 the upper femur bones contribution to the upper leg is estimated and added to the upper leg body.

The left upper leg assembly is modeled in a similar fashion.

3.3.8 Tibia

The tibiae are modeled using NULL-material shells and a rigid body. The coordinate system frame in figure 3.22a designates the body local coordinate system for the left tibia. This rigid body is attributed the measured mass properties as listed in 2.12.

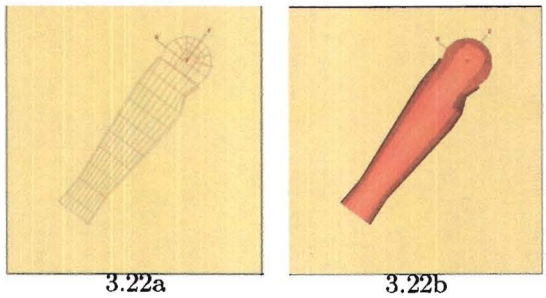

3.22a 3.22b

Figure 3.22: DoTSID tibea.

Subsequently a mesh of NULL-material is supported to this body, figure 3.22b. The tibia compliance is taken into account in the contact function. Naturally, the right tibia is modeled in a similar fashion.

3.3.9 Feet

The feet are modeled using NULL-material shells and a rigid body. The coordinate system frame in figure 3.23a designates the body local coordinate system for the left foot. This rigid body is attributed the measured mass properties as listed in Table 2.16.

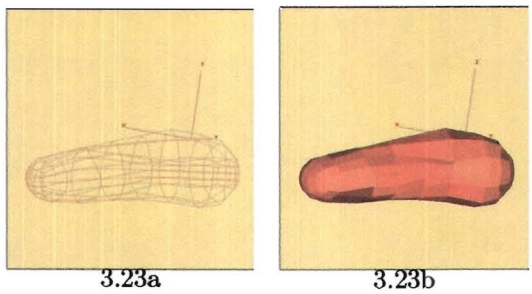

3.23a 3.23b

Figure 3.23: Foot

Subsequently, a mesh of NULL-material is supported to this body, figure 3.23b. The foot compliance is taken into account in the contact function. The right foot is modeled in a similar fashion.

Chapter 4

Calibration and Validation of the DoTSID Model

This chapter describes the calibration and validation process. First, from the available tests at TNO, a selection was made to comprise the test matrix. Subsequently, the test matrix is divided in calibration and validation tests and the optimization procedure described in section 3.1.3 can commence.

4.1 Test matrix

When composing a test matrix the objective should be to cover a scatter of impacts at different locations and velocities on material, component, assembled component and full dummy level, preferably at different impact directions and severities.

Table 4.1 lists the selection of validation tests performed on the DoTSID model. This selection was based on availability, quality and relevance. Note that no material tests are listed, therefore, the bulk of the material parameters had to be derived from literature and calibrated using assembled component tests. The model of the neck, damper and spine are derived directly from the multibody DoTSID model, therefore, these tests will not be further assessed. Thorax and pelvis component tests are included in this matrix as they are considered key parts of the model since all relevant sensors are located in these parts. The full dummy tests are a reasonable representation of the available different lateral loading conditions.

Table 4.1: Test matrix DoTSID calibration and validation

Test #	Component	Test type	[kg]	[m/s]
01	Neck	Static flexion/extension	–	–
02		Static lateral flexion/extension	–	–
03		Static oblique flexion/extension	–	–
04		Static torsion	–	–
05	Damper	Dynamic impact	4.7	3.1/4.5/6.5
06	Spine	Static flexion/extension	–	–
07		Static torsion	–	–
08		Static compression/extension	–	–
09		Static shear	–	–
10	Thorax	Linear Guided impact	20.75	4.1/8.3
11		Linear Guided impact	9.9	3.5/4.5/6.5
12	Pelvis	Linear Guided impact	9.9	3.5/4.5
13	Full Dummy	Staggered LGI 50/00/00	35.95	4.4/6.3
14		Staggered LGI 00/100/00	36.42	4.3/6.2
15		Staggered LGI 00/00/50	35.95	6.4
16		Staggered sled test 00/50/50	32767	10.3

The following critical remarks should be made with respect to the comprehensiveness of this test matrix:

- No test data on material level, especially concerning the arm foam and abdomen foam

- No abdomen component test data
- Only one pelvis component test series
- No oblique thorax component test data
- No dynamic component test data for lumbar spine and neck
- No oblique full dummy test data
- Only one high severity full dummy test

During lateral impact on the thorax the arm foam, which is considered to be strain rate dependent, compresses and bottoms out. The abdomen forms an important load path to the lumbar spine, that in its turn connects the thorax with the pelvis. Because the arm foam, abdomen and lumbar spine are all components that are crucially positioned in the load path their characteristics will play an important part in the response of the dummy. The omission of oblique test data and especially the shortage of high severity test data in the matrix may restrict the useful range in which the model can be used. Furthermore, only one out of seven full dummy level tests are performed with a deforming barrier (test 16). While rigid impactors make good sense in terms of modeling simplicity, this relatively small amount of tests with deforming barriers potentially jeopardizes the models predictive capabilities in a (deforming) vehicle environment.

Tests 1 through 15 are made available for calibration purposes. Since these tests are all performed with a rigid barrier, they can be simulated using a simpler model then what will be needed to simulate tests 16. This elimination of unknowns will facilitate the model calibration process. Test 16 is reserved for model validation, as this impact condition bears the most similarity to an actual vehicle crash standard.

4.2 Calibration of the DoTSID model

Numerous, often iterative, steps for many model parameters were undertaken during the DoTSID model calibration. For the sake of clarity, this section will only discuss a few of these steps.

4.2.1 Component tests

This section describes the experiments that were performed on the spine, neck, damper, thorax and pelvis components.

Spine, neck and damper

The spine, neck and damper unit are all modeled as rigid bodies with FE `NULL`-material. The joint properties of these models have been validated during the development of the multibody US-DoTSID and are copied for use in the hybrid MB-FE DoTSID model. Pertaining this validation, the reader should note that only the damper unit has been validated using test data from dynamic impacts, as can be seen in table 4.1. For additional information the reader is referred to [33].

Thorax

As table 4.1 indicates, two tests series are available for thorax component testing. During the evaluation of the test data from test series 11, however, it appeared that all signals show unexpected vibrations. These vibrations are most likely due to the aluminium impactor plate used in this impact and the relatively low impactor mass with respect to the tested component. Because the results of test series 10 are trusted above those of series 11 and test series 10 has a higher (more applicable) energy level, series 11 is disregarded in favor of series 10.

In these test series, the thoracic spine is mounted to support brackets by using the interface mountings with the neck bracket and lumbar spine. A linear guided impactor with an effective mass of 20.75 kg and an impactor face of ∅ 165 mm was used to provide lateral impact, as depicted in figure 4.1.

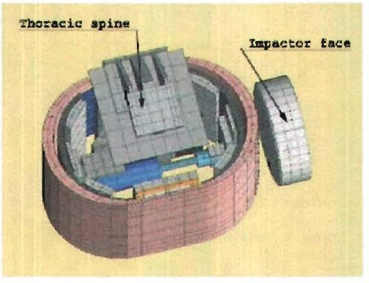

Figure 4.1: Test set-up for thorax component test.

The impact velocities where: 4.1 m/s and 8.3 m/s. During these tests the following signals were measured:

- Damper displacement [m]
- Lateral upper and lower rib accelerations [m/s^2]
- Bumpstop load (N)

The results for the 4.1 m/s impact velocity are shown in figure E.1. From these graphs, it can be concluded that for the low velocity the rib accelerations are predicted very well. The initial simulation of the 8.3 m/s impact velocity (depicted in orange in figure 4.2), however, displays rib accelerations that are leading and overshooting the experimental curves (in red).

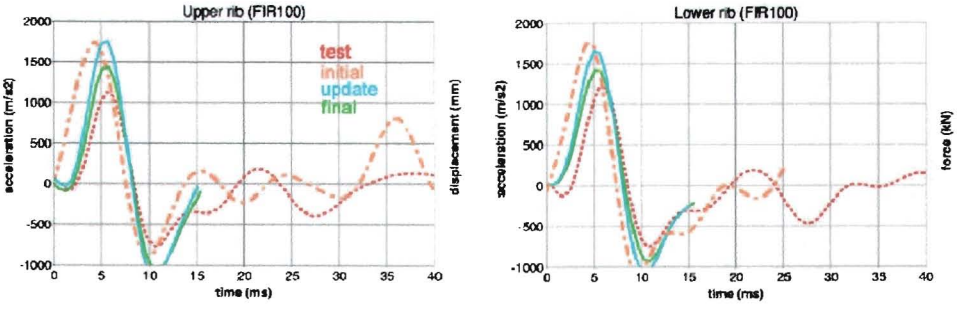

Figure 4.2: Results for thorax component test (v = 8.3 m/s). Test results vs. initial, updated and final predictions.

The fact that the rib signals show an immediate loading, even prior to actual impact, is due to the FIR100 [68] filtering of this signal. Because the damper is a validated and therefore trusted component and the rib padding and hinge material properties are unknowns, further investigation is needed into the latter components. Since the thorax model predicts the lower velocity impact well and behaves to stiff at the higher velocity, a possible cause could be a an overestimation of the rib padding's strain rate dependency.

After gradually lowering the strain-rate dependency, the rib padding was adjusted to include no strain-rate dependency at all. The updated results are displayed in figure 4.2 signal (blue line). The rib acceleration peak has shifted in timing, but not enough. The lower velocity response remained unchanged throughout this process. Because no more gain in timing could be achieved with lowering the strain-rate dependency, the reference loading curve initial loading is adjusted by lowering the initial linear elastic stiffness and densification plateau. The final results are shown in 4.2 (green line). Timing wise the result is very good, but the peak levels still show a clear overshoot.

Other variations , such as modifying the densification or bottoming-out stiffness of the foam, resulted in identical curves indicating that other factors are contributing to this phenomenon[1]. For now these results are deemed adequate to proceed to full dummy calibration.

[1] Further testing, performed after this thesis, casted doubts on the validity of this particular experiment in favour of the numerical model.

Pelvis

Using the interface mountings with the lumbar spine, the lower torso is mounted to a support bracket. A flat, round, aluminium impact face with diameter of 152 mm is used for these dynamic tests. The effective mass of the impactor was 9.9 kg. Due to this set-up, only the impactor dynamics could be assessed. Furthermore, these tests suffer from the same shortcomings as the thorax component test series 11, since they too are performed with a aluminium faced impactor that had a relatively low mass. The test data from the 4.5 m/s impact, therefore, was not usable and the data from the 3.5 m/s impact was of only marginal quality. Because no other tests are available, the 3.5 m/s test is admitted into the test matrix. Figure 4.3 shows experimental and predicted results.

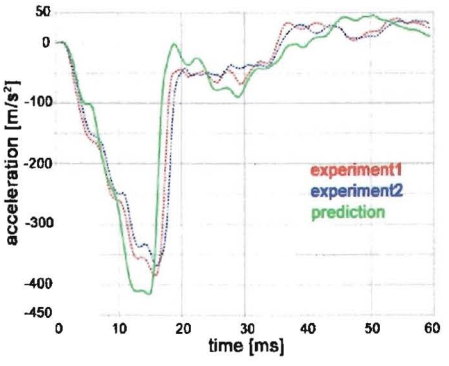

Figure 4.3: Predicted (green) vs experimental (blue and red) impactor acceleration for the pelvis component test.

The prediction leaves room for improvement, however, because of the low quality of the available test data, it is opted for to calibrate the pelvis response using full dummy tests.

4.2.2 Full dummy tests

All of these tests where performed using a Linear Guided Impactor (LGI). Figure 4.4 shows the LGI and the DoTSID in test configuration.

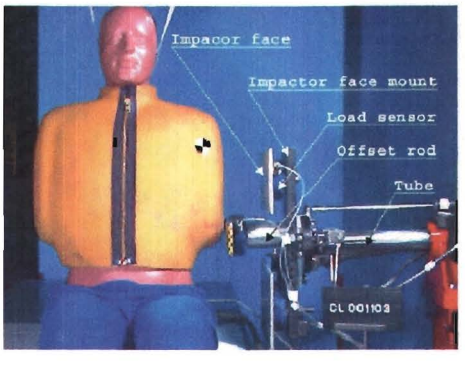

Figure 4.4: DoTSID crash test dummy in an abdomen leading linear guided impactor test set-up.

The DoTSID is sitting on a backless bench on two layers of Teflon, ensuring very low sliding friction. The dummy is supported in its upright position by two pieces of break away tape fastened to the head. The pants are pulled down slightly to enable a better view of the dummy kinematics. Furthermore the DoTSID is equipped with its standard array of equipment, see table 2.1.

The impactor probe consist of a chrome-plated steel tube, 60 mm in diameter and a length of 770 mm, with an impactor face mount to fix different impactor faces. This probe is guided by three Teflon bearings and can be propelled to the required velocity by two steel springs. The impactor face mount provides mounts for three separate aluminium plates: one at thorax height, one at abdomen height and one at pelvis height. All three plates carry their own load sensor to help in comparing the load introduction between test and simulation. By installing aluminium rods between a plate and the impactor face a relative offset between the

plates can be achieved. By using different rod lengths one can now vary the impact conditions. In figure 4.4, the abdomen plate is leading by 100 mm, therefore this impact is abbreviated with the index: 00/100/00. The first digits denote the offset of the thorax plate, the second pertain the offset of the abdomen plate and the third specifies the offset of the pelvis plate. Thus an 50/00/00 impact configuration designates a situation where the thorax plate would be leading the abdomen and pelvis plate by 50 mm. The effective mass of the impactor is approximately 35 kg.

Modeling the linear guided impactor

The impactor is modeled with `NULL`-material and four rigid bodies, one for each plate and one for the impactor probe. The load cells are modeled by specifying the `CONSTRAINT LOAD` output for each multibody plate. The rigid bodies representing the plates are each assigned the mass of their respective plates plus the mass of one load cell half. The probe rigid body is assigned the probe mass plus three times (the other) half of the load cells mass, plus the mass of the impactor face mount, plus the mass of any offset rod. In this way the mass in front of the load cells is split from the mass behind the load cells.

The probe multibody is fixed to `INERTIAL SPACE` with a translational joint that is given the initial velocity as measured from each test just prior to impact. Any velocity changes due to friction loss is not accounted for, but is assumed to be negligible during the short impact phase.

Staggered linear guided impact: 50/00/00

This configuration denotes a thorax leading staggered impact. This test series was performed at 4.4 m/s and 6.25 m/s.

First the higher (6.25 m/s) velocity will be discussed. More emphasis is placed on calibrating the model in for this particular speed as it is more representative of FMVSS-like velocities. The orange lines in figure 4.5 correspond with the initial model predictions.

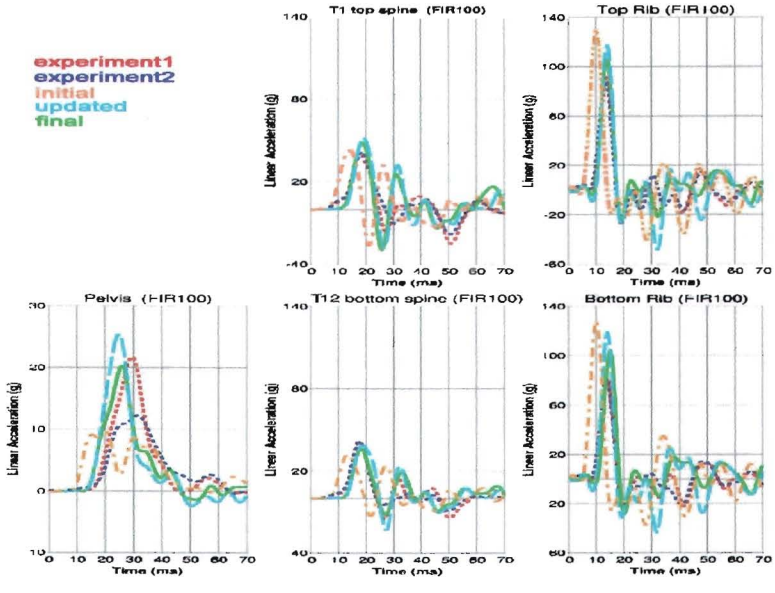

Figure 4.5: Analysis of the 50/00/00 stagered LGI test (v = 6.25 m/s).

The predictions for the rib accelerations an overshoot of approximately 50 percent, when compared to the experimental values. The pelvis and spine predictions show a slightly leading peak value with an acceptable margin of error.

First and primary concern for model optimization is to evaluate the signals "chronological" order, by first analyzing the (timing of the) experimental signals. This cause-and-consequence analysis is an invaluable aid in discerning an internal loadpath. Understanding this loadpath (for both simulation and model) is crucial when calibrating a model as complex as regarded here.

For instance, in the regarded 50/00/00 6.25 m/s impact, the impactor thorax plate load (in figure 4.6) shows a gradual loading while compressing the jacket and arm foam and at approximately 9 ms displays a sudden rise, indicating a hard impact. During these first 9 ms the pelvis does not respond at all, indicating

that none of this load is transferred to the pelvis. In fact, the pelvis only starts to respond at approximately 17 ms when the impactor pelvis plate load becomes positive, indicating impact. The initial negative values for abdomen and pelvis plate load are due to inertia effects in the impactor when the thorax plate is decelerated by the impact. Also the bottom spine acceleration is already at its peak value showing no influence on pelvis acceleration. This indicates that the pelvis response is dominated by the pelvis plate impact. The abdomen plate does not come into play at all, so no significant load is introduced externally through the abdomen area. The rib accelerations follow the rise of the thorax plate load. Slightly lagging the rib accelerations are the spine accelerations, indicating that the spine is loaded through the ribs.

Concluding; The load is first transferred from the impactor thorax plate to the jacket and arm foam into the rib cage, where it is registered by the rib accelerometers. This load is then transferred through the hinge and damper unit to the thoracic spine. The pelvis response is dominated by the pelvis impactor plate.

Applying these conclusions to the model and its performance in the current simulation, we start comparing the first available information in this load chain: the impactor thorax plate load. From figure 4.6 (orange line) it can be observed that the prediction of this load is premature and overshoots the experimental value almost 40 percent. Also, the gradient of the predicted curve is steeper than the experimental gradient. These are clear indications that the contact between the dummy model and impactor plate is modeled too stiff. The rib accelerations, as shown in figure 4.5, follow the behavior of the impactor thorax plate load.

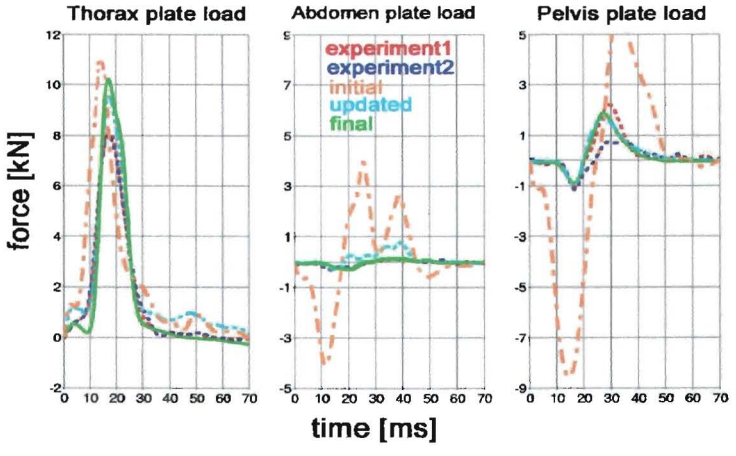

Figure 4.6: Impactor plate loads for the 50/00/00 stagered impact test

As the results of the thorax component calibration does not warrant the magnitude of error that occurs in this simulation, the "too-stiff" component has to be either the arm foam or the jacket. From the model kinematic file it can be deduced that the arm foam compresses approximately to half its original width of 8 cm. Upon inspection of the DoTSID arm it proved relatively easy to compress the foam to under one cm before it bottomed out. Traveling at 6.25 m/s this 3 cm delay in load transfer could very well account for the error in the predicted rib acceleration timing. Therefore, the arm foam loading curve was adjusted to display densification (or bottoming out) at 90 % compression. From the load path analyses it was concluded that the pelvis acceleration was not directly induced through this load path, so it is likely that the results for this prediction will remain similar after this modification.

The updated results are shown in figures 4.6 and 4.5 (blue line), and show a much better prediction of the regarded signals. The timing of the predicted rib acceleration peaks have both shifted towards the experimental peaks and also the magnitude of the predictions show a clear improvement over the previous prediction. Also, the prediction for both the upper and lower spine have improved, whereas the prediction of the pelvis acceleration has not significantly altered.

In an attempt to decrease the rib accelerations even more, the loading curve of the arm foam before densification has been lowered. The results for this simulation also can be found in figures 4.6 and 4.5 (green line). The timing of the predicted peak rib accelerations has not changed, but the magnitude shows better correlation to the experiment, while the other predictions remained unaffected. Lowering the arm foam loading curve even further produced numerical instabilities.

The lower speed (4.2 m/s) variant of this experiment was subsequently calibrated using the strain-rate dependency (see appendix B.2.2) of the arm foam material model. The final results for this simulation can be seen in figure E.3.

Staggered linear guided impact 00/100/00

Initial results for the 6.2 m/s abdomen leading impact are shown in figure 4.7 (orange line). The most striking conclusion that can be drawn from these graphs, is that the all predictions, except for the pelvis acceleration, are lagging. The magnitude of the error in timing between test and prediction cannot simply be justified by a weak contact. To correct this problem, the original mesh for the jacket C was replaced by a new jacket mesh, that included a bridge between jacket and shelf (shown in figure 3.19). This addition of material between the impactor and T12 was thought to improve the timing of the T12 prediction and ensure a correct load path to T1. Figure 4.7 shows the updated results. The timing for the T12 prediction has improved, however, the prediction for T1 did not benefit from this update in the same extent as the prediction for T12 did. Moreover the prediction for T12 now shows a premature peak at 14 ms. and the prediction for the pelvis acceleration is now premature. The results seem to indicate that at an early stage of the impact, between 10-20 ms, too much energy is transferred from the abdomen region to the pelvis area. In order to correct this, the lining of the jacket (see section 2.2.4) is included in the model. This lining gives the jacket a high stiffness in extension only. When the jacket is compressed in the abdomen area, the lining will divert load from the pelvis to the thorax. The results are shown in figure 4.7 (green line). Clearly the model response for both T1 and T12 and pelvis has improved.

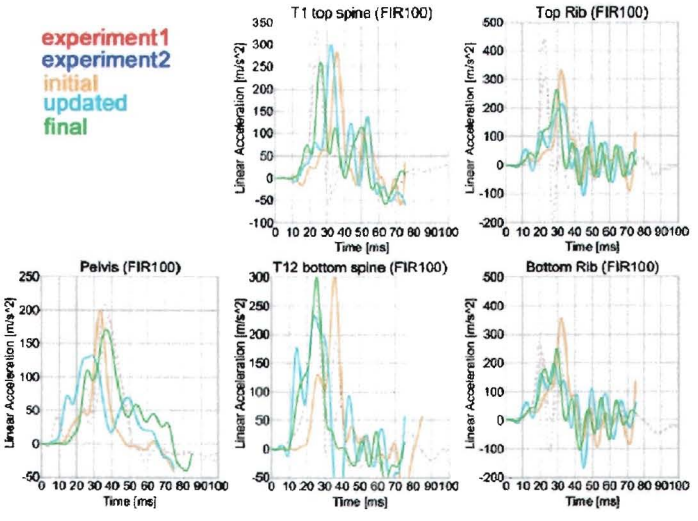

Figure 4.7: Results for 00/100/00 LGI test (6.2 m/s)

The predictions for the rib accelerations are unacceptable, however, with the new and, geometrically, accurate jacket model in place, the calibration of this test would rely on the tuning of the material properties for the jacket and the abdomen foam. Also the lumbar spine joint model, that was only validated under static loading conditions could be included in this process. The large numbers of unknowns proved to frustrate the calibration, perforce, calibration for this test was discontinued.

Staggered linear guided impact 00/00/50

Displayed in figure E.4 are the results for the pelvis leading impact. The predictions for all the regarded dummy response are satisfactory.

4.3 Validation of the DoTSID model

After calibrating the DoTSID model, as described in the previous section, the models performance is now assessed in a deforming barrier test (test 16 in table 4.1). This test has been performed by NISSAN Motor Company JAPAN and made available to TNO for validation of the multibody DoTSID model. The test set-up features a 32767 kg sled mounted impactor traveling at a velocity of 10.2 m/s. The impactor faces are urethane and polypropylene foam blocks, arranged in a 00/50/50 configuration. NISSAN supplied test data for the foam blocks on the impactor and for the dummy response during the test.

A previously conducted study [78], describes the modeling and validation of the deforming barrier and assesses the performance of the multibody DoTSID in this test. This test will serve as a validation test for the

hybrid MB/FE DoTSID model and will allow a comparison of the hybrid model to the multibody DoTSID model.

4.3.1 00/50/50 deforming barrier test

The original barrier model for this test, as validated by M.G.C. Rekveldt in [78] is used for this analysis. The multibody DoTSID model is replaced by the hybrid MB/FE DoTSID and contact definitions with the environment are set to accommodate the finite element parts of the hybrid SID model. Figure 4.8 shows the test set-up.

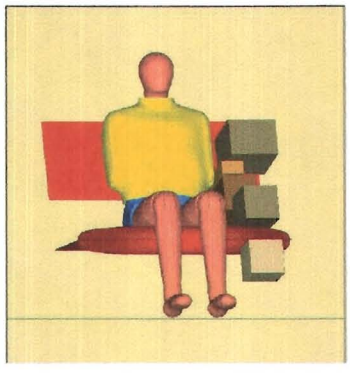

Figure 4.8: Analyses of the 00/50/50 deformable barrier impact.

Results for the 00/50/50 deforming barrier test

Results for this test are depicted in figure 4.9 and show very acceptable correlation for all signals. When comparing the predictions of the MB/FE model to the multibody model with respect to the experimental signals, the following observations can be made. In the hybrid model, the experimental rib accelerations are predicted more accurately in terms of shape and timing of the signals, while the pelvis acceleration prediction has improved in both shape and peak magnitude. The quality of the lower spine acceleration prediction is similar in both models. The peak level of the upper spine acceleration is predicted better by the MB/FE SID. The shape of the experimental upper spine acceleration in not predicted well with both dummies. The MB/FE model is able to correctly register the second peak in the upper rib's experimental signal, but it also wrongfully predicts an oscillation in the upper spine acceleration during the time of the primary peak. The magnitude of the upper spine acceleration is predicted better by the MB/FE model.

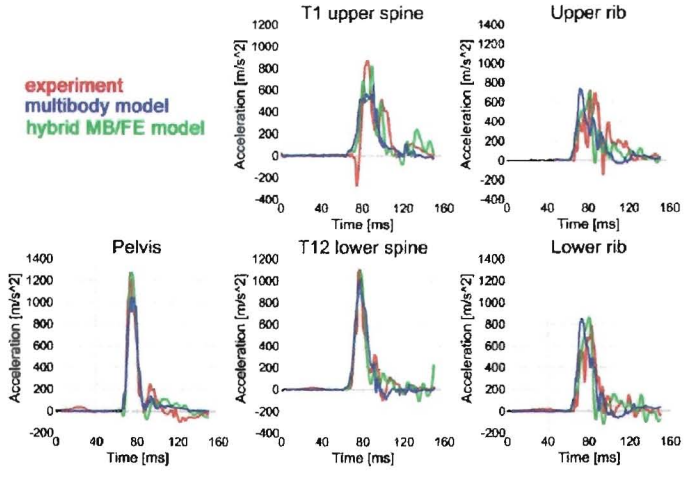

Figure 4.9: Results for 00/50/50 deforming barrier test. A comparison between the predictions of the hybrid MB/FE DOTSID model and the multibody model with respect to the experimental values.

All in all, it can be concluded that in this validation test the hybrid MB/FE DoTSID model performed well and even outperforms the multibody DoTSID model.

Chapter 5

Application of the DoTSID Model

Ultimately, one of the most important benchmarks for any numerical ATD model that is to be used in a production environment, is its ability to predict dummy response in the regulatory standards. These standards can be regarded as the application field for the numerical model. This chapter deals with the DoTSID models performance in two such standards: the FMVSS214 and FMVSS201.

5.1 Moving deformable barrier standard (FMVSS214)

The FMVSS214 Moving Deformable Barrier (MDB) standard is a standard that all US car manufacturers need to comply with. Since this standard includes the DoTSID crash test dummy, it can be considered as a crucial application field for the US-DoTSID model.

5.1.1 FMVSS214 test set-up

The FMVSS214 standard mandates an impact between a moving deforming barrier and a US-DoTSID seated in a stationary test vehicle. General Motors (GM) motor company, supplied a finite element model of one of their vehicles and the MDB model was developed within TNO [32]. Figure 5.1, depicts the vehicle model and the barrier in the correct test set-up. The weight of the barrier is 1358 kg and this particular vehicle weighs 1697 kg.

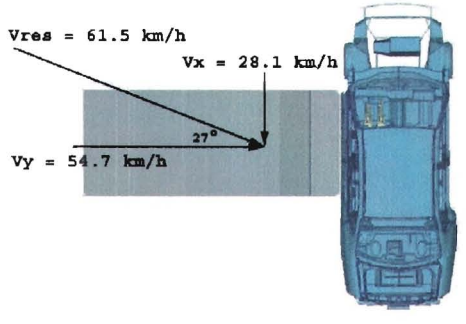

Figure 5.1: Test set-up for FMVSS201 procedure.

General Motors also supplied TNO with the experimental signals derived from the actual test, except for the dummy pelvis acceleration. Also, GM was unable to provide information pertaining the dummy positioning and seat characteristics.

5.1.2 Results of the FMVSS214 analyses

The results for this simulations are compared to the experimental values in figure 5.2. Obviously, large discrepancies between the prediction and the test can be observed. Determining the cause, though, proved to be an arduous task.

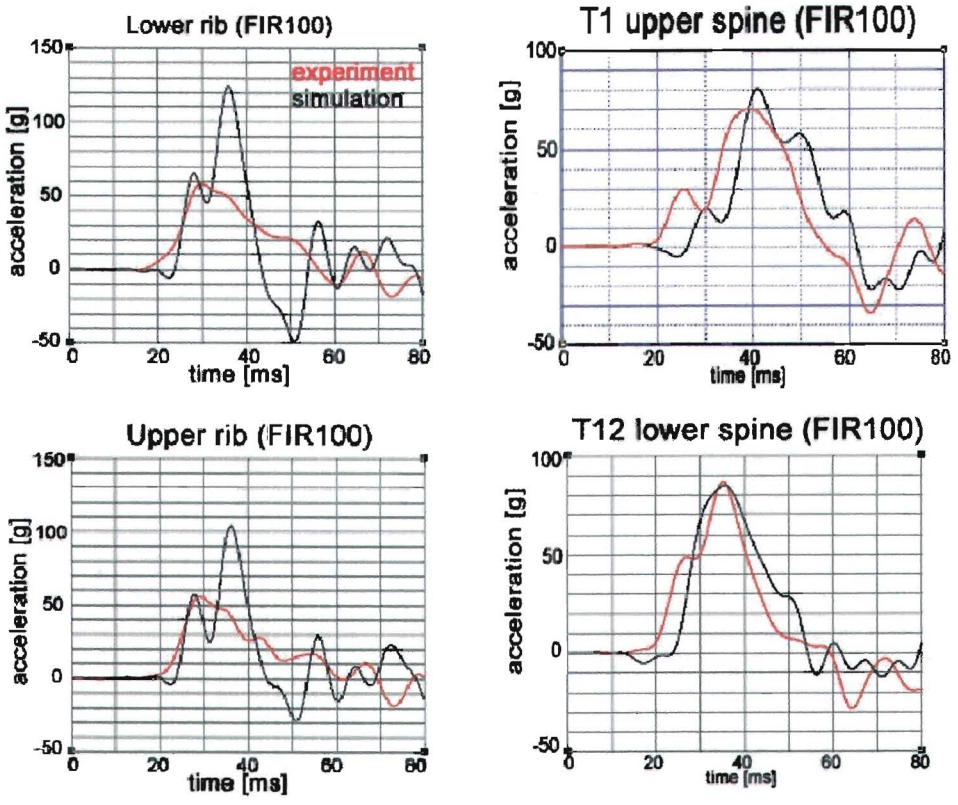

Figure 5.2: Analysis of GM-vehicle FMVSS214 impact. Red lines denote the experiment, black lines denote the predicted values.

As can be seen in figure 5.3, the door trim of the vehicle model exhibits a considerable deformation before striking the dummy. On t = 17 ms, when the experimental dummy already displays sensor output, the dummy model is hardly in contact with the door panel, see 5.3b. Shifting the dummy towards the door panel to improve the timing is considered valid, since the precise positioning of the dummy is not known, but this did not improve the overall response. GM was not able to provide TNO with additional information pertaining the material properties of the door panel, nor was it inclined to submit video footage of this particular experiment for comparison with the model kinematics.

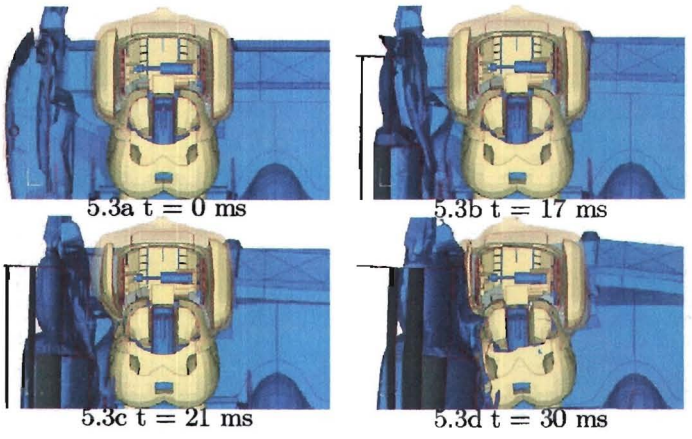

Figure 5.3: Analysis of GM-vehicle FMVSS214 impact.

All that, analytically, remained was a thorough comparison of the experimental loadpath to the numerical loadpath based on the information that is available. From the experimental results it can be deduced that the lower spine acceleration is loaded first and it also reaches the highest peak level at 35 ms. At t = 25 ms, the experimental upper spine (T1) acceleration drops as the lower spine (T12) acceleration remains at the

same magnitude. Since T1 and T12 are rigidly connected through the thoracic spine, this would indicate a rotation of the torso towards the door. This rotation must be induced by a predominant hard contact in either the abdomen or pelvis region. The pelvis acceleration signal is not available however, leaving this question unanswered. At 30 ms, both spine accelerations show a sudden rise. Since no direct contact occurs between door panel and spine, load must have been transferred through either the thorax or the abdomen/pelvis region. It is not likely that this load has been transferred through the thorax, as the rib accelerations show no indication of this. Once again, based on the available data, it is difficult to make an assumption on where the load was introduced.

Not knowing the dummies exact position poses a concern, when unraveling the loadpath within the ATD and comparing this to the ATD model. Shifting the dummy up or down influences the door trim's point of impact and thus, the simulated loadpath. Not having access to the critical pelvis acceleration signal, combined with the other limitations on available data (such as: dummy position and video footage) makes further analyses rather speculative.

One thing could be deduced from the available data, with respect to the performance of the combined vehicle-dummy model. In the predicted results, see figure 5.4, an initial positive pelvis acceleration can be observed at t = 12 ms, indicating that the pelvis is moving away from the door panel.

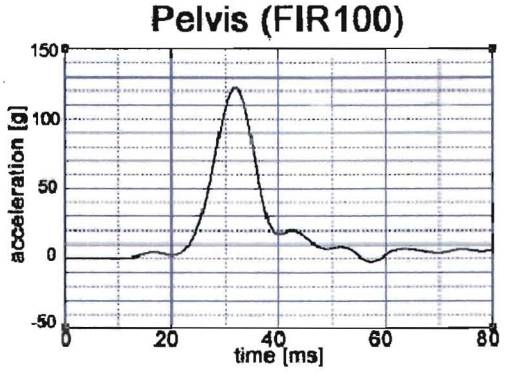

Figure 5.4: Prediction of pelvis acceleration in GM-vehicle FMVSS214 impact.

At the same time, the initial predicted spine accelerations are both negative, meaning that the dummies torso is rotating towards the door during the initial stage of the impact. This rotation could very well be the cause of the second peak in the rib accelerations that occur only in the prediction, at approximately t = 31 ms. Figure 5.3d visualizes the origin of this peak as the thorax impacts the upper part of the door trim. The experimental initial spine accelerations are positive and the rib accelerations show no indication of a second peak. Moreover, at 31 ms both rib accelerations are gradually decreasing, indicating that in reality this contact does not occur, or at least, does not occur in the same magnitude as predicted. Working on the conjecture that this initial rotation causes these phenomena, a likely conclusion would be that controlling the initial pelvis motion could beneficially influence the predictions.

Various perturbations on dummy model positioning, door trim and door panel material properties lead to the following observations:

- Changing the material property of the trim influences the dummy response significantly.
- Positioning of the dummy has a great influence on the signal response.

None of these parametric study cases led to promising results though. Given the number of unknowns in this problem and the limitations on available experimental data, this benchmark was discontinued for the time being.

5.2 Rigid pole impact standard (FMVSS201)

The FMVSS201 standard specifies the use of a SID/HIII dummy, however, given the similarity between the DoTSID and SID/HIII, this particular test can be regarded as a good test case for evaluating the models performance.

5.2.1 FMVSS201 test set-up

The rigid pole impact standard describes a lateral impact of the moving test vehicle onto a 254 mm diameter rigid pole. The vehicle travels at 29 km/h and strikes the pole at the drivers location. Figure 5.5 shows the DoTSID model in a General Motors Sport Utility Vehicle (GM-SUV). This vehicle is equipped with a curtain air bag unfolding from the roof rail (marked red) to control excessive head acceleration.

The model of the GM-SUV was developed and validated at TNO [79] and provides a good starting point for assessment of the performance of the DoTSID model in this application.

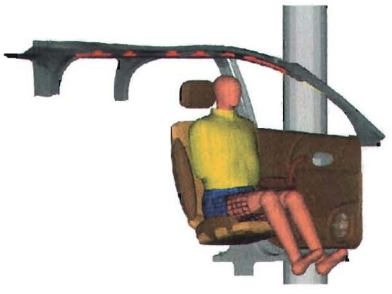

Figure 5.5: Analysis of GM-SUV FMVSS201 pole impact.

General Motors supplied the experimental data derived form the actual test, except for the upper spine (T1) acceleration. Since the actual test was performed using a SID/HIII, the head acceleration has been disregarded for the purpose of signal comparison.

5.2.2 Results of the FMVSS201 analyses

As can be deducted from the test results shown in figure 5.6, correlation for the upper and lower rib is very good. The discrepancies between simulation and test after 45 ms are less relevant (see section 3.1.3), but can be explained when regarding the experimental unfiltered signals. Figure 5.6 depicts the experimental filtered and unfiltered lower rib acceleration versus the filtered prediction. Clearly, the experimental signal loses quite some information in the 43 ms to 53 ms time interval, that the model did retain after filtering.

The general shape of the experimental lower spine acceleration curve is captured by the prediction. The prediction, when compared to the experimental curve, peaks 5 ms prematurely at 93 % of the magnitude of the experimental peak value. This error margin is considered to be acceptable.

The predicted pelvis acceleration, though, shows an overshoot of 60 % when compared to the experimental curve, also the prediction is leading the experiment by 7 ms. When comparing the amount of energy contained by the experimental and simulated pelvis signal, though, they appear almost the same. This observation, combined with the fact that the simulated signal shows an premature overestimation with regard to the experimental signal, indicates that the pelvis is behaving too stiff in this application. Reducing the pelvis stiffness (or perhaps the stiffness of the pelvis-to-doorpanel contact) would very likely lead to a better correlation of the simulated pelvis acceleration signal with respect to the test. Moreover, this reduction could also beneficially delay the timing of the lower spine acceleration, as less load will be transferred through the pelvis to the lower spine during the first 40 ms.

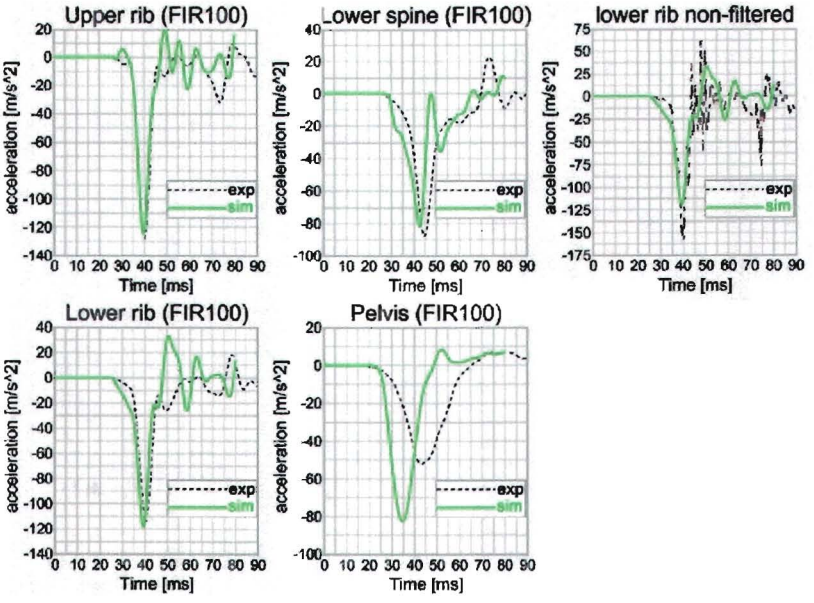

Figure 5.6: Results for GM-SUV FMVSS201 impact.

Chapter 6

Additional tests

Spurred by the poor performance of the model in the FMVSS214 application and the abdomen leading staggered impact calibration tests, additional testing was performed within the scope of this thesis. The objective of these tests were twofold:

1. Gain insight into abdominal entry loading conditions
2. Improve model performance in FMVSS214-like applications

Objective one was thought to be reached best by performing a test that reduced the number of unknowns by de-coupling the jacket to abdomen interaction. To this end two test were proposed: one impact with the 00/100/00 configuration on a dummy *without* jacket and one using an identical setup on a dummy *with* jacket.

For objective two the goal was to perform a test that would yield similar loading conditions on the dummy as seen in the FMVSS214 test. This surrogate FMVSS214 test could then be used as a tool to validate or improve the DoTSID model in the, more complicated, FMVSS14 application. Also in this respect it was deemed important to test the models sensitivity in predicting slight alterations in impact conditions. Because the precise location of the armrest during impact is crucial in controlling TTI and pelvic acceleration (as described in section 2.1), correct model sensitivity for these variations is considered paramount.

6.1 Test set-up

In order to meet the aforementioned objectives, a suitable test set-up needs to be designed. This section will discuss, the (configuration of) the impactor, the instrumentation of the DoTSID ATD and the test matrix.

6.1.1 Impactor configuration

When designing an impactor, four important factors need to be taken into account:

1. Impactor material
2. Impact velocity
3. Impactor mass
4. Impactor configuration

The impactor material is to be aluminium, since this can be considered rigid and relieves the necessity to extensively validate the impactor model itself.

The velocity of the impactor throughout the impact is a function of its initial velocity, friction between the impactor and its environment (excluding the dummy contact friction) and velocity loss due to dummy contact interaction (both contact friction loss and kinetic energy transfer). The initial velocity, just prior to impact, can easily be measured and modeled and the friction loss to the environment is negligible in the short time interval that impact occurs. The influence of the contact interaction with the dummy on the impactor velocity is clearly the hardest to capture. To minimize the influence that the dummy response has on the motion of the impactor, and facilitate the calibration process, the impactor needs to have a sufficiently high mass. This mass threshold is determined by conducting a series of simulations with an increasingly large impactor mass.

Figure 6.1 shows that for masses from 720 kg and up the dummy response is nearly equal. Another advantage of a high mass impacter would be that signal oscillations due to eigenfrequencies are more likely to be avoided.

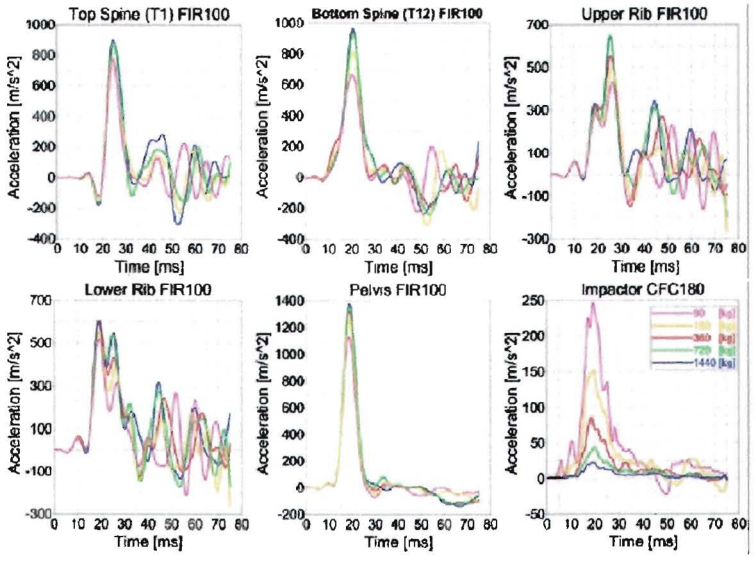

Figure 6.1: Mass sensitivity study for the 00/150/100 rigid impactor.

Based on the door panel intrusion from the FMVSS201 application kinematics, see figure 5.3, an impactor configuration (relative offset of the impactor faces) was estimated in order to attain a similar loading condition as seen in the full vehicle application. Perturbations on this impactor configuration and impact velocity indicated that, an 720 kg rigid impactor[1], a staggered impactor configuration of 00/150/100 and an initial velocity of 8 m/s should provide a similar response as seen in the FMVSS201 experiment. Figure 6.2 compares the experimental signals derived from the FMVSS214 experiment to the model predictions for a 720 kg 00/150/00 rigid impactor traveling at an impact velocity of 8 m/s.

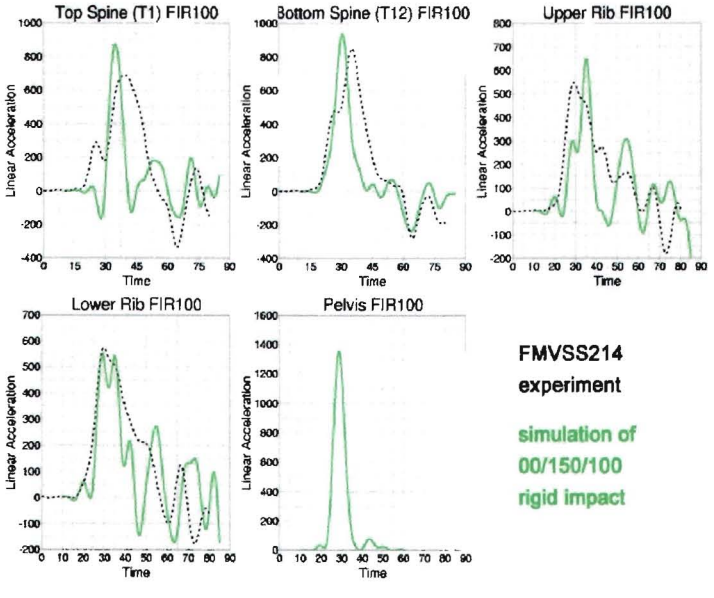

Figure 6.2: Comparisson of the GM-FMVSS214 experiment (black) with the 00/150/00 rigid impactor model prediction (green).

[1] The relatively high mass and speed of the impactor ruled out the possibility of using the linear guided impactor used in the previous test. Instead, the "*Elastische Bots Simulator*" (EBS) provided a suitable alternative. This test device can propel masses up to 720 kg to a velocity of 8 m/s.

Upper and lower spine accelerations are approximated well in this model. However, the peak width of the experimental accelerations can not be captured, this is thought due to the rigidness of the virtual impactor as opposed to the deforming door trim that more gradually loads the thorax. However, since the peak values have are comparable in magnitude and timing, this is deemed acceptable.

For the 00/100/00 impact configurations an initial velocity of 5 m/s was opted, since higher velocities could well damage the crash test dummy.

6.1.2 Test matrix for additional testing

Summarizing the previous section, table 6.1 lists the additional test that are to be performed on the DoTSID using the "*elastische bots simulator*" (EBS) in TNO.

Table 6.1: Test matrix for EBS DoTSID testing

Test #	Test description	[kg]	[m/s]	Remarks
17	Sled test 00/150/100	700	5	Repeat
18	Sled test 00/150/100	700	5	3cm up
19	Sled test 00/100/00	700	8	Repeat
20	Sled test 00/100/00	700	8	No jacket

Test 18 is a deliberate perturbation on test 17 and will provide insight in the sensitivity of both experiment and model. Figure 6.3 shows the experiment set-up for the 00/150/100 EBS test.

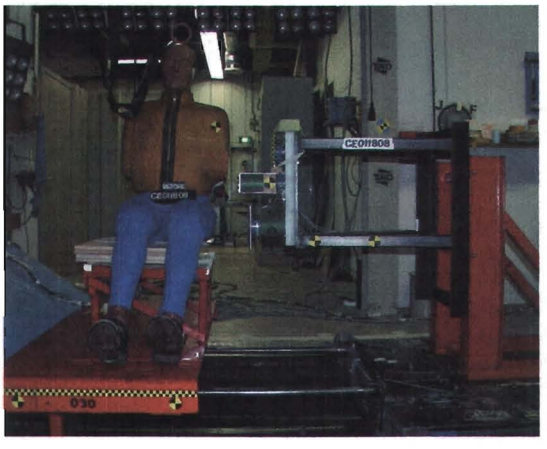

Figure 6.3: Test set-up for 00/150/100 EBS test.

6.1.3 DoTSID instrumentation

The cost of experimental testing is highly dependent on the number of recorded signals. To maximize the number of tests that can be performed on a certain budget, an optimum had to be found between cost and cost-effectiveness of signals. The test matrix will, therefore, be executed with the instrumentation listed in table 6.2.

Table 6.2: Instrumentation EBS DoTSID testing

	Location	Sensor
Dummy	Upper spine	tri-ax accelerometer
	Lower spine	uni-ax accelerometer
	Upper rib	uni-ax accelerometer
	Lower rib	uni-ax accelerometer
	Pelvis	tri-ax accelerometer
	Lumbar spine	tape-switch
Sled	front	uni-ax accelerometer
	back	uni-ax accelerometer
Impactor	Thorax plate	uni-ax accelerometer
	Abdomen plate	uni-ax accelerometer
	Pelvis plate	uni-ax accelerometer

Furthermore, two high speed cameras are available for each test. One camera will be positioned directly in front of the dummy and the second camera will be ceiling mounted to provide footage directly from the top. During test 20, however, the frontal camera, will be repositioned to film the rear of the dummy in order to capture the motion of the lumbar spine. Finally, just prior to impact, the sled's velocity will be measured.

The tape switch in the lumbar spine is *non-standard* instrumentation. The tape switch is made of plastic and runs down the full length of the lumbar spine and is positioned to be crushed between the abdomen and lumbar spine during impact. Figure 6.4 shows a detail of the DoTSID ATD where the tape switch is highlighted in green.

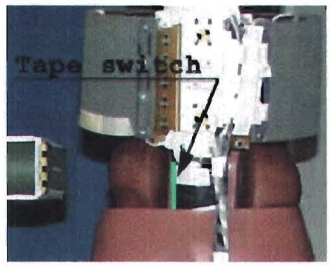

Figure 6.4: Tape switch instrumentation on DoTSID.

The outer shell of the tape switch is made of plastic and will yield under a certain pressure. When it does, two layers of conductive material on the inside make contact and a spike can be registered. This instrumentation is thought to be useful in determining the point where the abdomen foam densifies and starts to transfer load to the lumbar spine.

6.2 Assessment of the experimental results

Since all performed experiments were simulated before the actual tests were executed, the results of the experiments could immediately be compared to the predictions. Please note that since the model results were generated before the experiments were conducted, some model parameters such as: precise dummy position with respect to the impactor, initial sled velocity and impactor mass were estimated.

6.2.1 00/150/100 EBS surrogate test for FMVSS214

Figure 6.5 compares the (repeated) experimental results of the 00/150/100 impact with the predictions. The repeatability of the experiment is considered to be very good. The predictions show a good correlation to the experimental results. The bottom spine and pelvis acceleration predictions show good correlation in timing, peak magnitude and shape of the curve. The prediction for the upper spine acceleration overshoots the experiment by 40 percent, but the shape of the experimental curve is captured acceptably by the prediction, notwithstanding the 5 ms shift. The same holds true for the prediction of the upper rib, but in this case also the peak magnitude is predicted acceptably.

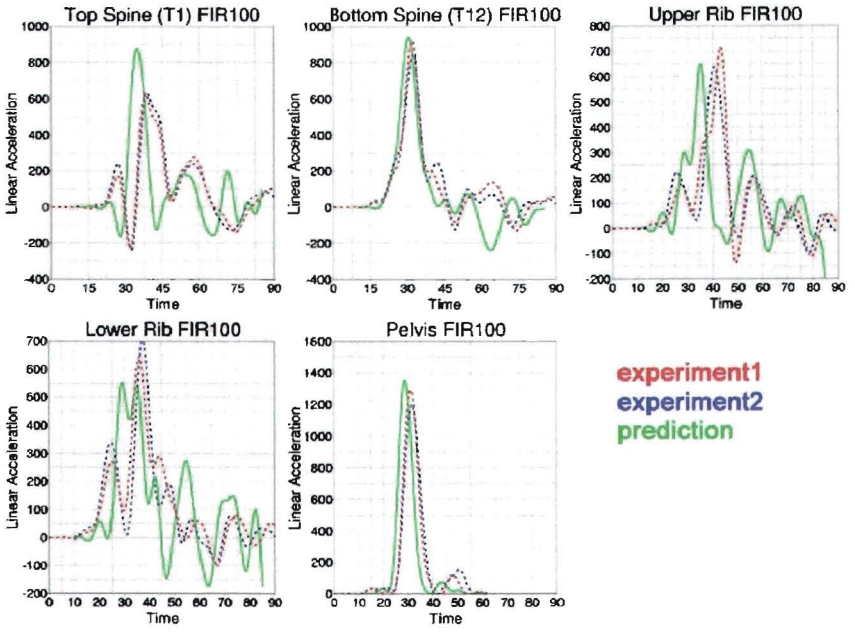

Figure 6.5: Preliminary results 00/150/100 EBS test

The lower rib acceleration gives some reason for concern pertaining the quality of the model. Especially the presence of the first predicted peak on 29 ms, as it is a likely cause to the underestimation of the important peak magnitude on 35 ms. From the model kinematics it could be deduced that the abdomen plate scrapes the lower rib while it penetrates the abdomen. This could account for the presence of the first peak in the predicted signal of the lower rib acceleration. Video footage provided no means for comparison with the model kinematics though, as the complete abdomen and thorax are obscured by the jacket.

6.2.2 00/150/100 EBS sensitivity test

Test impact 18 (see table 6.1), where the dummy is moved upwards with respect to the impacter by 3 cm, shows very surprising results. With the impactor now hitting the ATD 3 cm lower, the abdomen plate should hit the pelvis directly. As a consequence the pelvis acceleration should display a smooth peak of greater magnitude that would have been shifted in timing with respect to the original 00/150/100 test. However, as figure 6.6 shows the experimentally derived pelvis acceleration (red line) contains a double peak of substantially lower maximum value than the previously conducted tests.

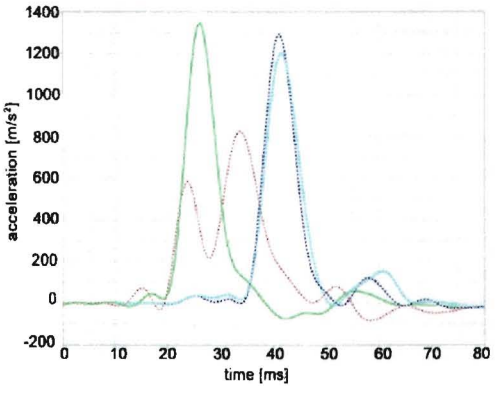

Figure 6.6: A comparisson of the predicted pelvis accelerations (g) for the 00/150/100-3cm-up simulation (green), the 00/150/100-3cm-up (red) experimental results and the experimental results from the 00/150/100 test (blues).

An explanation can be found when studying the film data of this test. Figure 6.7 shows frames of this film taken at 22 and 24 ms.

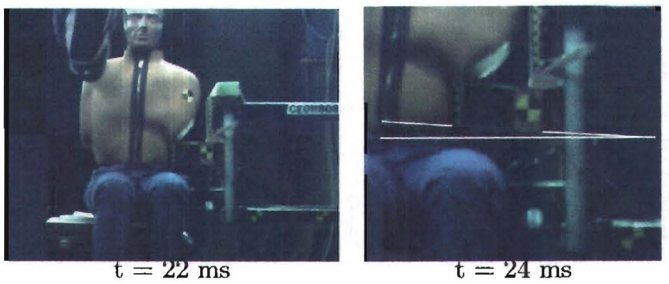

t = 22 ms t = 24 ms

Figure 6.7: Frame and detail of frame from 00/150/100 EBS impact, taken at 22 and 24 ms.

Most likely due to the shape of the pelvis and the hard contact with the pelvis bone, the abdomen plate rotates and slips over the left iliac wing. The timing coincides with the drop in the experimentally derived pelvis acceleration. Repeatability for this test was not assessed, but can assumed to be poor. The exact rotation of the abdomen plate will very likely be hard to capture in a numerical model. This makes the experiment unsuited for calibration purposes and, therefore, it will be disregarded for further analysis in this thesis.

6.2.3 00/100/00 EBS test *with* jacket

The test results for the 00/100/00 *with jacket* experiment (in figure E.5) show a marginal, but acceptable, repeatability for the experiment. The model predictions for the top and lower spine accelerations are acceptable. The predictions for the lower and upper rib accelerations both do not register the first experimental peak and overestimate the second peak. The pelvis acceleration prediction can be called acceptable with respect to one of the experimental signals, but unacceptable with respect to the other.

6.2.4 00/100/00 EBS test *without* jacket

No repeat was executed for this experiment, since there was a genuine concern that these impact conditions could well damage the ATD. The predictions for the experimental signals from the 00/100/00 *without jacket* test, as depicted in E.6, are arguably of a lesser quality then the predictions for the 00/100/00 *with jacket* experiment. This is surprising, since the *without jacket* simulation is a more straightforward simulation, with fewer unknowns due to the omission of the jacket and arm foam. The predictions for both the spine and the pelvis accelerations show are leading the experimental curves and start rising immediately after impact occurs. This observation leads to the assumption that the abdomen is behaving much too stiff in this simulation. This is supported by comparing the model kinematics to the test video, where it can be seen that the abdomen in the model does not show as much compression as during the experiment. The fact that the same abdomen model is used in the 00/100/00 *with jacket* simulation, implies that the jacket and/or arm foam model are partly obfuscating the modeling error in the abdomen.

Working on the premises that the aforementioned assumptions hold true, this can be seen as a typical weak-spot of the applied modeling approach, as basic material and component level validation have been skipped for the abdomen component in favor of validation on full dummy level. The abdomen, jacket and arm foam, that all play crucial roles in a 00/100/00 impact, were insufficiently validated to warrant a calibration attempt with a 00/100/00 impactor. The number of unknowns in this problem forced a multitude of iterations that resulted in a "local optimum" for the model parameters and guided the modeling process in a wrong direction.

6.3 Reassessment of the DoTSID model

Tests 17, 19 and 20 (see table 6.1), are all first reevaluated by specifying the correct initial dummy position, impactor mass and impactor velocity, as measured in each in individual test.

In the predictions for the 00/100/00 tests, no significant changes could be observed. The 00/150/100 test prediction, however, did improve. Conclusions pertaining this simulation are discussed in section 6.3.1.

Re-calibration for the 00/100/00 impacts started with the *without jacket* case first. This test can be used for tuning the properties for the abdomen component. Only when this simulation yields acceptable results, it is suggested to proceed to the *with jacket* variant in order to tune the jacket and possibly the arm foam. Better still though, is to conduct dynamic material and component tests for the jacket, arm foam, abdomen

and lumbar spine before continuing model calibration in 00/100/00-like applications. Within the scope of this thesis, however, no time is left for either approach[2].

6.3.1 00/150/100 EBS surrogate test for FMVSS214

Figure 6.8 shows the experimental curves as well as the original (orange) and the updated (green) predictions. The pelvis acceleration prediction improves in both timing and peak value and nearly matches the experimental curve. The prediction for the bottom spine show a slight improvement in the shape and timing of the curve, but a larger overshoot with reference to the experimental signal when compared to the base simulation. The overall quality of the rib acceleration predictions show a slight improvement. The accuracy of the maximum peak magnitude prediction for the upper rib acceleration has decreased, whereas it increased for the lower rib acceleration. The timing for both predictions shows, a slight, improvement. The predicted upper spine acceleration displays better timing and peak value for the new simulation with respect to the experimental signal.

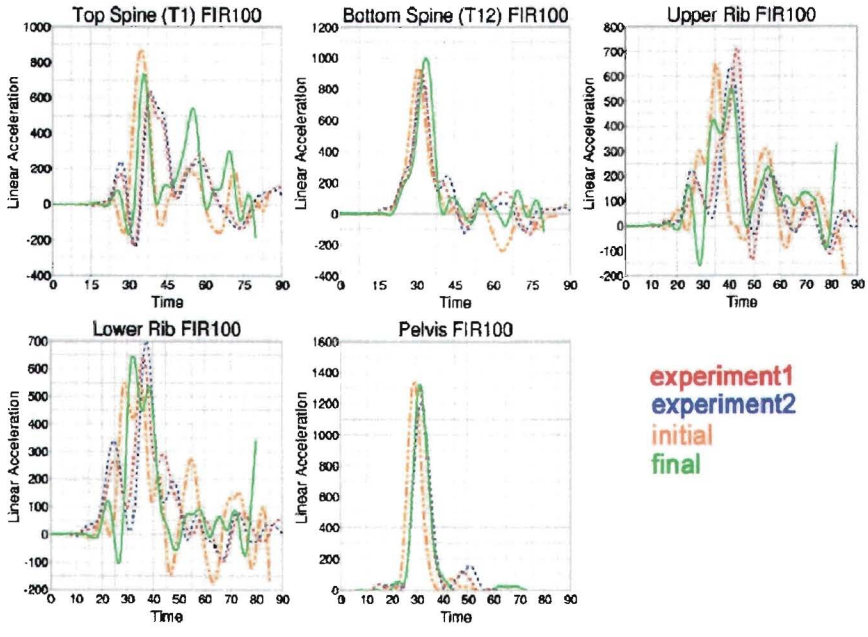

Figure 6.8: Results for 00/150/100 EBS test

These findings support the claim that the hybrid MB/FE model is capable of predicting dummy response in FMVSS214 applications. Therefore, until indications suggest otherwise, the poor model response in the FMVSS214 benchmark (section 5.1.1) is attributed to the vehicle model.

[2] The 00/100/00-nojacket test was reassessed within the scope of this thesis. By decreasing abdomen foam and pelvis foam stiffness, the results in figure E.7 could be attained. The influence of these changes on the other impact simulations, however, has not been assessed. Therefore these results are included for reference only.

Chapter 7

Discussion

This section will address the objectives that were stipulated out in section 1.2 and contains an analysis of the employed methodology, an assessment of the model's quality, the conclusions and, finally, the recommendations.

7.1 Analysis of methodology

The implementation of multibody components has accelerated the development of the hybrid MB/FE DoTSID model. In itself, the hybrid MB/FE modeling approach has proven to be an improvement and a flexible addition to traditional FE modeling. It allowed for a fast and accurate modeling of the DoTSID's joints and joint properties. The presence of these multibody joints also facilitated the positioning of the dummy. The method is flexible because the designer can choose what part to model using rigid bodies and what part to model using finite element techniques. Additionally, the presence of a rigid body in a component allows for an efficient and very accurate control over that components inertia properties, that cannot easily be attained by using traditional FE modeling techniques. Furthermore, the substitution of finite element components with rigid bodies allowed a more cpu efficient model.

Having said this, the proposed calibration method in section 3.1.3, could not be executed. This was because of a lack of reliable test data on particularly material level and to a lesser extent on component level. The uncertainties pertaining the validity of material and component models hampered the calibration process on complete dummy level. There are even indications that these shortcuts resulted in unnecessary modeling errors for some components, as discussed in section 6.2.4.

Therefore, it can be concluded that the hybrid MB/FE modeling approach is useful symbioses of multibody and finite element modeling. However, validation on a material and component level deserves much more emphasis in the development of such a model when compared to a traditional multibody model.

7.2 Quality assessment of the DoTSID model

Objective and standardized criteria for determining the quality of a model do currently not exist, although in 1997 an attempt was made by a subcommittee of the SAE [48]. The result of their efforts is summarized in table 7.1.

The committee was composed of occupant modelers from the automotive industry, code developers and the academia. This proposed validation index was agreed upon in principle, but various issues such as: comparing two time varying responses, the total number of required tests and the region of validation remained unsolved. As a result, the index was never finalized. The proposed validation index consisted of various levels of validation of a model, with the higher levels implying a higher quality of model predictions of a reference test event(s).

When implementing this scale to index the quality of the hybrid MB/FE US-DoTSID model, the question arises to which simulations to apply this table to. The total collections of tests, including the complete test matrix, the validation tests and the additional tests, or only the validation tests. Should tests be indexed separately, if so, is the total model's index an (weighed) average of these indices, if not, how should the index be applied to predictions pertaining different reference events.

It is difficult for a designer of a model to select the tests by which his model will be judged. However, it is decided to use the 00/50/50 deforming barrier validation test, the 00/150/100 rigid impactor test and the FMVSS201 application for indexing the quality of the hybrid MB/FE DoTSID model. Both the 00/150/100 rigid impactor test and the deforming barrier test are sensible choices to use in the index. The rigid impact

Table 7.1: Summary of proposed validation index levels

Class	Characteristic
Level 0	No agreement between predictions of model and "reference event"
Level 1	Qualitative agreement: a) Trends of predicted parameters are the same b) Qualitative correspondence for kinematics
Level 2	HIC and similar indicator predicted by the model are within 20% of those obtained in reference event
Level 3	Peak values of important occupant responses limited to a relative error of 20% and 11.31 deg on vector direction
Level 4	Same as level 3 except 5%
Level 5	Timing of peaks of important vector responses limited to 5% relative difference
Level 6	All peaks and valleys in the duration of the time-dependant predictions must match the reference event within 10%
Level 7	Same as level 6 except 5%
Level 8	1% relative error, point by point, over the durations of the reference and predicted events

test proved to be a repeatable test that approximates the model's intended application area. The deforming barrier test also is representative of the model's intended application area. The FMVSS201 application, though, is not entirely fit to serve as an index test. In this simulation a complex environment is present that interacts with the dummy model. So actually the FMVSS201 model results are a product of both models and, since no model is perfect, it will invariably influence the DoTSID model score. Moreover, these full scale vehicle crashes usually exhibit a poorer repeatability then tests performed in a more controllable (impactor) environment. Out of a sense of completeness, with respect to covering the DoTSID model's application area, the FMVSS201 application will be used for model indexing purposes. Furthermore, it is important to note that none of these test have been calibrated. This quality makes these tests more suited for an objective indexing than the calibration tests. In table 7.1 several times the term: *important occupant responses*, is mentioned. It is assumed that all occupant responses that are used to calculate TTI and pelvis injury index fall into this category. Table 7.2 summaries the results for indexing the important occupant responses for all three tests.

Table 7.2: Validation index for DoTSID model

	00/50/50	00/150/100	FMVSS201	
Upper rib acceleration	5	3	5	4
Lower rib acceleration	5	3	5	4
Lower spine acceleration	5	3	5	4
Pelvis acceleration	5	5	1	3
	5	3	1	

When rigidly applying Prasad's validation index, taking the lowest value from each individual test (bottom row), the overall result would be 1. This would indicate that the DoTSID model only shows qualitative agreement to a reference event. Perhaps a more valid way to apply the final index would be to take the average index over the range of tests for all the different signal predictions. When these averages are rounded down (right column), they represent a meta test that allows for a more objective final index. When applying this method, the hybrid MB/FE DoTSID model would be attributed a 3 on the Pradad's validation index.

In either procedure that could be used for the indexing, it can be deducted that only the low score for the pelvis prediction in the FMVSS201 application degrades the models ultimate index. When compared to the relatively good indices for the pelvis predictions in the other two simulations, the question could be raised if the previously mentioned objections to admitting the FMVSS201 application into this indexing procedure should have been heeded.

The thesis objective included the statement that: *"The model should be predictive and accurate within a useful range of applications"*. However, since *predictive* and *accurate* have not been quantified in the validation index levels nor the in the objective, it is left to the readers discretion to determine whether or not this objective has been met.

7.3 Conclusions

Summarizing the previous sections it can be concluded that:

1. The implementation of multibody components accelerated the development of the hybrid MB/FE DoTSID model
2. The hybrid MB/FE modeling approach provides a flexible integration with finite element models and can be considered to be an improvement upon traditional FE modeling, since the hybrid technique:
   - Allows the designer to choose the most suited modeling technique (i.e. rigid body or finite element) for each component
   - Provides accurate control over a components inertia properties through inertia compensation in rigid bodies, without the need for detailed meshing
   - Allows for the implementation of a supported non-deforming mesh (NULL-material) that, for certain components, yields a sufficiently accurate and very cpu efficient alternative to traditional finite element modeling
   - Offers a more user friendly positioning of the model when compared to traditional finite element models through the rigid body joints.
3. In a range of different impact scenarios, the hybrid MB/FE DoTSID model demonstrated its usefulness as a tool for side impact analysis
4. Validation on a material and component level deserves much more emphasis in the development of a hybrid MB/FE dummy model than is the case with traditional multibody models
5. On Prasad's *proposed validation index levels for numerical models* the hybrid MB/FE DoTSID model scores a validity rating of 3

7.4 Recommendations

Any further calibration of the assembled hybrid MB/FE DoTSID model should include material and component validation, especially pertaining the jacket, arm foam, abdomen and lumbar spine.

In general, the development of a hybrid model would benefit from a more accurate mesh then the one that was used for the DoTSID model. Uncertainties pertaining the quality of the mesh, particularly in the pelvis region (see section 3.1.1), will hamper further calibration. A more accurate mesh could be derived from CAD data or be obtained through 3-d surface scan measurements.

In addition to these recommendations pertaining the MB/FE DoTSID model and the hybrid MB/FE modeling approach, a few observations can be made with respect to the MADYMO solver.

When supporting nodes to a rigid body, the mass of those supported nodes is, erroneously, omitted. While this is not insuperable for FE NULL-material (as this material model does not support density), it leads to (larger) aberrations when supporting (a higher percentage) of nodes of a material that is associated with any other material model. Furthermore, MADYMO does not support a simulation to start with pre-stressed materials[1]. This precludes the correct positioning of the MB/FE-DoTSID model, as the pelvis is not able to retain the stress that is associated with the initial pelvis deformation due to contact with the seat under the influence of gravity. The suggested work-around is to simply position the pelvis, and any other FE components that are in initial contact, very close to their point of contact. This, however, entails that the initial position of the dummy model will slightly different then is the case in the experiment[2]. Moreover any initial friction between the dummy and the seat is cannot be accounted for in the numerical model.

Solving the "*supported nodes*" issue and including the option in MADYMO to start a simulation with pre-stressed materials is highly recommended in order to allow for a better performance of hybrid MB/FE models in general.

[1] An additional, and conclusive, reason not to model the spine and neck using finite elements.
[2] In the regarded impactor simulations, this error was compensated for by moving the impacter up by the same amount.

Bibliography

[1] *Exposure Data For Travel Risk Assessment*, European Transport Safety Council, June 1999

[2] *Laboratory test procedure for FMVSS201 Rigid Pole Side Impact Test*, U.S. Department of transportation National Highway Traffic Safety Administration, TP-201P-00, October 14 1997

[3] *Laboratory test procedure for FMVSS214 "Dynamic" side impact protection*, U.S. Department of transportation National Highway Traffic Safety Administration, TP-214D-05, August 2, 1999

[4] R.H. Eppinger, J.H. Marcus, R.M. Morgan, *Development of Dummy and Injury Index for NHTSA's Thoracic Side Impact Protection Program*, SAE paper 840855, Society of Automobile Engineers, Inc., May 1984

[5] *Side Impact Dummy (SID) Users Manual*, 1First Technology Safety Systems Inc., May 1994

[6] *FTSS Product Catalog*, 1First Technology Safety Systems Inc., 2 October 1999

[7] U.S. Department of Transportation, National Highway Traffic Safety Administration, *Advanced anthropomorphic test device (AATD) development program, phase I reports: concept definition*, 1985

[8] *VITES Part B RTD Project Proposal for the Programme: Competitive and Sustainable Growth*, Virtual Testing for Extended Vehicle Passive Safety, March 31 2000

[9] R.R. McHenry, *Analysis of the Dynamics of Automobile Passenger Restraint systems*, Proc. 7^{th} Stapp Car Crash Conference, pp. 207-249, 1963

[10] R.R. McHenry, K.N. Naab, *Computer Simulation of the automobile crash victim in a frontal collision– a Validation Study*, Cornell Aeronautic Laboratory Inc., Rep. No YB-2126-V-IR, 1966

[11] R.R. McHenry, D.J. Segal, *Computer Simulation of automobile crash victim.* Cornell Aeronautic Laboratory Inc., Rep. No VJ-2492-V-1, 1967

[12] D.J. Segal, *Revised Computer Simulation of automobile crash victim*, Cornell Aeronautic Laboratory Inc., Rep. No VJ-2759-V-2, 1971

[13] J.P. Danforth, C.D. Randall, *Modified ROS occupant dynamics simulation user manual*, General Motors Corp. Research Labs., Pub. No. GMR-1254, 1972

[14] D.H. Robbins, R.O. Bennet Jr, B.M. Bowman, *User-oriented mathematical crash victim simulator*, Proc 16^{th} Stapp Car Crash Conference, pp.128-148, 1974

[15] A.I. King, C.C. Chou, *Mathematical Modelling, Simulation and Experimental Testing of Biomechanical system crash response*, Journal of Biomechanics, Vol. 9, pp 301-317, 1976

[16] J.A. Bartz, *Development and Validation of a computer simulation of crash victim in three dimensions*, Proc 16^{th} Stapp Car Crash Conference, pp.105-127, 1972

[17] J.T. Fleck, F.E. Butler, *Validation of the Crash Victim Simulator, Volumes 1-4, Report No. ZS-5881-V-1*, DOT-HS-6-01300, December, 1981

[18] A.J. Padgaonkar, K.W. Krieger, A.I. King, *A Three-Dimensional Mathematical Simulation of Pedestrian-Vehicle Impact with Experimental Verification*, Journal of Biomechanical Engineering (ASME), 99K: 116-123, 1977

[19] P. Niederer, F. Waltz, *Stability Considerations in the Mathematical Reconstruction of Traffic Accidents*, SAE, Paper No. 760775, 1976

[20] W.L. Kruse, *Calspan-Chrysler Research Safety Vehicle Front End Design for Property and Pedestrian Protection*, Proc. 6^{th} International Technical Conference on Experimental Safety Vehicles, 1976

[21] J.E. Fowler, R.K. Axford, K.R. Butterfield, *Computer Simulation of the Pedestrian Impact Development of the Contact Model*, Proc. 6^{th} International Technical Conference on Experimental Safety Vehicles, 1976

[22] M.K. Verma, B.S. Repa, *Pedestrian Impact Simulation- A Preliminary Study*, SAE 831601, Proc. 27^{th} Stapp Car Crash Conference, 1983

[23] A.J. Padgaonkar, P. Prasad, *Simulation of Side Impact Using the CAL3D Simulation Model*, SAE 791007, Proc. 23^{th} Stapp Car Conference, 1979

[24] K.F. Newman, N.D. Grew, G. Dowzall, *CAL3D: Its Use in Bl Cars Limited*, Proc. of the CAL3D User Conference Sponsored by MVMA and NHSTA, May 1981

[25] D.J. Segal, *Computer Modeling of Side Impact penetration of Dummies of Various Sizes Into Padding*, MGA Report G 37-V-3, DOT-NH-22-82-C-07047, August 1983

[26] D.J. Segal, *Side Modelling Using Lumped Mass and CAL3D CVS Simulations*, SAE publication P-146, Mathematical Simulation of Occupant and Vehicle Kinematics, pp. 51-63, SAE Paper No. 840859, 1984

[27] D.H. Robbins, J. Becker, R.O. Bennet, B.M. Bowman, *Accident Data Simulation pedestrian and Side Impact-3D*, HSRI Rep. No. UM-HSRI-80-75, December 1980

[28] Y.C. Deng, *Side Impact Simulation and Thoracic Injury Assessment*, presented at the11th International Technical Conference on ESV, 1987

[29] I. Kaleps, L.A. Obergefell, J. Ryerson, *Simulation of restrained Occupant Dynamics During vehicle Rollover*, Final Report for DOT Interagency Agreement DTNH22-83-X-07296

[30] L.A. Obergefell, I. Kaleps, A.K. Johnson, *Prediction of an Occupant's Motion during Rollover Crashes*, 30^{th} Stapp Car crash conference, SAE Paper No. 861876, 1986.

[31] G.D. Frish, *Simulation of Occupant-Crew Station Interaction During Impact - Impact Injury of the Head and Spine*, Edited by Ewing *et al*, Charles C. Thomas, Publisher, Springfield, Illinois

[32] TNO Automotive, *MADYMO v5.4 Users Manual*, May 1999

[33] TNO Automotive, *MADYMO v5.4 Database Manual*, May 1999

[34] C. Erbelding, A. Kurz, A. Schelke, *Development of Finite Element Side Impact Dummies: A Contribution to efficient occupant simulation*, Berechnung und Simulation im Fahrzeugbau, Tagung Würzburg, VSDI-Gesellschaft Fahrzeug-und Verkehrstechnik, VDI Berichte: 1283, ISBN 318 091283, pp. 263-282, 1996

[35] J. Hasewaga, H. Motojima, Y. Ogawa. *Development of a Finite Element Model of the Side Impact Dummy and Application for the Side Impact Protection*, ESI Paper No. 96-S8-0-12, 1996

[36] C. Pal, H. Ichikawa, K. Sagawa, I. Hagiwara, *Development of a Finite Element Side Impact Dummy (SID) Model Based on Dynamic Behavior*, ESI Paper No. 96-S8-0-13, 1996

[37] T.C. Low, P. Prasad, *Dynamic Response and Mathematical Model of the Side Impact Dummy*, 34^{th} Stapp Car crash conference, SAE Paper No. 902321, 1990

[38] L.S. Pauls, *An Improved Side Impact Model for Use on Micro Computers*, 35^{th} Stapp Car Crash Conference, SAE Paper No. 910602, 1991

[39] PSI, *PAM-CRASH^{tm} PAM-SAFE^{tm} Version 2000 Level 18 Notes Manual*©, PAM System International, March 2000

[40] E. Haug et al., *FEM-CRASH Berechnung eines Fahrzeugfrontalaufpralls, VDI-Tagung*, Berechnung im Automobilbau, 1986

[41] E. Haug, D. Ulrich, *The PAM-CRASH Code as an Efficient Tool for Crashworthiness Simulation and Design*, The 2^{nd} European Car/Trucks Simulation Symposium, 1988

[42] R. Hoffmann, D. Ulrich, *Finite Element Analysis of Occupant Restraint System Interaction with PAM-CRASH*, Proc. 34^{th} Stapp Car Conference, SAE, SAE P-236, pp 289-300, Paper No 902325, 1990

[43] B. Pletschen, *An Advanced 50 percentile Hybrid III Dummy Database: Validation*, Second Int. MADYMO User Meeting, 1990

[44] U. Franz, M. Walz, O. Graf, *Enhancements to the FAT Dummies using Specific features of LS-DYNA*, CAD-FEM GmbH, 1999

[45] U. Franz, O. Graf, *Accurate and Detailed LS-Dyna FE Models of the US- and EuroSID: A Overview of the German FAT Project*, CAD-FEM GmbH, 2000

[46] B. Moisey, Shkolnikov, D. Bhalsod, *LS-DYNA3D Finite Element Model of Side Impact Dummy SID*, SAE Paper No. 971525, 1997

[47] NHTSA web pages, *HTTP://www-nrd.nhtsa.dot.gov/include/nrd10/nrd1/ fea.html*, last updated 16/18/00

[48] P. Prasad, *Occupant Simulation Models: Experiment and Practice*, edited by J.A.C. Ambrósio et al, *Crashworthiness of transportation Systems: Structural Impact and Occupant Protection*, pp. 209-219, Kluwer Academic Publishers, 1997

[49] Department of Transportation, *United States Code of Federal Regulations (CFR) 49 Part 572 Subpart-F*, October 30, 1990

[50] Department of Transportation, *United States Code of Federal Regulations (CFR) 49 Part 572 Subpart-B*, August 1, 1973

[51] National Highway Traffic Safety Administration, *Preliminary Regulatory Impact Analysis New Requirements for Passenger Cars to Meet a Dynamic Side Impact Test FMVSS 214*, PB89-149736, January 1988

[52] National Highway Traffic Safety Administration, *Technical Report Evaluation of FMVSS 214 Side Impact Protection Dynamic Performance Requirement*, DOT HS 809 004, October 1999

[53] K.L. Campbell, R.J. Wasko, S.E. Henson, *Analysis of Side Impact Test Data Comparing SID and BIOSID*, Proc. 34^{th} Stapp Car Crash Conference, SAE Paper No. 902219, 1990

[54] Randa Radwan Samaha, Louis N. Molino, Matthew R. Maltese, *Comparative Performance Testing of Passenger Cars Relative To FMVSS 214 And the EU 96/EC/27 Side Impcat Regulations: Phase I*, National Highway Traffic Safety Administration U.S. DOT, appendix B - ESV Conference Paper 98-S-0-09, 1998

[55] H. Mertz, A. Irwin, *Biofidelity Ratings of SID, EUROSID, and BIOSID*, ISO/TC22/SC12/WG5, N288, October 1990.

[56] H Mertz, J. Kortge, R. Daniel, J. Brinn, *An Evaluation of APR and SID Side-Impact Anthropomorphic Dummies Volume I*, Society of Automotive Engineers, May 5 1983

[57] H.B. Helleman, *Development of a Database for the Model 572 Side Impact Dummy (DOTSID)*, TNO Road Vehicles Institute, TNO Report No. 751060095-SID, 1992

[58] TNO Automotive, *MADYMO v5.4 Theory Manual*, May 1999

[59] B.W. Been, Mechenical properties of new generation crash dummy materials, TNO Road Vehicles Institute, TNO Report No. 98-OR.BV.032.1/BWB, 1998

[60] J.G.M. Thunissen, *The behavior of foam materials in crash conditions*, TNO Road Vehicles Institute, TNO Report No. 95-OR.BV.002.1/JTH, 1995

[61] M.H.J.W. Paas, *The implementation of a versatile foam model in MADYMO*, TNO Road Vehicles Institute, TNO Report No. 97-OR.BV.028.1/MPA, 1997

[62] R. Happee, E.T.J. Klompen, *Development of material testing and modelling methods for crash testing at Eindhoven University*, TNO Road Vehicles Institute, TNO Report No. 98-OR.BV.034.1/RHA, 1998

[63] K. Ando et al, *Foam Material Calibration For The Side Impact Simulation*, NIHON ESI K.K., Paper No. 96-S8-W-15, 1996

[64] M. Th. P. van Slagmaat, The DoTSID lumbar spine, TNO Road Vehicles Institute, TNO Report No. 98.OR.BV.003.1/MTVS, 1998

[65] R.M.H.P. van Haaster, *Update of Version 2.2 US DOTSID MADYMO database - Version 3.1*, TNO Road Vehicles Institute, TNO Report No. 97.OR.BV.041.1/RVH, 1997

[66] R.S.J.M. Verhoeve, *Improvement of the MADYMO DoTSID ellipsoid model - Appendix I in Side Impact Simulation Study Phase 1*, TNO Road Vehicles Institute, TNO Report No. 00.OR.BV.015.1/EVO, July 2000

[67] H.M.G. van Oorschot, P. Slaats, M. Kortehaas, *Side Impact Simulation Study Phase 1*, TNO Report No. 00.OR.BV.015.1/EVO, October 2000

[68] *Instrumentation For Impact Test-Part 1-Electronic Instrumentation*, SAE J211/1, March 1995

[69] M. H. Ray, K. Hiranmayee, S. J. Kirkpatrick, *Performance Validation of Two Side Impact Dummies*, Proceedings of IJCRASH'98, 1998

[70] Y. Zhu, J.M. Cavanaugh, Y. Huang, A.I. King, *Pelvic Biomechanical Response and Padding Benefits in Side Impact Based on Cadaveric Tests*, Proc 37^{th} Stapp Car Crash Conference, SAE Paper No. 933128, 1993

[71] J.M. Cavanaugh, T. Walilko, A. Walbridge, Y. Huang, A.I. King, *An Evaluation of TTI and ASA in SID Side Impact Sled Tests*, Proc. 38^{th} Stapp Car Crash Conference, SAE Paper No. 942225, 1994

[72] K. Tominaga, S. Yamaguchi, K. Kizuki, *Numerical Analysis of Side Impact Phenomena Using MADYMO 3D DOT-SID Dummy*, Proc. 40^{th} Stapp Car Crash Conference, SAE Paper No. 962414, 1996

[73] S. Sundararajan, C.C. Chou, G.G. Lim, J.A. Prater, R.R. Clements, *Dynamic Door Component test Methodology*, Society of Automotive Engineers, SAE Paper No. 950877, 1995

[74] Werkhoven van, Slagmaat van, *MADYMO DoT SID Validation-Internal Report*, TNO Road-Vehicles Research Centre, TNO Report No 750292185, 1993

[75] J. Chung, J.M. Cavanaugh, M. Mason, A.I. King, *Development of a Sled-to-sled Subsystem side impact Test Methodology*, Society of Automotive Engineers, SAE Paper No. 970569, 1997

[76] P.M. Miller, H. Gu, *Sled test Procedure for Side Impact Testing*, Society of Automotive Engineers, SAE Paper No. 970570, 1997

[77] D.J. Stein, *Apparatus and Method for Side Impact Testing*, Society of Automotive Engineers, SAE Paper No. 970572, 1997

[78] M.G.C. Rekveldt, *Evaluation of the MADYMO US-DoTSID ellipsoid model. Parameter identification method and sled modelling*, TNO Road Vehicles Institute, TNO Report No. 00.OR.BV.060.1/MRE, 30 January 2001

[79] TNO-MADYMO-NA, *Side Impact Modeling for Curtain Airbag Development - Final Report*, TNO MADYMO North America, August 16 2000

Appendix A

Injury Parameters

The field of injury biomechanics deals with the effect of mechanical loads on the human body, in particular impact loads. Due to the mechanical load a body region will experience mechanical and physiological changes, the so-called biomechanical response. Injury will take place if the biomechanical response is of such nature that the biological system deforms beyond a recoverable limit, resulting in damage to anatomical structures and alteration in normal functions. The mechanism involved is called *injury mechanism*, the severity of the resulting injury is indicated by the expression *injury severity*. An injury parameter is a physical parameter or function of several parameters that correlates well with the injury severity of the body region under consideration.

Many schemes have been proposed for ranking and quantifying injuries. Anatomical scales describe the injury in terms of its anatomical location, the type of injury and its relative severity. These scales rate the injuries itself rather than the consequences of injuries. The most well known worldwide accepted anatomical scale is the *Abbreviated Injury Scale* (AIS). Although originally intended for impact injuries in motor vehicle accidents, the updates to the AIS allow its application now also for other injuries like burns and penetration. The AIS distinguishes the seven levels of injury, see figure A.1.

Figure A.1: The abreviated injury scale

The AIS is a so-called "Threat to life" ranking. The numerical values have no significance other then to designate order.

A biomechanical tolerance is the magnitude of a biomechanical response of the human body due to an impact that causes a certain defined level of injury, often given by an AIS level. It is important to note that the tolerance is not the same for each individual in a population and varies from low to high values within the population. Thus the tolerance in general is related to a certain percentage of the population to be protected.

An *Injury Criterion* (IC) can now be defined as a biomechanical index of exposure severity that, by its magnitude, indicates the potential for impact induced injury.

Many injury criteria are based on accelerations, forces, displacements and velocities. Each IC has an accompanying threshold value, referred to as injury criterion limit. When a certain IC limit is breached, the sustained injury is no longer likely to be that of level 2 or lower on the AIS scale (indicated by the green color in figure A.1).

There are several reasons why injury criteria are developed. The search for a valid criterion improves the understanding of injury mechanisms and the situations for which injuries occur. An injury criterion also relates loading conditions during impacts on human bodies to certain levels on injury scales, such as the AIS scale. Another practical reason is that experiments with cadavers, animals and crash dummies provide only measurements of forces, displacements, velocity and accelerations and not directly of injuries.

A.1 Thoracic Trauma Index (TTI)

TTI stands for Thoracic Trauma Index and is calculated as:

$$TTI = 1.4 * AGE * \left(\frac{T12(G) + RIB(G))}{2} \right) * \frac{M}{M_{std}}. \tag{A.1}$$

Where:

AGE	=	age of test subject in years
$T12(G)$	=	maximum absolute value of acceleration in g's of the 12^{th} thoracic vertebra, in lateral direction
$RIB(G)$	=	greater of the maximum absolute values of accelerations in g's of the 4^{th} and 8^{th} rib on struck side, in lateral direction
M	=	test subject mass in kg
M_{std}	=	standard reference mass of 75 kg

As dummies have no meaningful age and a standard mass of 75 kg formula A.1 translates to:

$$TTI(d) = \frac{T12(G) + RIB(G))}{2} \tag{A.2}$$

for 50^{th} percentile ATD's. This criterion's limit is set at 85G for an ATD in 4-door cars and 90 in 2-door cars. Required filtering for the component signals is FIR100[68].

Appendix B

MADYMO

MADYMO (MAthematical DYnamic MOdel) is a computer program that simulates the dynamic behavior of physical systems emphasizing the analysis of vehicle collisions and assessing injuries sustained by passengers. Although originally developed for studying occupant behavior during car crashes, MADYMO is sufficiently flexible to analyze collisions involving other means of transport such as trains, aeroplanes, motorcycles and bicycles. It also allows assessments to be made of the suitability of various restraint systems, including seat belts and air bags. MADYMO combines in one simulation program the capabilities offered by multi-body and finite element techniques, as shown in figure B.1.

A model can be created with only finite element models, or only multi-bodies, or both. MADYMO offers a set of standard force models for belts, air bag and contact between bodies or with the surroundings.

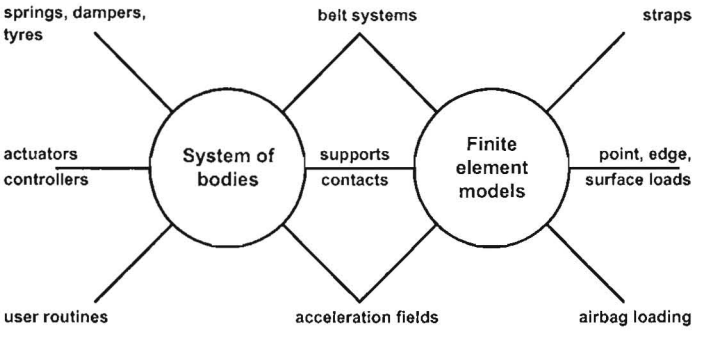

Figure B.1: General MADYMO solver structure

To create a MADYMO input data file, the user first selects the number of multi-body systems and finite element structures to be included in the simulation model. The input data file specifies the mass distribution of the bodies, the connections between the bodies and the joint properties. For the finite element mesh, the element types and the material properties must be specified.

B.1 Multibody concept

In general a multibody system is a system of rigid bodies. Any pair of bodies in the same system can be interconnected by one kinematic joint. The MADYMO multibody for generating the equations of motion is suitable for systems of bodies with a tree structure and systems with closed chains. Systems with closed chains are reduced to systems with a tree structure by removing a kinematic joint in every chain. Removed joints are subsequently considered as closing joints. For each (reduced) system with a tree structure, one body can be connected to the reference space by a kinematic joint, or the motion relative to the reference space of one body can be prescribed as a function of time.

A rigid body is defined by:

- Its mass,
- the location of the centre of gravity,

- and the moments of inertia and the products of inertia.

The shape of a body is not relevant to the equations of motion except when a body contacts other bodies or its environment. Only in the latter case it is necessary to define the shape of the bodies. In order to quantify body data, the user must choose a body local coordinate system. The user can choose the origin and orientation of this coordinate system depending on the users needs. Normally the axes are chosen such that they can be easily recognized in order to facilitate measurement of geometric data. The local coordinate system of a body i will be denoted by (x_i, y_i, z_i). Data corresponding to a specific body is defined with respect to this body local coordinate system.

The location of the centre of gravity is denoted with the vector g_i. The components of g_i are expressed in the local coordinate system of body i. The three moments of inertia and three products of inertia must be specified relative to a coordinate system, the inertia coordinate system, with its origin in the centre of gravity of the body. The orientation of this coordinate system must be specified when it differs from the orientation of the body local coordinate system. The products of inertia are equal to zero when the axes of the inertia coordinate system are parallel to the principal axes of inertia.

A kinematic joint restricts the relative motion of the two bodies it connects. A specific type of kinematic joint is characterized by the way the relative motion of two bodies is constrained. The relative motion allowed by a joint is described by the joint degrees of freedom. The number depends on the type of joint. In MADYMO, the most common joint types are available including spherical joints, translational joints, revolute joints, cylindrical joints, planar joints and universal joints. A system of bodies is defined by:

- The geometry (locations of the bodies centres of gravity and the locations of kinematic joints)
- The mass distribution of the bodies
- The type of kinematic joints and the bodies they connect
- The initial conditions

In addition, the shape of bodies may be needed for contact calculations or postprocessing (graphics) purposes.

B.1.1 Kinematics of rigid bodies connected by joints

A kinematic joint can connect only two bodies. Assume a pair of bodies interconnected by an arbitrary kinematic joint. The bodies are numbered i and j. In MADYMO, the motion of a body j is described relative to the corresponding parent body i. The joint degrees of freedom define the motion within the joint. Their number, n_{ij} , equals the number of degrees of freedom of the joint. They will be contained in the column matrix $\underline{q}_{ij}$

On each body, a body-fixed joint coordinate system (ξ,η ,ζ) is introduced in order to describe the relative motion of body j relative to body i. Let the orientation of the coordinate system of joint j on body i (j) relative to the body local coordinate system on body i (j) be specified by the time-independent rotation matrix C_{ij} (C_{ji}). Let the orientation of the joint coordinate system on body j relative to the joint coordinate system on body i be specified by the rotation matrix D_{ij}. This matrix is a function of the joint degrees of freedom. Let the orientation of the local coordinate system of body i and body j be specified by the rotation matrix A_i and A_j, respectively. Using these rotation matrices, A_j can be written in terms of A_i as

$$\underline{A}_j = \underline{A}_i \underline{C}_{ij} \underline{D}_{ij} \underline{C}_{ji}^T \tag{B.1}$$

Let c_{ij} and c_{ji} be the position vectors of the origins of the joint coordinate systems on body i and j, respectively, relative to the origin of the local coordinate system of the corresponding body. For a rigid body, the components of these vectors relative to the corresponding body local coordinate system are constant. The vector from the origin of the joint coordinate system on body i to the joint coordinate system on body j is given by the vector d_{ij} . The components of this vector relative to the joint coordinate system on body i, d_{ij} , are a function of the joint degrees of freedom only. The position vector of the origin of the local coordinate system on body j, r_j , can be written in terms of the position vector of the origin of the local coordinate system on body i, r_i , as

$$r_j = r_i + c_{ij} + d_{ij} + c_{ji} \tag{B.2}$$

Applying equations B.1 and B.2 successively for a body connected to the reference space until the peripheral body of each branch yields the positions and orientations of all the local coordinate systems relative to the

reference space coordinate system. Taking the first time derivative of equations B.1 and B.2 yields the following expressions for the angular and linear velocity.

$$\omega_j = \omega_i + \omega_{ij} \tag{B.3}$$

$$\dot{r}_j = \dot{r}_i + \omega_i \times c_{ij} + \dot{d}_{ij} - \omega_j \times c_{ji} \tag{B.4}$$

ω_{ij} is the angular velocity vector of body j relative to body i. Taking the time derivative of equations B.3 and B.4 yields similar expressions for the angular and linear acceleration. The kinematics of a joint, the relative motion of the joint coordinate systems, is defined by the rotation matrix D_{ij} and the components of the relative translation vector with respect to the joint coordinate system on body i, d_{ij}. These quantities depend only on the joint position degrees of freedom q_{ij}.

B.2 Finite Element concept

In the finite element module, truss, beam, membrane, shell and brick elements are implemented. Several material models such as elastic, elasto-plastic, Mooney-Rivlin and hysteresis can be used. The interaction between the multi-body model and the finite element model is explained in Figure B.2.

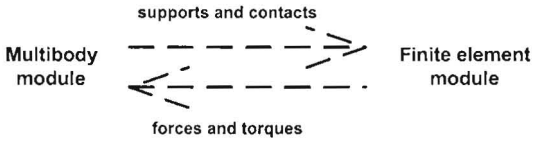

Figure B.2: Interaction between multi-body and finite element modules

Two kinds of interactions, supports and contacts, generate forces between finite element models and the multi-body systems.

This approach allows the use of different time integration methods for the equations of motion for the finite element and the multi-body modules. For short duration crash analysis, explicit integration methods are preferred. For a MADYMO analysis with a finite element model, the 4^{th} order Runge-Kutta or Euler method must be used for the time integration of the equations of motion of the multi-body module. The central difference method is used for the time integration of the equations of motion of the finite element models. Actual positions and velocities at each time step of the central difference method determine the support and contact forces. The forces acting on the multi-body system are accounted for in each main time point of the 4^{th} order Runge-Kutta and each time step of the Euler method. Explicit methods are conditionally stable and therefore put limitations on which time step can be used. Due to the fine spatial discretization often required, a much smaller time step is needed for finite element models than for multi-body models. To increase the efficiency of the entire analysis, the finite element analysis is sub-cycled with respect to the multi-body analysis using a different constant time step for each finite element model. If contacts between different finite element models are specified, the time step is identical for all the finite element models that are in contact. MADYMO automatically selects the smallest time step used in any of the finite element models defined.

The response of solid structures is governed by a set of partial differential equations for the unknown state variables. A direct method or a variational method can be used to generate these equations. In the absence of thermo-mechanical effects, the basic equations are:

- the momentum equation,
- the constitutive equation,
- the strain-displacement relationship.

For given initial and boundary conditions, the system response is embedded in these equations. However, an analytic solution of the resulting partial differential equations satisfying the initial and boundary conditions exists only for very simple cases, and thus a numerical procedure must generally be used. This is the method used to reduce a continuum to a discrete numerical model. The continuum is divided into relatively simple finite elements representing its shape. These elements can be volumes, surfaces, lines or combinations of these. The elements are interconnected at a discrete number of points, the nodes. MADYMO uses a Lagrangian

description. This means that the nodes, and therefore also the elements, are fixed to the material and thus move through space with the material. The system is discretized by interpolating the displacement, velocity and acceleration of any point in an element in terms of the same quantities at the nodes connected to this element. The interpolation functions, the element shape functions, must be such that rigid body motions, motions for which the strains are zero, can be described.

The state of stress results from the strains and the constitutive equation of the material. In quasi-static analyses the equilibrium requirements for each element, are established in terms of the motion of the nodes which can be solved for successive points in the deformation process. Therefore the displacements of the nodes will be the basic unknown parameters for quasi-static analyses.

In dynamic analyses, the equilibrium requirements for each element are established in terms of the motion of these nodes which can be solved for successive points in time. Therefore, the displacements, the velocities and the accelerations of the nodes are the basic unknowns for a dynamic analysis. A well-defined problem includes the definition of the geometry in terms of nodal coordinates and element connectivities. In addition to that, material and geometrical properties of the elements need to be specified. Initial conditions, such as initial displacements or velocities, as well as boundary conditions, such as prescribed motions, contacts and loads can be specified to complete the model definition.

B.2.1 Time integration method

The finite element method is used to reduce a solid structure to a discrete numerical model. The equations of motion of a finite element model can be written as:

$$\underline{M}_{\underline{a}} + \underline{D}_{\underline{v}} + \underline{K}_{\underline{u}} = \underline{F}_{ext} \tag{B.5}$$

where $\underline{M}$, $\underline{D}$ and $\underline{K}$ are the mass, damping and stiffness matrices; $\underline{F}_{ext}$ is the applied load column; and $\underline{a}$, $\underline{v}$ and $\underline{u}$ are the nodal acceleration, velocity and displacement vectors, respectively. The matrix $\underline{D}$ is in general not assembled from element damping matrices, but is constructed by using the mass and stiffness matrix of the complete element assemblage, and Rayleigh damping is assumed:

$$\underline{D} = \alpha \underline{M} + \beta \underline{K} \tag{B.6}$$

where α and β are damping coefficients. α is a function of time and $\beta = 0$. The equilibrium equations can now be transformed into:

$$\underline{M}(a + \alpha \underline{v}) = \underline{F}_{ext} - \underline{F}_{int} \tag{B.7}$$

where $\underline{F}_{int} = \underline{K}_{\underline{u}}$ is called the internal nodal force vector. An observation resulting from the solution of the equations of motion in this form is that each degree of freedom must have a non-zero contribution in the mass matrix. It is also clear that for a diagonal mass matrix the set of differential equations is uncoupled. In general the mass matrix is not diagonal. However, it can be made diagonal by a technique called mass lumping.

In addition to the spatial discretization, a time discretization is necessary. This means the quantities describing the structural behavior are calculated at a discrete number of points in time. A direct time integration method is used so that the equations of motion are satisfied only at discrete time points. The concept on which a direct integration method is based on the assumption that there is a variation of displacements, velocities, and accelerations within each time interval. The form of this variation determines the accuracy, stability, and the costs of the solution procedure. In the MADYMO finite element module, a central difference method with a constant time step and a variable time step is available. The relations for the central difference method with a constant time step are:

$$\begin{aligned} \underline{v}_{n+\frac{1}{2}} &= \underline{v}_{n-\frac{1}{2}} + \Delta t \underline{a}_n \\ \underline{u}_{n+1} &= \underline{u} + \Delta t \underline{v}_{n+\frac{1}{2}} \end{aligned} \tag{B.8}$$

Subscripts $n - \frac{1}{2}$, $n + \frac{1}{2}$and $n + 1$ correspond with time points $t - \frac{\Delta t}{2}$, $t + \frac{\Delta t}{2}$ and $t + \Delta t$ respectively, where t is the current time point. Incorporating the central difference equations in the equations of motion leads to:

$$\underline{v}_{n+\frac{1}{2}} = A_1 \underline{v}_{n-\frac{1}{2}} = A_2 \underline{M}^{-1} (\underline{F}_{ext} - \underline{F}_{int}) \tag{B.9}$$

where:

$$A_1 = \frac{1 - \frac{\alpha}{2\Delta t}}{1 + \frac{\alpha}{2\Delta t}}$$

$$A_2 = \frac{\Delta t}{1 + \frac{\alpha}{2\Delta t}}$$

A lumped mass distribution is used so that the mass matrix $\underline{M}$ is diagonal and the determination of the inverse of the mass matrix $\underline{M}$-1 becomes insignificant. By default, no damping is used ($\alpha = 0$).

In the central difference method, the displacements and velocities are calculated from quantities at previous points in time only. This method is called an explicit time integration method. This method is conditionally stable, meaning that is the time step must be small enough to ensure that the solution does not grow without bound. For undamped linear systems, the time step is limited by:

$$\Delta t \leq \frac{2}{\omega} \tag{B.10}$$

where ω is the maximum eigenfrequency appearing in the mesh. This is the *Courant* stability condition. For a linear truss element with two nodes, it can be shown that:

$$\Delta t \leq \frac{L}{c} \tag{B.11}$$

where c is the dilatational wave speed and L is the characteristic length of the element. This condition requires that the time step is small enough to ensure that a sound wave may not cross the smallest element during one time step. The speed of sound for linear elastic material is a function of the elasticity and density of the material:

$$c \leq \sqrt{\frac{E}{\rho}} \tag{B.12}$$

where E is the Youngs modulus and ρ the density of the material. Thus the critical time step for stability depends on the size of the smallest element as well as the elasticity and density of the material modelled. For nonlinear systems, a similar stability criterion cannot be derived. However, for most practical nonlinear problems an extra 10% reduction on the Courant condition is sufficient.

When the constant time step integration is used, the time step is based on the Courant criterion calculated for the initial geometry. This time step can be reduced by specifying a smaller time step. Large element distortions, however, can make this time integration unstable because the characteristic lengths of the elements become smaller and/or the stiffness of the material increases. In such cases the variable time step integration is more suitable because it is based on the Courant criterion calculated for the current geometry.

B.2.2 Material models

All structural materials are elastic to a certain extent, if the applied loads do not exceed a certain limit, the deformation disappears with the removal of the loads. When loaded beyond the elastic limit, plastic deformations remain after removal of the loads. Often the material is assumed to be:

- homogeneous meaning that the smallest part cut from the body possesses the same specific mechanical properties as the body
- isotropic implying that material properties are the same in all directions.

Structural materials usually do not satisfy all of the above assumptions. Even metals consist of crystals that vary in size and orientation. However, as long as the dimensions of a body are large in comparison to the dimensions of a single crystal the assumption of homogeneity can be used, and if the crystals are oriented at random the material can be treated as isotropic. In this section, a material description will be provided for all the material models used in modelling the DoTSID.

Elastic material

The mechanical behavior of materials is specified as the relationship between the stresses and strains, constitutive equations. Hookes law is the general constitutive equation for linear elastic material behavior that shows a linear relationship between the six strain components and six stress components. This relationship can be written in matrix notation as:

$$\underline{\sigma} = \underline{S}\,\underline{\varepsilon} \tag{B.13}$$

where $\underline{S}$ is the stiffness matrix with elasticity coefficients and where $\underline{\sigma}$ and $\underline{\varepsilon}$ are column matrices with the following stress and strain components:

$$\underline{\sigma}^T = (\sigma_{xx}, \sigma_{yy}, \sigma_{zz}, \tau_{xy}, \tau_{yz}, \tau_{zx}),\ \varepsilon^T = (\varepsilon_{xx}, \varepsilon_{yy}, \varepsilon_{zz}, \psi_{xy}, \psi_{yz}, \psi_{zx}) \tag{B.14}$$

The stiffness matrix can be inverted in order to obtain the strains in terms of the stresses:

$$\underline{\varepsilon} = \underline{C}\,\underline{\sigma} \tag{B.15}$$

with $\underline{C}$ denoting the compliance matrix.

For isotropic material, the behavior in all directions is the same and the compliance matrix can be expressed as:

$$\underline{C} = \begin{bmatrix} 1/E & -\nu/E & -\nu/E & 0 & 0 & 0 \\ & 1/E & -\nu/E & 0 & 0 & 0 \\ & & 1/E & 0 & 0 & 0 \\ & \textit{symmetrical} & & 1/G & 0 & 0 \\ & & & & 1/G & 0 \\ & & & & & 1/G \end{bmatrix} \tag{B.16}$$

where E is Youngs modulus, ν is Poissons ratio (0.5 for isotropic materials) and G the shear modulus. The relationship between these constants is:

$$G = \frac{1}{2}E(1+\nu) \tag{B.17}$$

This means that only two constants, E and ν, have to be specified for linear isotropic material behavior. In MADYMO 5.4 this material is denoted with the keyword `ISOLIN`.

For fabrics, it is necessary to model a material behavior that only resists elongations. During compression, wrinkling prevents the build-up of stresses. To account for this nonlinear behavior, the stress components are first calculated and transformed into principal stresses. Negative principal stresses are discarded during the reverse transformation. The resulting stresses are then used to calculate the internal nodal forces. This tension only material behavior can only be used for membrane elements and can be specified using the keyword `ISOTEN`.

Material damping Most biological materials and polymers exhibit some form of material damping. In addition to a linear visco-elastic material model (`LINVIS`), a similar model can be used in which the damping is represented by a linear dependence on strain rate

$$\underline{\sigma} = \underline{S}\,\underline{\varepsilon} + \gamma\dot{\underline{\varepsilon}} \tag{B.18}$$

with S the stiffness matrix and γ a rate sensitivity parameter, which is chosen as:

$$\gamma = E\ d\ (\mu + (1-\mu)\Delta t_e) \tag{B.19}$$

with E, d, Δt_e denoting the Youngs modulus, a damping constant and the element time step according to the undamped stability criterion, respectively. The parameter μ can have two discrete values:

$$\mu = 0 \Longrightarrow \gamma = E\ d\Delta t_e \tag{B.20}$$

Damping depends on the element time step and as a result on element size; small elements show less damping than large elements, or:

$$\mu = 0 \Longrightarrow \gamma = E\ d \tag{B.21}$$

Damping is identical for all elements irrespective of size.

Material damping also influences the time step criterion. As a result of damping, stability is obtained for:

$$\Delta t = \min\left[\sqrt{(\gamma/E)^2\,\Delta t_e^2} - \gamma/E\ |_{0<e\leq N_{elem}}\right] \tag{B.22}$$

In the absence of damping ($d = 0$), the finite element time step equals the undamped Courant time step. Damping is available for `ISOLIN`, `FABRIC` and `MOONRIV` material models, using the keyword `DAMPING`.

Moony-Rivlin material

To model rubber-like material behavior, a Mooney-Rivlin material model has been implemented in MADYMO based on the strain energy function:

$$W = A(J_1 - 3) + B(J_2 - 3) + C(J_3^{-2} - 1) + D(J_3 - 1)^2 \tag{B.23}$$

With J_1, J_2, and J_3 the invariants of the right Gauchy-Green strain tensor $\underline{\varepsilon}$.

$$J_1 = trace(\underline{\varepsilon}) \tag{B.24}$$

$$J_2 = \frac{1}{2}\left(trace^2(\underline{\varepsilon}) - trace(\underline{\varepsilon}^2)\right) \tag{B.25}$$

$$J_3 = \det(\underline{\varepsilon}) \tag{B.26}$$

C and D are functions of the material parameters A and B.

$$C = \frac{1}{2}A + B \tag{B.27}$$

$$D = \frac{A(5\nu - 2) + B(11\nu - 5)}{2(1 - 2\nu)} \tag{B.28}$$

The incompressibility of the material can be taken into account by setting Poissons ratio to nearly 0.5. The resulting large value for the penalty factor D forces the third invariant J_3 to 1, resulting in incompressible material behavior. The 2^{nd} Piola-Kirchhoff stress sensor is obtained by differentiating the strain energy function W with respect to the right Cauchy-Green strain tensor $\underline{\varepsilon}$.

$$\underline{S} = \frac{\partial W}{\partial \underline{\varepsilon}} \tag{B.29}$$

This material behavior can be used for brick elements only. The user must specify the material constants A, B and ν. The material model sets limits on the possible values of Poissons ratio:

$$0.460 < \nu < 0.499 \tag{B.30}$$

This material model in MADYMO is denoted with the `MOONEY-RIVLIN` keyword.

Foam material

The behavior of solid foams can be described as highly non-linear and strain-rate dependent with high energy dissipation characteristics and hysteresis in cyclic loading. Low density combined with high energy dissipation capacity make foams attractive for energy absorbing functions in automotive applications. However, its discontinuous nature makes it difficult to construct constitutive equations that accurately describe the mechanical behavior of foam.

Foams are typically used under compression (see figure B.3). At small strains, the mechanical behavior is close to linear elastic, followed by a large order of magnitude reduction in slope. Then, there is a long region, or plateau, in which the slope changes gradually. This stage corresponds to the collapse of cells. After the cells have collapsed, the final stage of densification is reached in which the cells come in contact with one another, causing a sharp increase in the stress.

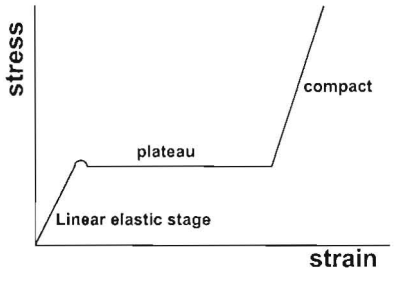

Figure B.3: Typical stress-strain relationship for foam materials in compression.

Strain-rate dependency is a very important factor that must be considered when modelling the characteristics of foam. If the dynamic stress-strain relationship from experiments is used directly in a simulation without considering strain rate effects, the foam model will almost certainly be either stiffer or softer than the real foam.

The `FOAM` material model uses an experimental stress-strain curve rather than a material law. It is available for brick elements only. The model is based on the following two assumptions

1. There is no coupling between stresses and strains of different principal directions, which means Poisson effects are neglected.

2. Strain rate effects can be characterized by a strain rate dependent scaling factor.

As a result, the stress-strain curve can be determined from uni-axial compression and tension tests for different loading rates. Mathematically, the stress-strain relationship has the following form:

$$g(\dot{\varepsilon})\ \sigma_r \tag{B.31}$$

where g is a scaling factor that depends on the effective strain rate, and σ_r is a user specified reference stress curve. This curve represents the quasi-static uni-axial behavior of foam under both compression and tension. The reference stress curve must be defined in terms of nominal stresses vs. logarithmic strains. A piecewise linear interpolation is used. Currently, both hysteresis models 1 and 2 can be applied for this curve. However, hysteresis model 2 is preferred because it works better with the physical behavior of foams. The effective strain in the scaling factor is defined as

$$\varepsilon = \sqrt{tr(\underline{\varepsilon} \cdot \underline{\varepsilon}^T)} \tag{B.32}$$

Two analytical laws are available for scaling up the user-defined stress-strain curve, the `Cowper-Symonds`

$$g(\dot{\bar{\varepsilon}}_n) = 1 + \left(\frac{\dot{\bar{\varepsilon}}_n}{\mathrm{D}}\right)^{\frac{1}{\mathrm{p}}} \tag{B.33}$$

and the `Johnson-Cook` formulations.

$$g(\dot{\bar{\varepsilon}}_n) = 1 + \mathrm{p}\ ln\left(max\left(1, \frac{\dot{\bar{\varepsilon}}_n}{\mathrm{D}}\right)\right) \tag{B.34}$$

where D and p are user specified positive constants. These empirical laws are based on nominal strain rates so a transformation of logarithmic strain rates to nominal strain rates must be carried out. Taking the derivative of the effective strain with respect to time and using the relationship between nominal and logarithmic strains, the nominal strain rate is obtained as

$$\dot{\bar{\varepsilon}}_n = \exp(\mathrm{s}\ \varepsilon)\varepsilon^{-1}\ \mathrm{tr}(\underline{\varepsilon} \cdot \dot{\underline{\varepsilon}}^T);\ \ \mathrm{s} = \mathrm{sign}\left[\min(\underline{\varepsilon}) + \max(\underline{\varepsilon})\right] \tag{B.35}$$

The nominal strain rate is adjusted depending on the sign of the largest absolute value of the principal strains. As a result, the stresses are scaled up much more for loading than for unloading.

The computation of the stress increments is carried out at each cycle by first transforming the logarithmic strain tensor to its principal axes. The principal strains are used to determine the stresses by interpolating directly from the specified reference stress reference curve σ_r. The interpolated stresses are transformed back to the inertial coordinate system. Then, Jaumann stress increments are computed by subtracting the stresses calculated at the previous time point from the current stresses. Finally, taking into account the rate dependency of the foam materials, the Cauchy stresses are computed.

B.3 Deriving material parameters for `FOAM` material

In order to derive accurate material properties for `FOAM` material models, the following method is proposed.

First a loading (and unloading) curve for the regarded foam specimen should experimentally be derived under quasi-static loading conditions. This loading curve can then represent σ_r in equation B.31. In tension, a Young's modulus can be attributed that is equal to the initial Young's modulus in compression.

In addition to the static calibration, a dynamic calibration should be carried out to determine the parameters D and p, as described in equations B.33 and B.34. These parameters can be determined directly if two stress-strain relations for two different constant strain rate tests are available as there are two unknown variables. However, when working with experimental data derived from drop tests, strain rate is not a constant. Therefore, a method of curve fitting is required. This can be done by simulating the foam impact experiments using different combinations of D and p. A nonlinear numerical optimization technique can be applied to determine the value of the material parameters appropriate to the different dynamic impact conditions. The optimization problem can be defined as follows:

Minimize the Objective Function

$$\sqrt{\sum_{p_i} \left(\frac{F_i^C - F_i^E}{F_i^E} \right)^2} \tag{B.36}$$

subjected to

$$F^E - 10\% \leq F^C \leq F^E + 10\% \tag{B.37}$$

for points P1, P2 an P3 and

$$D^E - 10\% \leq D^C \leq D^E + 10\% \tag{B.38}$$

for point P3.

Here F and D are the force and the displacement respectively, the superscripts E and C signify the points obtained by the experiment an the calculation. In this scenario, three points (P1, P2 and P3) are used to approximate dynamic the experimental curve (see figure B.4).

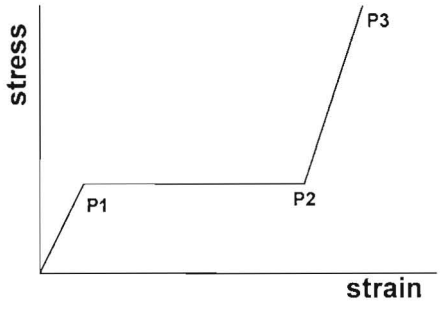

Figure B.4: Three point representation of a typical foam loading curve.

Point P1 coincides with the end of the linear elastic phase, P2 denotes the beginning of the compact phase and P3 signifies the stress that related to the highest recorded strain in the experiment. The subscript i is the number of points that should be mapped to the experimental curves. For n different experiments this index will therefore vary from 1 to $3n$.

The constraints expressed by B.37 and B.38 are defined to avoid iteration to a local minimum.

Appendix C

Previous DoTSID models

Several attempts have been made to capture the DoTSID's response in a numerical model, using either multibody or finite element techniques. The hybrid DoTSID model will be based on two earlier released models: TNO's multibody model and the and a LS-DYNA finite element model circulated by NHTSA for research purposes in 1997 (figure 3.2).

C.1 MADYMO DoTSID multibody model

The MADYMO DoTSID multibody model was originally developed at TNO Delft in 1991. Since then it has been improved in several update steps. The latest update to model version 3.4 was made in July 2000 [66] and showed significant improvement over its predecessor in the calibration tests. A study performed in October 2000, however, showed that this model in FMVSS214 conditions still showed unacceptable correlation with respect to test data [67].

C.2 NHTSA DoTSID FE model

In 1997 NHTSA released the 3^{rd} update to their finite element DoTSID model in the LS-DYNA code that the agency circulates for research purposes. The overall response of this FE DoTSID model was verified under a variety of linear impactor tests which included impacts in the thorax and pelvis area with changes in the impact angle, padded and rigid wall sled tests and finally FMVSS214 side impact and an angled movable deformable barrier (MDB) to vehicle side impact test. In 1998, the model was examined in pole impacts [69] and was found to severely underestimate pelvic accelerations. In addition, the model was found to contain a number of deficiencies [47], which notably include the absence of the cable in the lower lumbar spine area and the absence of the anti sag device in the thorax. It was also concluded that certain refinements were necessary to achieve a fully validated model to study the behavior of the SID in various side impact situations. Such refinements include:

1. Re-meshing certain components in the thoracic, pelvis and thigh areas and redefining, particularly, the soft foam materials to preclude elements from inverting during simulation
2. Reworking the contact interfaces between interacting materials to prohibit excessive penetration
3. Improving the damper properties of the rib structure
4. Re-characterizing the stiffness of the joints
5. Remodeling of the head-neck area.

Appendix D

Calibration Data Acquisition Methods for Side Impact

Occupant models can best be calibrated against test apparatuses instead of vehicle test because the former are more repeatable and allow for a better validated environment. The type of test best suited to generate calibration data depends on the application of the model. In a typical side impact event, a stationary occupant is impacted or "punched" by the intruding door. The door is accelerated from rest by the impacting object and accelerates quickly to a high velocity before picking up structural members in the car frame, that transfer energy to the rest of the vehicle. The energy transferred to the occupant depends on the complex interaction between occupant and door. Occupant to door spacing, trim compliance and geometry, door velocity time history, seat interaction and occupant position are all important variables that must be taken into account when using a component test to simulate a full-scale crash event.

Many researches have used the Heidelberg type sled test procedure for evaluation of side impact [37][70][71]. In these type of tests a sled and occupant are accelerated up to impact velocity and then the sled is quickly decelerated to rest allowing the occupant to slide and impact a rigid or padded wall . The Heidelberg sled test is in fact more representative of a frontal type impact situation, where the occupant is injured during a "secondary" impact with the interior, than it is of a side impact, where the door moves and strikes the stationary occupant. As a result, Heidelberg tests cannot accurately capture the interaction and energy transfer between door and occupant as it occurs in a side impact crash environment.

Other sled-type component tests exist in which the stationary occupant is hit by a sled-mounted door moving at a constant velocity[72][73]. Typically the door is tailored to reproduce the door velocity time history after the point of impact.

Another experimental apparatus is the linear guided impactor (LGI), where the stationary occupant is hit by a spring driven impactor face. The impactor face is mounted on a probe that is guided by a series of Teflon bearings ensuring a low friction. By changing the pre-load of the springs different test velocities can be obtained [74]. Using this approach the precise impact velocity cannot be controlled and has to be measured at impact.

Simulating the entire door velocity profile of a full-scale side impact test involves controlled acceleration and deceleration of the door. Only in 1997 a component test was developed addressing this complex problem [75] [76][77]. In this test, a fixture-mounted door structure is accelerated from rest using a pneumatic ram. The occupant is seated on a rail-mounted automobile seat allowing realistic positioning relative to the door. Door deceleration and motion of the seat can be controlled through a series of programmable hydraulic decelerators. In addition the door decelerators can be programmed to account for door pitching and yawing if necessary.

Appendix E

Comparison Between Experimental and Predicted Results

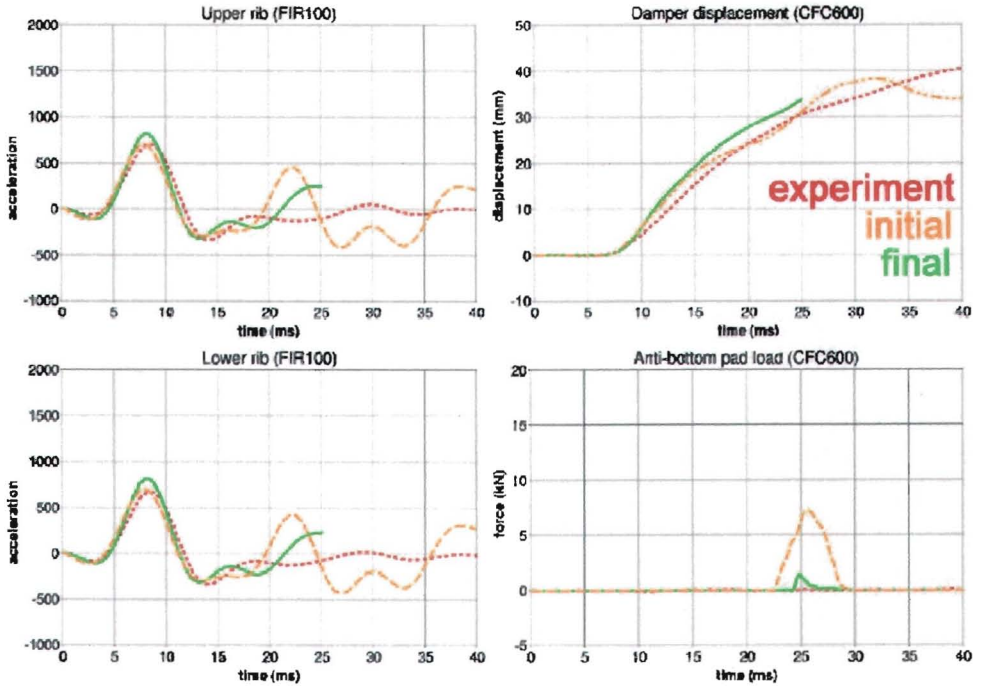

Figure E.1: Results for thorax component test (v = 4.1 m/s).

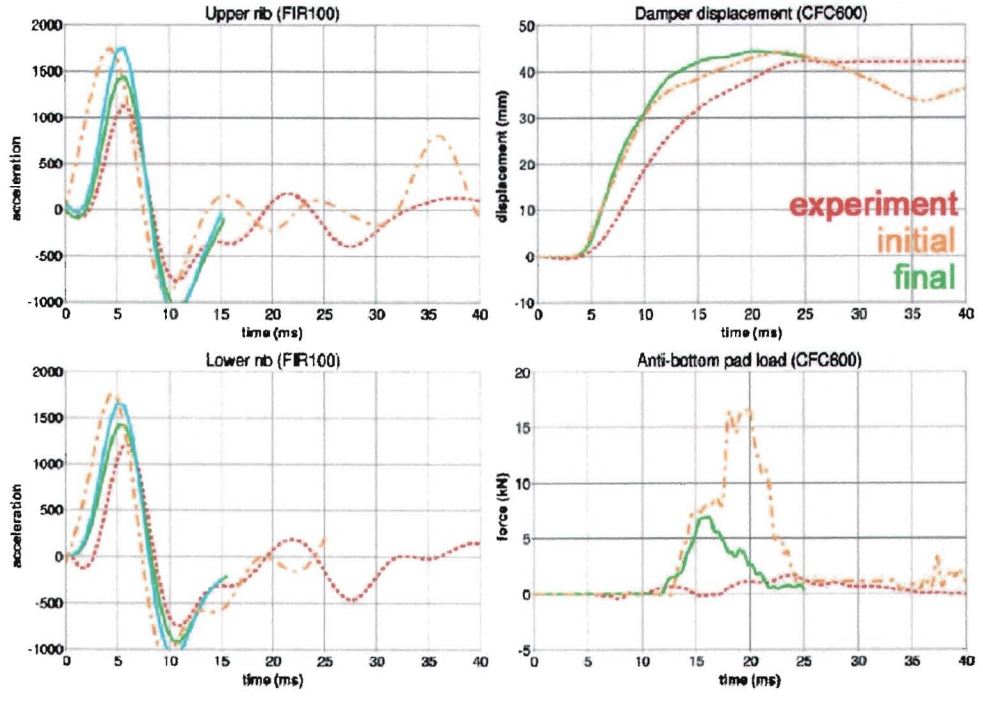

Figure E.2: Results for thorax component test (v = 8.3 m/s).

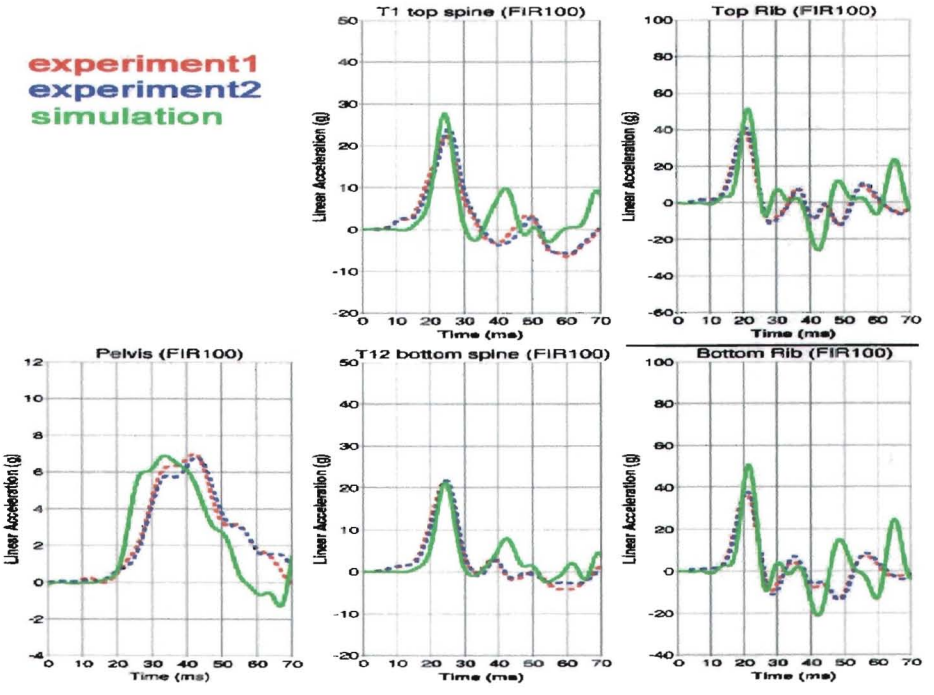

Figure E.3: Results for the 50/00/00 LGI test (v = 4.35 m/s).

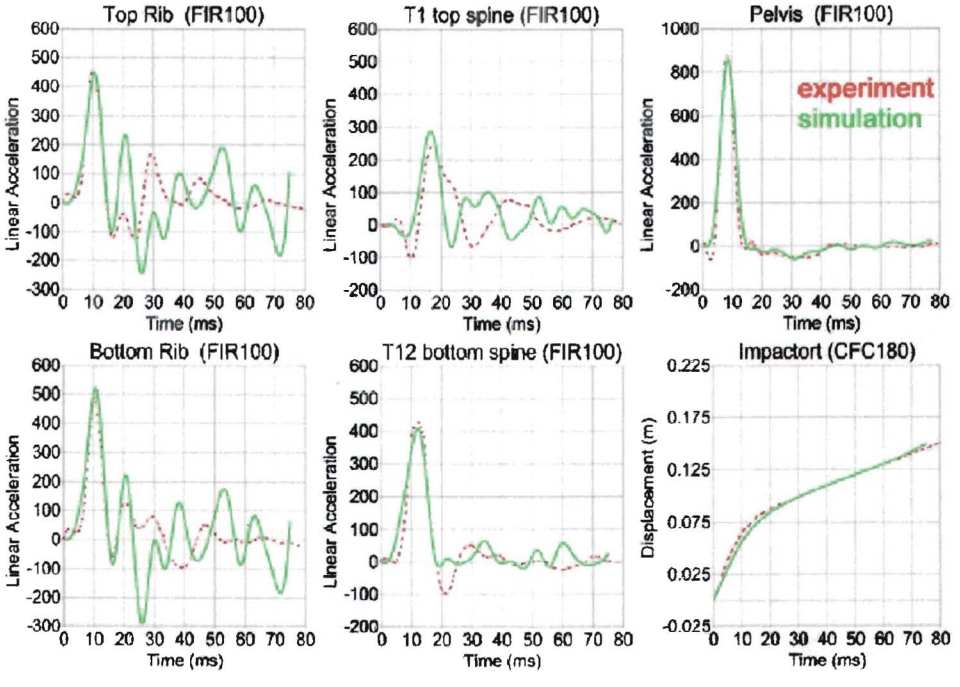

Figure E.4: Results for 00/00/50 LGI test (v = 6.36 m/s).

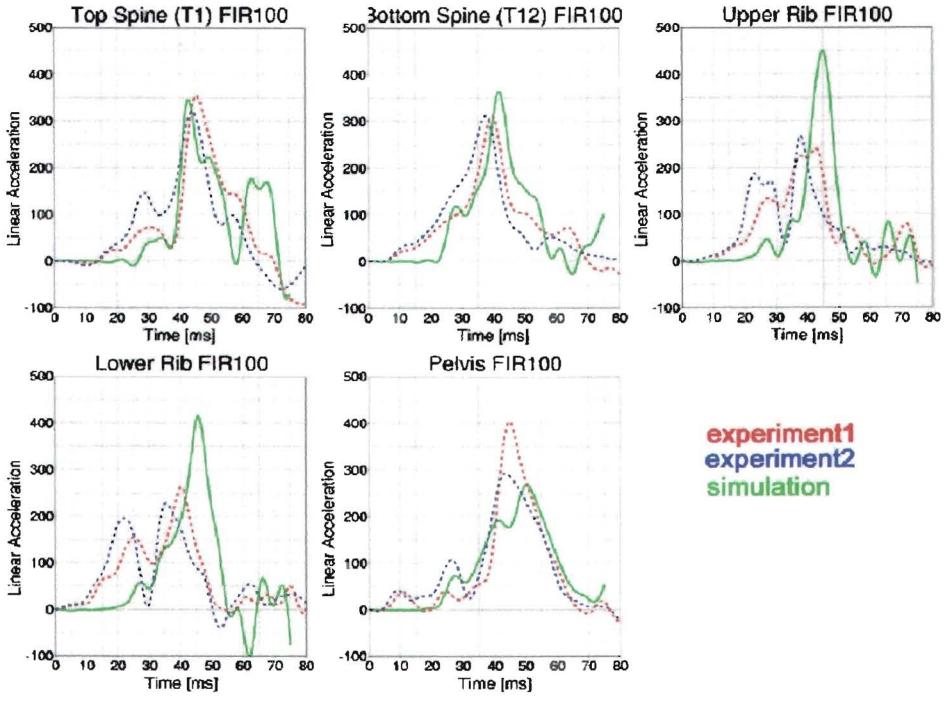

Figure E.5: Results for EBS 00/100/00-with-jacket test

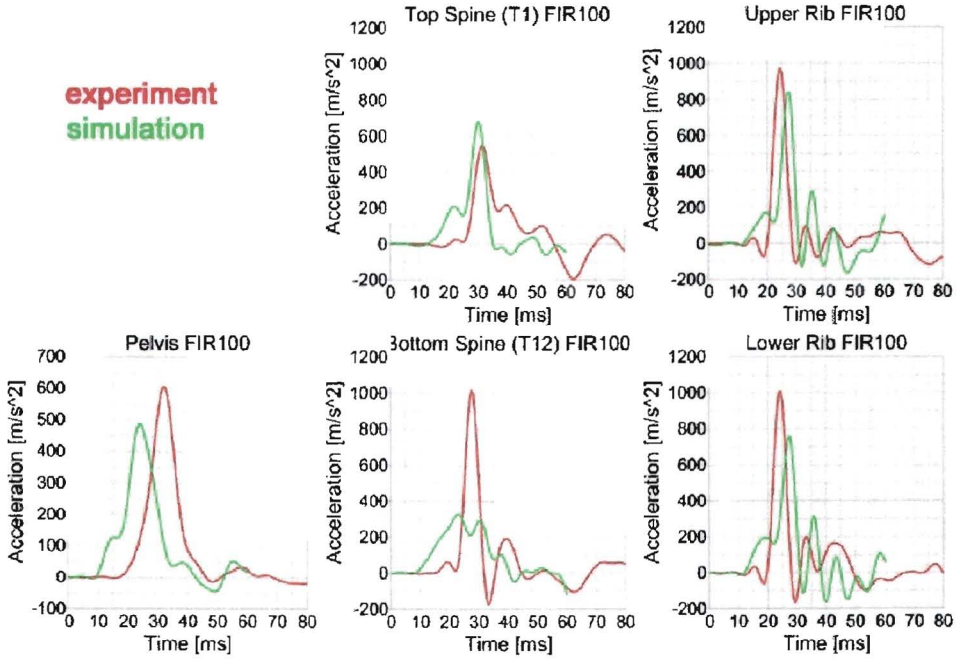

Figure E.6: Results for EBS 00/100/00-without-jacket test

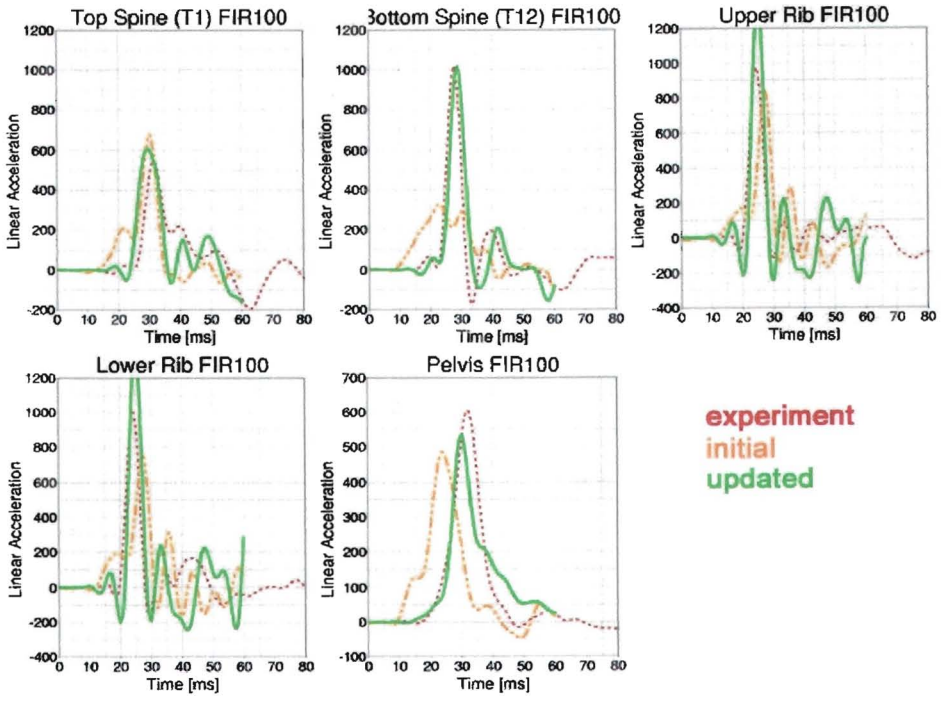

Figure E.7: Results for EBS 00/100/00-without-jacket test

Appendix F

DoTSID Set-up Table

Table F1: Setup of the hybrid MB-FE DoTSID dummy model in MADYMO

Child body	Parent Body	Joint Type		FE components	Element type	Material models	Material Parameters	Supports (to body)
1 Lower Torso		1 FREE	1	PelvisBone	MEM3/MEM4	NULL	E = 7E10	ALL (1)
			2	PelvisFlesh	SOLID1	FOAM (Cowper)	Dens = 360, D = 0.1, P = 2.3	Partly (1)
			3	PelvisOutsideSkin	SHELL4	ISOLIN	Dens = 1.15E3, E = 8.0E6, nu = 0.45	
			4	PelvisInsideSkin	SHELL4	ISOLIN	Dens = 1.15E3, E = 1.6.0E7, nu = 0.30	Partly (1)
			5	PelvisBackHole	SHELL4	ISOLIN	Dens = 7.8 E3, E = 2.07E11, nu = 0.28	Partly (1)
			6	LumbarPelvicAdaptor	MEM4	NULL	E = 7E10	ALL (1)
			7	UpperFemurLeft	MEM3/MEM4	NULL	E = 2.07E+11	ALL (7)
			8	UpperFemurRight	MEM3/MEM4	NULL	E = 2.07E+11	ALL (8)
2 LowerLumbarSpine	1 Lower Torso	2 Bracket	9	LumbarSpine	MEM4	NULL	E = 2.07E+11	ALL (2)
3 UpperLumbarSpine	2 LowerLumbarSpine	3 FREE	9	LumbarSpine	MEM4			ALL (3)
			10	AbdomenFlesh	SOLID1	FOAM (Johnsen)	Dens = 205, D= 0.1, p = 0.1	
			11	AbdomenSkin	SHELL4	ISOLIN	Dens = 1.35E3, E = 5.0E6, nu = 0.35	
4 ThoracicSpine	3 UpperLumbarSpine	4 Bracket	12	ThoraxSpineBox	MEM4	NULL	E = 2.07E+11	ALL (4)
			13	NeckBracket	MEM4	NULL	E = 2.07E+11	ALL (4)
			14	ShoulderPlate	MEM4	NULL	E = 2.07E+11	ALL (4)
			15	ThoraxLumbarAdaptor	MEM4	NULL	E = 2.07E+11	ALL (4)
			16	ShoulderFoam	SOLID1	FOAM (Johnsen)	Dens = 123, D= 15, p = 2	Partly (4)
			17	Bumpstop	SOLID1	MOONRIV	Dens = 1068E3, A = 3.322E5, B =1.641E5, nu = 0.48, damp = 1	Partly (4)
			18	Hinge	SOLID1	ISOLIN	Dens = 1.3868E3, E = 1.728E8, nu = 0.35	Partly (4)
			19	HingeMountBlock	SOLID1	ISOLIN (RIGIDS)	Dens = 2.68E3, E = 6.911E7, nu = 0.30	Partly (17)
			20	NutBarLeft	SOLID1	ISOLIN (RIGIDS)	Dens = 7.8E3, E = 2.07E8, nu = 0.30	
			21	NutBarRight	SOLID1	ISOLIN (RIGIDS)	Dens = 7.8E3, E = 2.07E8, nu = 0.30	
			22	RibSteelStrips	SHELL4	ISOLIN	Dens = 7.8E3, E = 2.07E11, nu = 0.35	
			23	RibDampingMaterial	SOLID8	ISOLIN	Dens = 1.5E3, E = 2.07E8, nu = 0.30	
			24	SternumBars	SOLID1	ISOLIN (RIGIDS)	Dens = 7.8E3, E = 2.07E8, nu = 0.35	Partly (18)
			25	SternumPlate	SOLID1	ISOLIN	Dens = 1.0E3, E = 3.87E6, nu = 0.45, damp = 1.0	Partly (18)
			26	RibBallastCushions	SOLID1	MOONRIV	Dens = 1.068E3, A = 1.243E5, B = 6.1404E5, nu = 0.49, damp = 1	Partly (17)
			27	RibBallastBarRight	SOLID1	ISOLIN (RIGIDS)	Dens = 1.0E4, E = 2.07E8, nu = 0.35	
			28	RibBallastBarFrontLeft	SOLID1	ISOLIN (RIGIDS)	Dens = 1.0E4, E = 1.38E8, nu = 0.35	
			29	RibBallastBarFrontRight	SOLID1	ISOLIN (RIGIDS)	Dens = 1.0E4, E = 1.38E8, nu = 0.35	
			30	RibBallastBarRearLeft	SOLID1	ISOLIN (RIGIDS)	Dens = 1.0E4, E = 1.38E8, nu = 0.35	
			31	RibBallastBarRearRight	SOLID1	ISOLIN (RIGIDS)	Dens = 1.0E4, E = 1.38E8, nu = 0.35	
			32	RibWrapFront	SHELL4	ISOLIN	Dens = 1.0E3, E = 3.87E6, nu = 0.45, damp = 1.0	
			33	RibWrapSides	SHELL4	ISOLIN	Dens = 1.0E3, E = 5.805E6, nu = 0.45, damp = 1.0	
			34	RibWrapRear	SHELL4	ISOLIN	Dens = 1.0E3, E = 3.87E6, nu = 0.45, damp = 1.0	
			35	RibPads	SOLID8	FOAM (Johnsen)	Dens = 123, D= 15, p = 2	
			34	Lower Neck	MEM4			ALL (4)
5 Neck	4 Thoracic Spine	5 SPHERICAL	34	Middle Neck	MEM4	NULL	E = 2.07E+11	ALL (5)
6 Head	5 Neck	6 SPHERICAL	34	Upper Neck	MEM4			ALL (6)
			35	HeadToNeckAdaptor	MEM4	NULL	E = 2.07E+11	ALL (6)
			36	Head	MEM4	NULL	E = 2.07E+11	ALL (6)
7 LeftFemur			37	UpperLegBoneLeft	MEM3/MEM4	NULL	E = 2.07E+11	ALL (7)
			38	UpperLegFleshLeft	SOLID1	FOAM (Cowper)	Dens = 360, D = 0.1, p = 2.3	Partly (7)
			39	UpperLegSkinLeft	SHELL4	ISOLIN	Dens = 1.15E3, E = 8.0E6, nu = 0.30	
8 RightFemur			40	UpperLegBoneRight	MEM3/MEM4	NULL	E = 2.07E+11	ALL (8)
			41	UpperLegFleshRight	SOLID1	FOAM (Cowper)	Dens = 360, D = 0.1, p = 2.3	Partly (8)
			42	UpperLegSkinRight	SHELL4	ISOLIN	Dens = 1.15E3, E = 8.0E6, nu = 0.30	
9 LeftPostKnee	7 LeftThigh	9 REVOLUTE	43	KneePostLeft	MEM3/MEM4	NULL	E = 2.5E+6	ALL (9)
			44	KneeCapLeft	MEM3/MEM4	NULL	E = 2.5E+7	ALL (9)
10 RightPostKnee	8 RightThigh	10 REVOLUTE	45	KneePostRight	MEM3/MEM4	NULL	E = 2.5E+6	ALL (10)
			46	KneeCapRight	MEM3/MEM4	NULL	E = 2.5E+7	ALL (10)
11 LeftTibea	9 LeftPostKnee	11 REVOLUTE	47	LowerLegLeft	MEM4	NULL	E = 2.5E+6	ALL (11)
12 RightTibea	10 RightPostKnee	12 REVOLUTE	48	LowerLegRight	MEM4	NULL	E = 2.5E6	ALL (12)
13 LeftFoot	11 LeftLowerLeg	13 REVOLUTE	49	FootLeft	MEM4	NULL	E = 2.5E+6	ALL (13)
14 RightFoot	12 RightLowerLeg	14 REVOLUTE	50	FootRight	MEM4	NULL	E = 2.5E+6	ALL (14)
15 Damper	4 Thoracic Spine	15 SPHERICAL	51	DamperShell	MEM4	NULL	E = 2.07E+11	ALL (15)
16 DamperRod End	15 Damper	16 TRANSLATIONAL	52	DamperRod	MEM4	NULL	E = 2.07E+11	ALL (16)
17 LeftSideRibs	16 DamperRod End	17 REVOLUTE	53	RibBallastBarLeft	MEM4	NULL	E = 2.07E+11	ALL (17)
			54	Clevis	MEM4	NULL	E = 2.07E+11	ALL (17)
			24	RibBallastCushions				Partly (17)
18 SternumBallast	4 Thoracic Spine	18 FREE	55	SternumBallastBars	MEM4	NULL	E = 2.07E+11	
			23	SternumPlate				Partly (18)
			56	ArmFoamLeft	SOLID1	FOAM (Johnsen)	Dens = 40, D = 0.1, p = 0.1	
			57	ArmSurfaceLeft	MEM4	NULL	E = 2.07E+11	
			58	ArmFoamRight	SOLID1	FOAM (Johnsen)	Dens = 40, D = 0.1, p = 0.1	
			59	ArmSurfaceRight	MEM4	NULL	E = 2.07E+11	
			60	Jacket	SHELL4	ISOLIN	Dens = 1.4E3, E = 1.0E7, nu = 0.45	
			61	Jacket shelf	SHELL4	ISOLIN	Dens = 1.4E3, E = 1.0E7, nu = 0.45	
			62	Jacket bridge	SOLID8	ISOLIN	Dens = 1.4E3, E = 1.0E7, nu = 0.45	
			63	Jacket lining	MEM4	ISOTEN	Dens = 0.8E3, E = 1.0E9, nu = 0.45	